# FINITE ELEMENT MODELLING OF REINFORCED CONCRETE BEAM COLUMN JOINT

A Thesis Report submitted in the partial fulfillment of

requirement for the award of the degree of

**MASTER OF ENGINEERING**

**IN**

**STRUCTURES**

Submitted By

**Priya Goyal**

**Roll No. 801122013**

Under the Supervision of

**Dr. Naveen Kwatra**

Head and Associate Professor,
Department of Civil Engineering
Thapar University, Patiala

**DEPARTMENT OF CIVIL ENGINEERING**

**THAPAR UNIVERSITY,**

**PATIALA- 147004, (INDIA).**

**JULY-2013**

# DECLARATION

I hereby declare that the work which is presented in this thesis report entitled "**Finite Element Modeling of Reinforced Concrete Beam Column Joint**", in partial fulfillment of the requirement for the award of degree of **MASTER OF ENGINEERING (STRUCTURAL ENGINEERING)** in the **CIVIL ENGINEERING DEPARTMENT, THAPAR UNIVERSITY, PATIALA**, is a n authentic record of the initial work carried out by her under the supervision of **Dr. Naveen Kwatra, Head and Associate Professor,** DEPARTMENT OF CIVIL ENGINEERING, THAPAR UNIVERSITY, PATIALA.

The matter embodied in this report has not been submitted in part or full to any other university or institute for the award of any degree.

Priya Goyal

Date: 15.07.13 (PRIYA GOYAL)

This is to certify that the above declaration made by the student concerned is correct to the best of my knowledge and belief.

15/7/13

**(Dr.Naveen Kwatra)**
**Head and Associate Professor,**
**Deptt. of Civil Engineering,**
**Thapar University, Patiala**

**(Dr. S.K. Mohapatra)**
**Dean Academic Affairs**
**Thapar University,**
**Patiala**

# ACKNOWLEDGEMENT

A dissertation cannot be completed without the help of many peoples who contribute directly or indirectly through there constructive criticism in the evolution and preparation of this work. It would not be fair on my part, if I don't say a word of thanks to all those whose sincere advice made this period a real educative, enlightening, pleasurable and memorable one.

I would like to express my deepest appreciation to my thesis supervisor, Head and Associate Professor **Dr. Naveen Kwatra** for their gracious efforts and keen pursuits, which has remained as a valuable asset for the successful instrument of my Thesis Report. His dynamism and diligent enthusiasm has been highly instrumental in keeping my spirit high. His flawless and forthright suggestions blended with an innate intelligent application have crowned my task a success.

I would also like to express my gratitude to my family, for their unconditional support and prayers at all times and constant encouragement during the entire course of my thesis work.

I am also like to offer my sincere thanks to all faculty, teaching and non-teaching of Civil Engineering (CED) TU, Patiala for their assistance. Thank you.

**PRIYA GOYAL**

M.E CIVIL STRUCTURES

ROLL NO 801122013

# ABSTRACT

To model the complex behavior of reinforced concrete analytically in its non-linear zone is difficult. This has led engineers in the past to rely heavily on empirical formulas which were derived from numerous experiments for the design of reinforced concrete structures.

The Finite Element method makes it possible to take into account non-linear response. The FE method is an analytical tool which is able to model RCC or retrofitted structure and is able to calculate the non-linear behavior of the structural members is Finite element method. For structural design and assessment of reinforced concrete members, the non-linear finite element (FE) analysis has become an important tool. The method can be used to study the behavior of reinforced and pre-stressed concrete structures including both force and stress redistribution.

The Finite Element method allows complex analyses of the nonlinear response of RC structures to be carried out in a routine fashion. FEM helps in the investigation of the behavior of the structure under different loading conditions, its load deflection behavior and the cracks pattern.

External wrapping with fiber-reinforced polymer (FRP) is a promising solution for retrofit of beam-column joints due advantages such as high strength-weight ratio, corrosion resistance, ease of application, low labour costs, and no significant increase in member size over other strengthening techniques. Also, recent research has attempted to simulate the behavior of reinforced concrete structures strengthened with FRP composites using the finite element method (FEM).

In the present study, the non-linear response of RC beam column joint under the incremental and cyclic loading and the stressed retrofitted (90% and 75%) RC beam column joint under the cyclic loading using FE Modelling has been carried out with the intention to investigate the relative importance of several factors in the non-linear finite element analysis of RC beam column joints. These include the variation in load displacement graph, the crack patterns, propagation of the cracks, the crack width and the effect of the non-linear behavior of concrete and steel on the response of control and stressed retrofitted beam column joint.

# TABLE OF CONTENTS

# LIST OF TABLES

# LIST OF FIGURES

# Chapter 1 INTRODUCTION

## 1.1GENERAL

Beam column joints are critical regions in multi-storey moment resisting reinforced concrete frames subject to inelastic response under severe seismic loading. Because seismic moments in columns and beams act in opposite directions across the joint, the beam–column joint is subjected to horizontal and vertical shear forces whose magnitude is often many times higher than those found in adjacent beams and columns. Since joints are also connecting elements of the load carrying columns, brittle failure such as shear or bond failure in the joints must be avoided. Therefore, in the design of the reinforced concrete beam–column joints against seismic load, it is desirable to limit joint strength degradation until the ductility capacity of the beam reaches the designed capacity.

The functional requirement of a joint, which is the zone of intersection of beams and columns, is to enable the adjoining members to develop and sustain their ultimate capacity. The demand on this finite size element is always severe especially under seismic loading. The joints should have adequate strength and stiffness to resist the internal forces induced by the framing members.

The RC beam column joints are the most vulnerable part and subjected to damage firstly. Recent earthquakes worldwide have illustrated the vulnerability of existing RC beam-column joints to seismic loading. Poorly detailed joints performed as “weak links” in RC frames. The commonly seen deficiencies of damaged beam-column joints may be characterized as

- Insufficient shear strength
- inadequate anchorage or bonding and
- insufficient flexural strength or ductility

The two major failure modes for the failure at joints are: (a) joint shear failure and (b) end anchorage failure as shown in Figure 1.1.

**(a)** **(b)**

**Figure 1.1 Major failure modes for a RC beam-column joint: (a) Joint shear failure; (b) Inadequate reinforcement anchorage [15]**

In the analysis of reinforced concrete moment resisting frames the joints are generally assumed as rigid. In Indian practice, the joint is usually neglected for specific design with attention being restricted to provision of sufficient anchorage for beam longitudinal reinforcement. This may be acceptable when the frame is not subjected to earthquake loads. There have been many catastrophic failures reported in the past earthquakes, in particular with Turkey and Taiwan earthquakes occurred in 1999 (Figure 1.2), which have been attributed to beam-column joints [15]. The poor design practice of beam column joints is compounded by the high demand imposed by the adjoining flexural members (beams and columns) in the event of mobilizing their inelastic capacities to dissipate seismic energy. Unsafe design and detailing within the joint region jeopardizes the entire structure, even if other structural members conform to the design requirements.

**Figure 1.2 Typical beam-column joint failures (1999 Turkey earthquake) [15]**

Reinforced Cement Concrete is one of the most important and widely used building materials being used in many types of engineering structures. The economy, the efficiency, the strength and the stiffness of reinforced concrete make it an attractive material for a wide range of structural applications

However, a vast majority of RC buildings worldwide consist of structures designed prior to the advent of modern seismic design codes. It has been identified that the deficiencies of joints are mainly caused by inadequate transverse reinforcement and insufficient anchorage capacity in the joint (**Liu, 2006**).

Figure 1.3(a) shows a few typical deficiencies found in the beam-column joints of old structures and Figure 1.3(b) shows the corresponding new ductile detailing recommended by new codes. To assure an increase of the shear strength after the cracking of the joint core by diagonal tension and sufficient rotational capacity, joint shear reinforcement is needed, this is therefore prescribed by the newer design codes (ACI 318-08; NZS 3101:1995; IS 13920-1993).

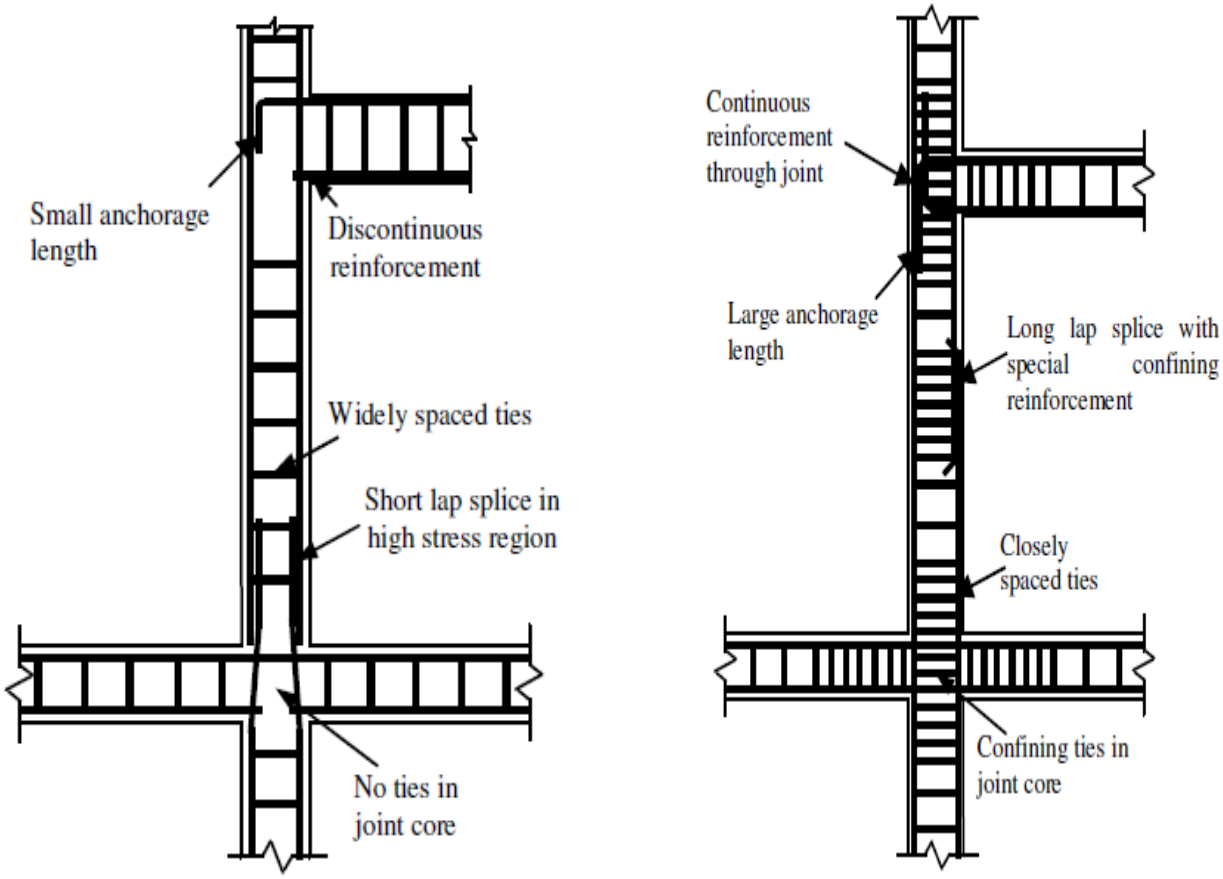


**Figure 1.3 (a) Typical non-ductile detailing prescribed by older codes; (b) Typical ductile detailing prescribed by newer codes [15]**

## 1.2 TYPES OF JOINTS

In a moment resisting frame, three types of joints can be identified viz. interior joint, exterior joint and corner joint as shown in Figure 1.4.

- When four beams frame into the vertical faces of a column, the joint is called as an interior joint.
- When one beam frames into a vertical face of the column and two other beams frame from perpendicular directions into the joint, then the joint is called as an exterior joint.
- When a beam each frames into two adjacent vertical faces of a column, then the joint is called as a corner joint. The severity of forces and demands on the performance of these joints calls for greater understanding of their seismic behaviour. These forces develop complex mechanisms involving bond and shear within the joint.

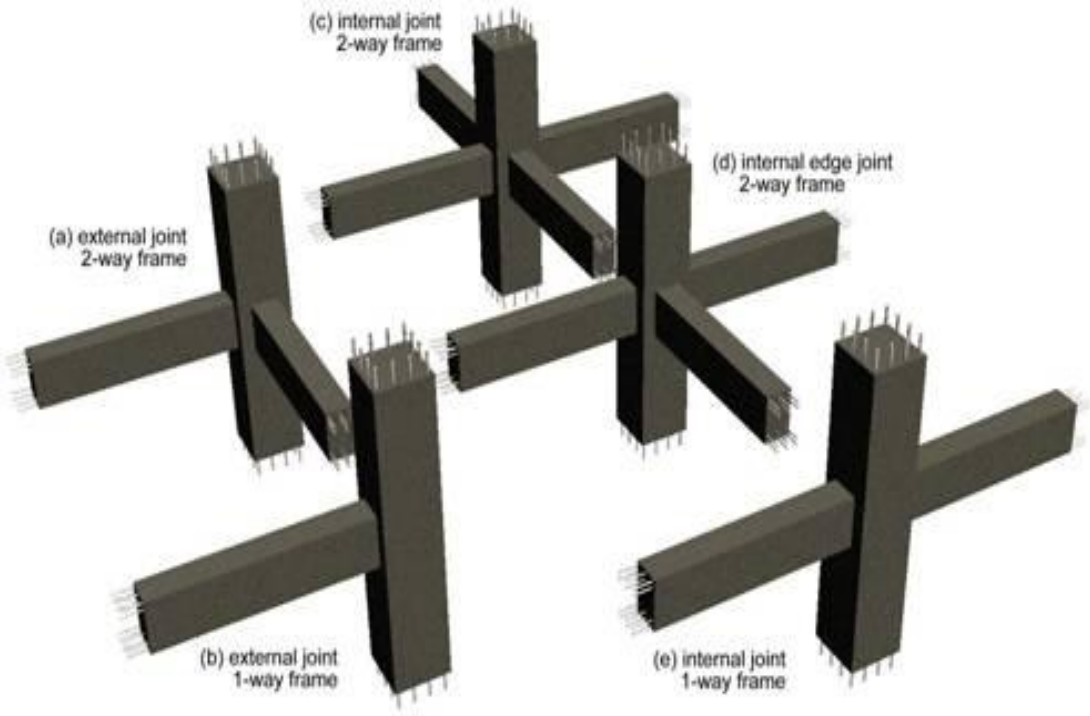


**Figure 1.4 Types of Joints in a frame (Megget, L.M. (2005)).**

## 1.3 FORCES ACTING ON A BEAM COLOUMN JOINT

The pattern of forces acting on a joint depends upon the configuration of the joint and the type of loads acting on it. The effects of loads on the three types of joints are discussed with reference to stresses and the associated crack patterns developed in them.

The forces on an interior joint subjected to gravity loading can be depicted as shown in Figure1.5.1 (a). The tension and compression from the beam ends and axial loads from the columns can be transmitted directly through the joint. In the case of lateral (or seismic) loading, the equilibrating forces from beams and columns, as shown in Figure 1.5.1(b) develop diagonal tensile and compressive stresses within the joint. Cracks develop perpendicular to the tension diagonal *A-B* in the joint and at the faces of the joint where the beams frame into the joint. The compression struts are shown by dashed lines and tension ties are shown by solid lines. Concrete being weak in tension,

transverse reinforcements are provided in such a way that they cross the plane of failure to resist the diagonal tensile forces [28].

The forces acting on an exterior joint can be idealized as shown in Figure 1.5.2. The shear force in the joint gives rise to diagonal cracks thus requiring reinforcement of the joint. The detailing patterns of longitudinal reinforcements significantly affect joint efficiency. Some of the detailing patterns for exterior joints are shown in Figure 1.5.2(b) and Figure 1.5.2(c). The bars bent away from the joint core as shown in Figure1.5.2 (b) result in efficiencies of 25-40 % while those passing through and anchored in the joint core show 85- 100% efficiency. However, the stirrups have to be provided to confine the concrete core within the joint [28].

The forces in a corner joint with a continuous column above the joint as shown in Figure 1.5.3 (c) can be understood in the same way as that in an exterior joint with respect to the considered direction of loading. Wall type corners form another category of joints wherein the applied moments tend to either close or open the corners. Such joints may also be referred as knee joints or L-joints. Opening corner joints tend to develop nascent cracks at the reentrant corner and failure is marked by the formation of a diagonal tensile crack.3.The detailing of the longitudinal reinforcement significantly influences the behavior of such joints. The forces developed in a closing joint are exactly opposite to those in an opening corner joint. The major crack is oriented along the corner diagonal. These joints show better efficiency than the opening joints. During seismic actions, the reversal of forces is likely and hence the corner joints have to be conservatively designed as opening joints with appropriate detailing. Failure of opening corner or knee joint is primarily due to the formation of diagonal tension crack across the joint with the outer part of the corner concrete separating from the rest of the specimen. Special and careful detailing is required to avoid failure of such joints so that the strength of adjacent members could be developed 4. The design and detailing schemes of these joints is beyond the scope of this paper and relevant information can be obtained elsewhere. The stress resultants from the framing members are transferred into the joint through bond forces along the longitudinal reinforcement bars passing through the joint and through flexural compression forces acting on the joint face. The joints should have enough strength to resist the induced stresses and sufficient stiffness to control undue deformations. Large deformations of joints result in significant increase in the storey displacement [28].

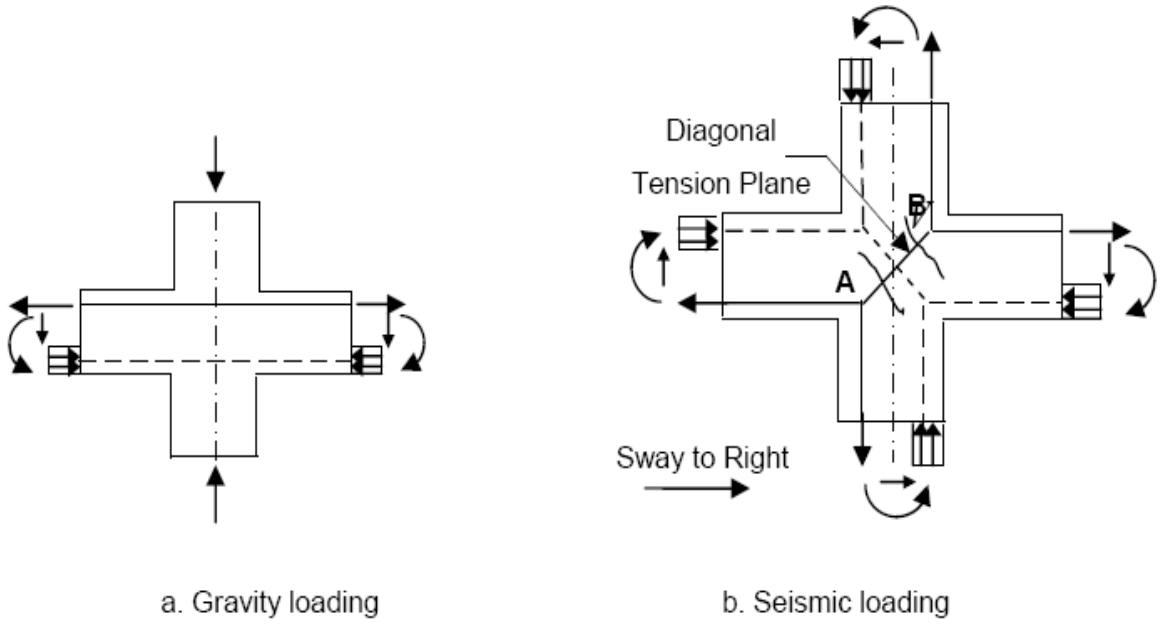


**Figure 1.5.1 Interior joint**

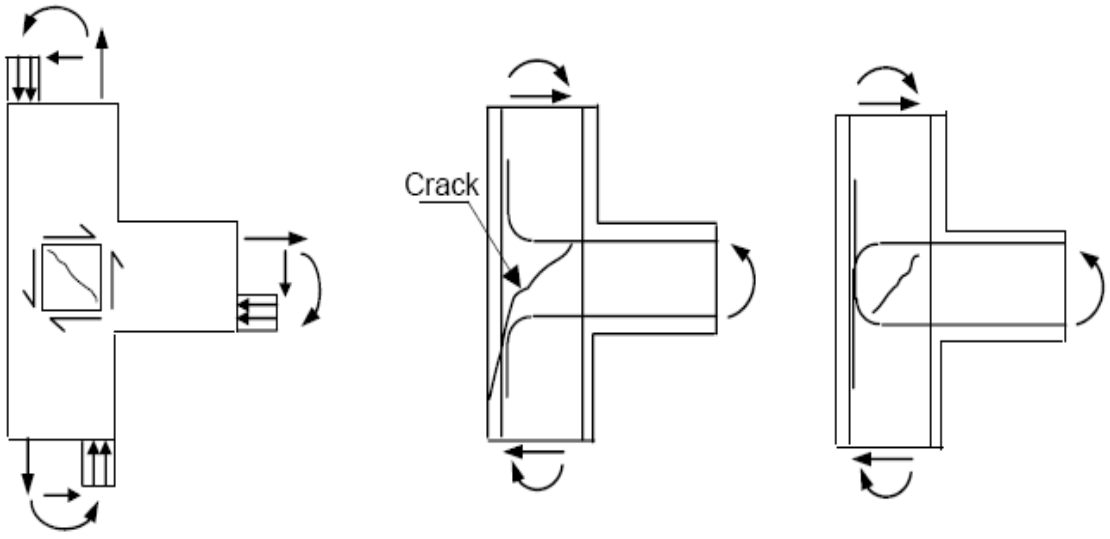


**Figure 1.5.2 Exterior Joint**

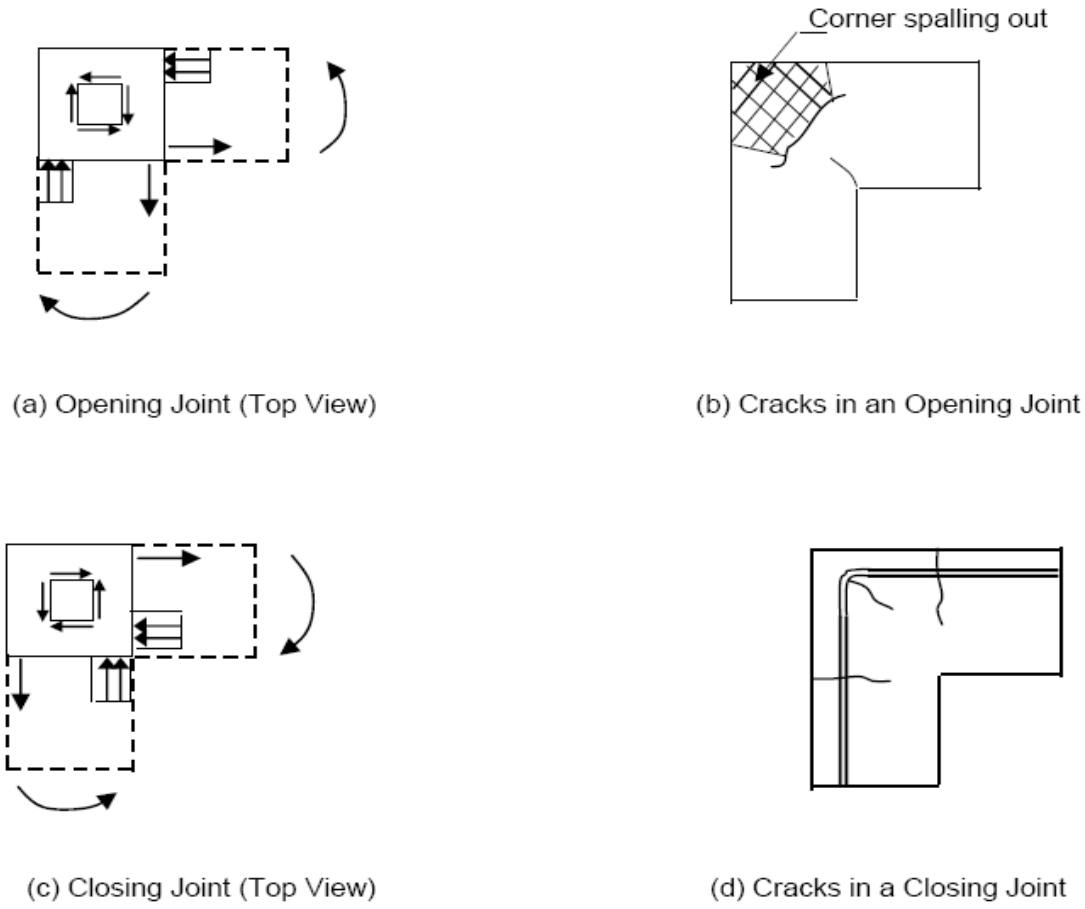


**Figure 1.5.3 Corner joints**

**Figure 1.5: Behavior of joints [28]**

## 1.4 EARTHQUAKE BEHAVIOR OF JOINTS

Under earthquake shaking, the beams adjoining a joint are subjected to moments in the same (clockwise or counterclockwise) direction as shown in Figure 1.6. Under these moments, the top bars in the beam-column joint are pulled in one direction and the bottom ones in the opposite direction as shown in Figure 1.7(a). These forces are balanced by bond stress developed between concrete and steel in the joint region. If the column is not wide enough or if the strength of concrete in the joint is low, there is insufficient grip of concrete on the steel bars. In such circumstances, the bar slips inside the joint region, and beams loose their capacity to carry load [27].

Further, under the action of the above pull-push forces at top and bottom ends, joints undergo geometric distortion; one diagonal length of the joint elongates and the other compresses as shown

in Figure 1.7(b). If the column cross-sectional size is insufficient, the concrete in the joint develops diagonal cracks.

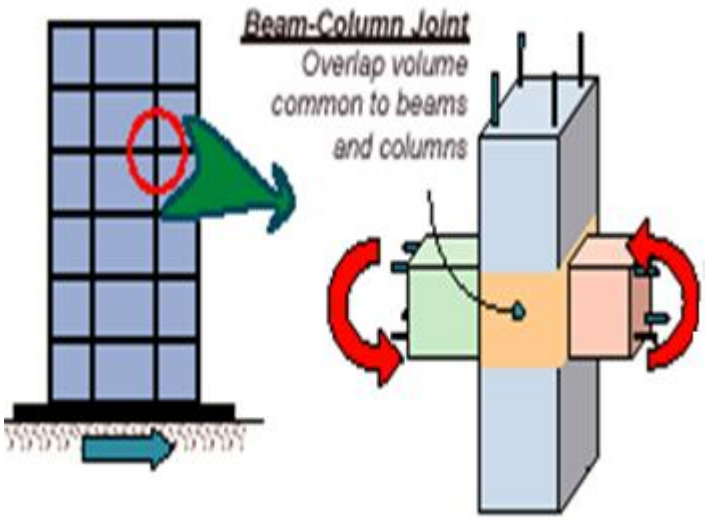


**Figure 1.6 Beam-Column Joints are critical parts of a building [27].**

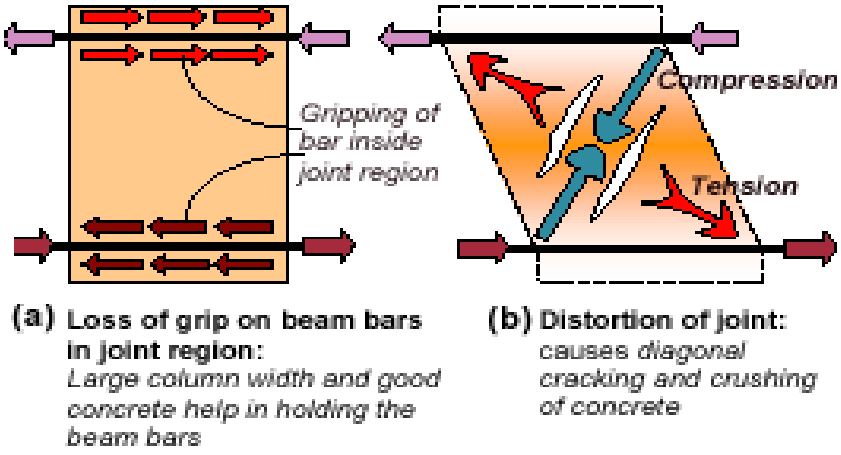


**Figure 1.7 Pull-push forces on joints cause two problems – these result in irreparable damage in joints under strong seismic shaking [27]**

Gupta and Agarwal (2012), examined the behavior of exterior RC Beam Column Joint strengthened with FRP under cyclic load. In this experiment, both confined and unconfined external RC beam column joint under cyclic excitation were tested and the same specimen after the test were retrofitted with FRP sheets in the damage area to restore their strength. Four RC T-joints were constructed with different detailing; two were unconfined (according to IS: 456-2000) and the other two confined (according to IS: 13920-1993). The cyclic load has been applied using Quasi-static testing technique. In the present study, the analytical results obtained from FE Modeling of RC beam column joint and the stressed retrofitted RC beam column joint (90%and75%) using finite element software package under cyclic loading are compared with the available experimental results.

### 1.5 IMPORTANCE OF FINITE ELEMENT MODELLING

To model the complex behaviour of reinforced concrete analytically in its non-linear zone is difficult. This has led engineers in the past to rely heavily on empirical formulas which were derived from numerous experiments for the design of reinforced concrete structures.

The Finite Element method makes it possible to take into account non-linear response. The FE method is an analytical tool which is able to model RCC or retrofitted structure and is able to calculate the non-linear behavior of the structural members is Finite element method. For structural design and assessment of reinforced concrete members, the non-linear finite element (FE) analysis has become an important tool. The method can be used to study the behaviour of reinforced and pre-stressed concrete structures including both force and stress redistribution [5].

With the advent of digital computers and powerful methods of analysis, such as the finite element method many efforts to develop analytical solutions which would obviate the need for experiments have been undertaken by investigators. The finite element method has thus become a powerful computational tool, which allows complex analyses of the nonlinear response of RC structures to be carried out in a simple way.

FEM is useful for obtaining the load deflection behaviour and its crack patterns in various loading conditions.

## 1.6 OBJECTIVES

In the present study, the non-linear response of RC beam column joint and the retrofitted RC beam column joint using FE Modelling under the incremental loading and cyclic has been carried out with the intention to investigate the relative importance of several factors in the non-linear finite element analysis of RC beam column joint. These include the variation in load displacement graph, the crack patterns, propagation of the cracks, the crack width and the effect of size of the finite element mesh on the analytical results and the effect of the non-linear behaviour of concrete and steel on the response of control frame and deformed frame.

The main objectives of the present study are:

1. To study the response and load-carrying capacity of beam column joint using non-linear finite element analysis.
2. To model the beam column joint in first phase of study and model the same with FRP wrapping in second phase using finite element method.
3. To compare the results of the control frame and the damaged retrofitted (90% and 75% stressed) beam column joint with the available experimental results from study done by Gupta and Agarwal, (2012) using finite element package "ATENA".

## 1.7 SCOPE OF THE WORK

The present work aims to study analytically the performance of beam column joint under cyclic loading. In the first phase of the present study of FE modelling of the control RC beam column joint under the incremental and cyclic loads has been analyzed using ATENA software and the results so obtained have been compared with available experimental results from Gupta and Agarwal, (2012).
The control RC beam column joint is analyzed using ATENA software up to the failure and the load deformation curves are plotted and the cracking behaviour is monitored. The control RC beam column joint has been analyzed and results have been compared with the experimental results.
In the second phase of the study, FE modelling the stressed/damaged retrofitted RC beam column joint is analyzed. The frame retrofitted by using GFRP is modelled and analyzed. The results obtained from the analysis of FF model have been plotted. Comparisons are made by the load deflection curves and values. Deflection and cracking behaviour of the RC beam column joint are also studied.

The following parameters are proposed to be measured:

i) Nonlinear load-deflection behaviour.

ii) Study of crack patterns at different load steps.

iii) Level/type of damage and location of damage.

The effect on the above parameters due to use of the retrofitting materials like FRP for strengthening of the joint (subjected to damage) is also studied.

## 1.8 ORGANISATION OF THE THESIS

The thesis is organized as par detail given below:

**Chapter 1**: Introduces to the topic of thesis in brief.

**Chapter 2**: Discusses the literature review i.e. the work done by various researchers in the field of performance of beam column joint and retrofitted beam column joint under cyclic loading. Past research on use of finite element modeling for concrete structures is also taken.

**Chapter3**: Deals with the details of beam column joint modelled in ATENA in its first part. Second part comprises of FEM modelling, theory related to the ATENA, material modelling and analytical programming procedure steps involved in modelling of the control RC beam column joint. It also deals with the description of the material behaviour of concrete, reinforced steel bars.

**Chapter4:** The results from the analysis, comparison between the analytical and the experimental results, results comparison between the control unconfined beam column joint and control confined beam column joint and the cracking behaviour of it, all are discussed in.

**Chapter5**: The results from the analysis for 90% and 75% stressed retrofitted, comparison of results b/w FE analysis and experimental results of beam column joint are discussed in this chapter.

**Chapter6:** Finally, salient conclusions and recommendations of the present study are given in this chapter followed by the references.

# CHAPTER 2 LITERATURE REVIEW

## 2.1 GENERAL

It would be difficult to present the detailed review of the literature related to FE modeling and retrofitted reinforced cement concrete structures so a brief review of previous studies on the application of the finite element method and experimental analysis of reinforced concrete beam column joint and retrofitted structures is presented in this chapter.

Earthquakes are the major nemesis of all the buildings. While analyzing and assessing the damage caused by earthquake it was inferred that building should not collapse total i.e. after a devasting earthquake it should not suffer such irreparable damage which would require demolishing and rebuilding and in case it sustain such damage it could be repaired quickly and easily to bring it to its usual functioning.[ISET 1981]

Significant research has been carried out in the last two decades to improve the seismic performance of reinforced concrete beam-column joints. This has resulted in the use of materials such as fiber-reinforced polymer (FRP). These materials provide continuous confinement of the joint area thereby enhancing yield load, initial stiffness and energy dissipation capacity considerably. In recent years, the use of finite element analysis to analyze concrete structural components has also increased. The finite element analysis provides a powerful tool to investigate the complex behavior of beam-column joints in addition to being much faster, and extremely cost-effective as compared to the experimental based testing.

## 2.2 FINITE ELEMENT MODELLING AND THE STRENGTHENING OF RC MEMBERS

**Hegger Josef, et al., (2004)** investigated the behavior of exterior and interior beam-column joints by nonlinear finite element analysis using ATENA, software for nonlinear analysis of reinforced concrete structures. The model has been calibrated using the results of the third author's tests. The behavior of exterior and interior beam-column turned out to be different .The parameters influencing the shear strength are not the same for both types of connections. Different parameters like effect of the material properties, effect of geometry of connection, effect of reinforcement,

effect of concrete compressive strength and joint slenderness. The parameters influencing the shear capacity are different for exterior and interior connections. The FE results were compared with the author's experimental results and the good agreement between the two was achieved [17].

**Mukherjee and Joshi, (2005)** examined the performance of fiber reinforced polymer composites (FRP) in up gradation of healthy beam-column joints with adequate and deficient reinforcements and also in rehabilitation of damaged joints. One set of joints had adequate steel reinforcements with proper detailing of reinforcements at the critical sections called "Ductile specimens". The other set of specimens had deficient bond lengths of the beam reinforcements at the junctions with the columns and were called "Non-Ductile specimens". The specimens were also strengthened by using carbon and glass FRP materials. The control specimens without FRP were used after testing to evaluate the rehabilitation of joints with FRP called "Rehabbed specimens". It was observed that for ductile specimens the load at yield was considerably higher in the FRP reinforced specimens than the control specimen. For the same tip load, the tensile force in steel was lower in the carbon reinforced specimen than in the glass reinforced specimens. Thus, the steel in the carbon reinforced specimens yielded at higher tip loads. The displacement at yield increased to a much lesser extent than the load due to FRP reinforcements. The load-displacement envelopes showed that all the FRP reinforced specimens had higher peak loads than the control specimen Stiffness degradation plots showed that all the FRP reinforced specimens had a total loss of stiffness at a higher displacement level than the control specimen. The carbon specimens had higher initial stiffness and slower rate of degradation. The cumulative energy dissipation graphs showed that the energy dissipation of the FRP reinforced specimens followed closely that of the control specimen because FRPs remain elastic until failure and not much dissipation of energy was expected through the deformation of the FRP. However, the FRPs had increased the ultimate deformation of the structure to a large extent. The photographs of the failed specimens showed that the confinement provided by the FRP reinforced joints impeded the creation of hinge through the spalling of concrete. The load versus displacement envelops for the rehabbed specimens showed that the use of composite system not only restored the original capacity of damaged specimen, but also upgraded the ultimate load capacity by 55%. Also displacement at ultimate load was increased by 30%. Stiffness versus displacement curve showed that there was 48% increase in initial stiffness. An increment of 57% was observed in energy dissipation capacity of structure after the rehabilitation [22].

**Gencoglu M., et al., (2007)** conducted an experiment on strengthening of the deficient RC exterior Beam-Column Joints using CFRP for Seismic Excitation. In order to strengthen the deficient external beam-column joints, CFRP fabrics were laid out on the tension face of column and beam and then both column and beam were wrapped fabric. The test results of the strengthened beam-column joints were compared with the test results of both RC exterior beam-column joint built in accordance with the requirements of ACI 318-02 and RC exterior beam-column joint disregarded the transverse requirements at ACI 318-02 in terms of load carrying capacity, total energy amounts, and ductility. Examination of the specimens after testing indicated that the strengthening method shifted the localization hinge of the specimen to the beam and the mode of failure of beam-column joints could be directly affected. CFRP sheets mounted onto the concrete surfaces of beam and column by using epoxy resins increase the load carrying capacity, the ultimate beam tip displacements, the absorbed total energy amounts and the RC exterior beam-column joint strengthened by two layers L CFRP sheets has the highest reversed cyclic load carrying capacity and the total absorbed energy amounts among other beam-column joint specimens [9].

**Ganesan .N et al., (2007)** analyzed ten steel fibre reinforced high performance concrete (SFRHPC) exterior beam-column joints under cyclic loading. The M60 grade concrete used was designed by using a modified ACI method suggested by Aïtcin. Volume fraction of the fibres used in this study varied from 0 to 1% with an increment of 0.25%. Joints were tested under positive cyclic loading, and the results were evaluated with respect to strength, ductility and stiffness degradation. The SFRHPC joints undergo large displacements without developing wider cracks when compared to the HPC joint indicating that steel fibres impart high ductility to the SFRHPC joints, which is one of the essential properties for the beam-column joints. Addition of fibres to the beam-column joints decreased the rate of stiffness degradation appreciably when compared to the joints without fibres. Load carrying capacity of the joints also increased with the increasing fibre content [8].

**Mahini S.S. et al., (2008)** studied the capability of nonlinear quasi-static finite element modeling in simulating the hysteretic behavior of CFRP-retrofitted RC exterior beam-column joints under cyclic loads using finite element method adopted by ANSYS. The finite element models are developed using a modified Hognestead model for concrete and anisotropic multi-linear model for modeling

the stress-strain relations in reinforcing bars while anisotropic plasticity is considered for the FRP composite. Both concrete and FRP are modeled using solid elements whereas space link elements are used for steel bars. The results obtained from the ANSYS finite element analysis are compared with the experimental data for 2 RC beam column connections before and after retrofitting by researchers. In this analysis procedure, an automatically reforming stiffness matrix strategy was used in order to simulate the actual seismic performance of the RC concrete after cracking, steel yielding and concrete crashing during the push and pull loading cycles. The comparisons were made for load-deflection curves at mid-span; and failure load. The results from finite element analysis were calculated at the same location as the experimental test of the beams. The accuracy of the finite element models is assessed by comparison with the experimental results, which are to be in good agreement. The load-deflection curves from the finite element analysis agree well with the experimental results in the linear range till peak load, as concrete's strain softening cannot be modeled by ANSYS [21].

**Pannirselvam N. et al., (2008)** presented the experimental work for Strength Modeling of Reinforced Concrete Beam with Externally Bonded Fibre Reinforcement Polymer. In this study, three different steel ratios are used with two different Glass Fibre Reinforced Polymer (GFRP) types and two different thicknesses in each type of GFRP were used. 15 beams were casted for this work in which 3 were used as a control beam and the remaining were fixed with the GFRP laminate on the soffit. Flexural test, using simple beam with two-point loading was adopted to study the performance of FRP plated beams in terms of flexural strength, deflection, ductility and was compared with the un-plated beams. The results obtained from this experiment showed that the beams strengthened with GFRP laminates exhibit better performance. The flexural strength and ductility increase with increase in thickness of GFRP plate. The increase in first crack loads was up to 88.89% for 3 mm thick Woven Roving's GFRP plates and 100.00% for 5 mm WRGFRP plated beams and increase in ductility in terms of energy and deflection was found to be 56.01 and 64.69% respectively with 5 mm thick GFRP plated beam. Strength models were developed for predicting the flexural strength (ultimate load, service load) and ductility of FRP beams [23].

**Hasballa M., et al., (2009)** studied the feasibility of using the GFRP bars as a longitudinal and transverse reinforcement for reinforced concrete frames subjected to high seismic loads. This paper focuses on the test results and analysis of two test prototypes. One prototype is totally reinforced with glass FRP bars and stirrups, while the other one is reinforced with steel. The experimental results showed that the joint drift capacity can reach more than 3.0% safely without any considerable damage; also GFRP bars were capable of resisting tension-compression cycles with no strength degradation. GFRP-reinforced joints satisfied both strength and ductility (deformability) requirements of earthquake-resistant structures. Steel reinforced specimen exhibited the basic joint-shear mode of failure, which resulted in degradation of the concrete strength inside the joint. On the other hand, GFRP reinforced specimen exhibited a flexural slippage failure due to the insufficient development length for the GFRP longitudinal reinforcement of the beam [11].

**Robert .R.S and Prince .A.G., (2010)** presented the experimental work on Behavior of Reinforced Concrete Beam Column Joints Retrofitted with GFRP-AFRP Hybrid Wrapping. Under this work, three exterior reinforced concrete beam-column joint control specimens (The columns had a cross section of 200 mm x 200 mm with an overall length of 1500 mm and the beams had a cross section of 200 mm x 200 mm with a cantilevered portion of length 600 mm) were tested to failure. Two specimens had reinforcement details as per code IS 456:2000. The other specimen had reinforcement details as per code IS 13920:1993. An axial load was applied on the column. Push and pull load was applied at the free end of the cantilever beam till failure. The failed two beam-column joint specimens designed as per code IS 456:2000 were retrofitted with GFRP-AFRP/AFRP-GFRP hybrid fiber sheets wrapping to strengthen the specimens. The performance of the retrofitted beam-column joints was compared with the control beam-column joint specimens. The load carrying capacity and energy absorption capacity of the reinforced concrete beam-column joint specimens designed and detailed as per code IS 13920:1993 was 10% -11% and10 % -13.8% more than the specimens detailed as per code IS 456:2000 respectively. The load carrying capacity and energy absorption capacity of specimen retrofitted with GFRP-AFRP hybrid sheet was 18.3 % and 26.6 % more than the control specimens respectively. The load carrying capacity and energy absorption capacity of specimen retrofitted with AFRP-GFRP hybrid sheet was 23.8 % and 33.2 % more than the control specimens respectively. In control specimen the failure was in the column portion of the joint but in the case of the wrapped specimens, the failure was in the beam portion

only and the column was intact and therefore preventing progressive collapse of the structure under seismic loads [27].

**Perumal.P and Thanukumari.B., (2010)** examined the effect of cocktail fibre reinforced concrete (1.5% of steel fibre and 0 to 0.6% polypropylene fibre) to increase the Seismic Performance of Beam-Column Joints using $M_{20}$ concrete. Six one fourth scale (to suit the loading and testing facilities) specimens were designed as per IS 456:2000 and one designed as per IS 1893 (Part 1): 2002 and detailed as per IS 13920-1993**.** The five specimens were similar to the first one but various combinations of cocktail fibre concrete in the joint region. Out of five fibre specimens four specimens were cast by using (constant 1.5% of steel fibre and 0 to 0.6% polypropylene fibres). The fifth fibre specimen was cast by using 1.5 % of polypropylene fibre only. The properties of ultimate strength, ductility, energy dissipation capacity and joint stiffness were compared. The increase in polypropylene fibre decreased the ultimate load carrying capacity. The energy absorption capacity increased by 87% by adding only steel fibre and 205% by adding cocktail with combination of 1.5% steel fibre and 0.2% polypropylene fibre. The specimen with 1.5% of steel fibre and 0.6% polypropylene fibre had the maximum ductility factor. The excess polypropylene fibre increases the ductility. In this paper it was observed that specimen consisting of 1.5% of steel fibre and 0.2% of polypropylene fibre have best performance considering the energy dissipation capacity and ductility factor but the ultimate load carrying capacity is reduced by adding polypropylene fibre. The addition of fibre cocktail to concrete prevents the brittle failure of the joint. The addition of polypropylene fibre increases the energy dissipation capacity when the dosage of polypropylene fibre is 0.2%. Further increase in polypropylene fibre was found to reduce the strength of the joint and also energy dissipating capacity. The rate of degradation of stiffness decreases in the case of specimens additionally reinforced with fibres [25].

**Rajaram.P et al., [2010],** studied analytically the structural behavior of interior RC beam column joint using standard software packages STAAD Pro and ANSYS. A two bay five storey reinforcement cement concrete moment resisting frame for a general building has been analysed and designed in STAAD Pro as per IS 1893:2002 code procedures and detailed as IS 13920:1993 recommendations. A beam column joint has been modeled to a scale of 1/5 th from the prototype and the model has been subjected to cyclic loading to find its behavior during earthquake.

Experimental results were compared with FEM model analysis in ANSYS, the behavior of the interior beam column joint are similar. Maximum stresses are occurred at the junction for the ultimate loading at the beam tip. The maximum stresses are developed in the FEM model at junction. The tensile stress at top exceeds the maximum tensile stress and compressive stress occurred at bottom in the forward cyclic loading. With the increase in the load there is degradation of stiffness. The relative energy absorbed during loading cycles increased with the increase in number of cycles [26].

**Choudhury .A.M., (2011)** investigated on ductility emphasizing size effect for plain and Retrofitted Beam-Column joint under cyclic loading. In this study, a typical full scale residential building with floor to floor height as 3.3 meters and the beam of 3.0 meters effective span was considered. Four types of specimens, namely, Beam-column joint with beam weak in shear: control, Beam-column joint with column weak in shear: control, Beam-column joint with beam weak in shear: retrofitted and Beam-column joint with column weak in shear : retrofitted were considered. In each type, three geometrically similar specimens of full scaled, two third scaled and one third scaled sizes were tested. Thus, total twelve specimens covering two different types and three different scales were tested under cyclic loading. Cyclic displacement was applied to all the specimens with the help of hydraulic dynamic actuators. Displacement controlled load with a frequency of 0.025Hz was applied to the test specimens. Amplitude of the displacement histories were scaled down for two-third and one-third models. The ultimate load carrying capacity due to retrofitting increased up to 12.18% for beam weak in shear large specimen. The ultimate load carrying capacity for all the specimens increased due to retrofitting and it was similar for column weak in shear specimens. Also the displacement ductility for all the specimens increased due to retrofitting and it was similar for column weak in shear specimens also. In this paper it was observed that displacement ductility and ultimate load carrying capacity due to retrofitting increases as the specimen size decreases. Large specimen has the least value and small specimen has the largest value. Both displacement ductility and ultimate load carrying capacity followed the principle of size effect for both control and retrofitted specimens [6].

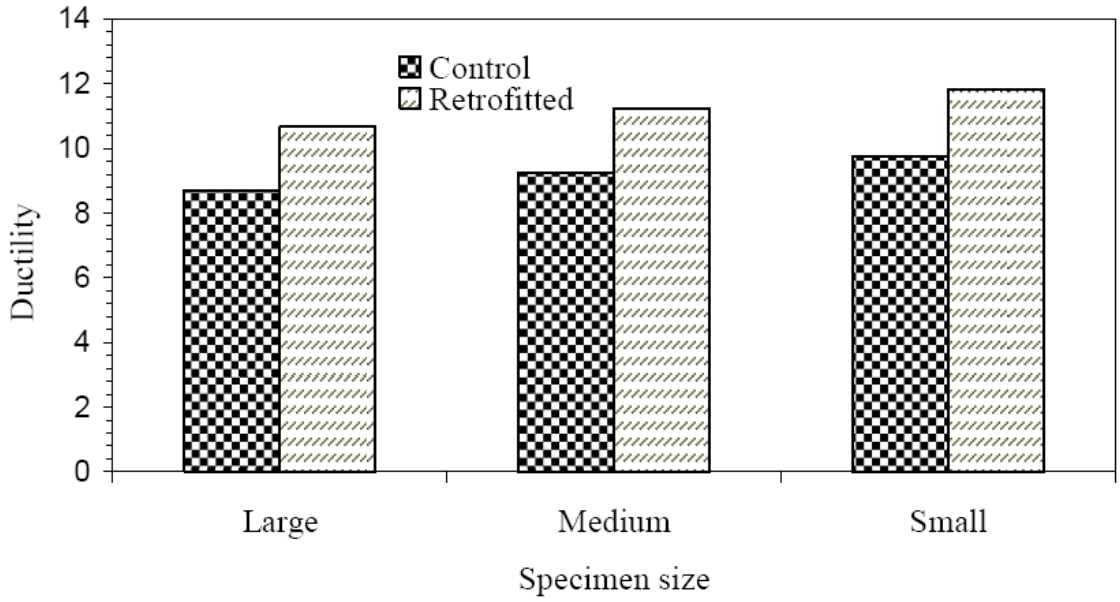


**Figure 2.1 Displacement Ductility of beam weak in shear control and retrofitted specimens**

**Xilin lu. et al., (2011)** presented the philosophy involving the use of additional diagonal bars within the joint under cyclic loading. In this paper, ten full-scale interior beam-column specimens were constructed with various additional reinforcement details. The specimens with additional bars compared with the ones without them showed fewer cracks in the column. With the increase of the ratio of bending moment of column to beam, the plastic hinges are more likely to develop in the beam, and the ductility of the joint improves. Additional diagonal bars, prevented cracks at the edges of joint interface between column and beam. Furthermore, these joints have been proven to behave in a ductile manner as beams undergo plastic hinging earlier than the columns. The specimens with additional bars effectively increase the strength capacity at the joint vicinity as well as sufficient development of ductility to the frame members under increasing lateral loading. The mechanism developed in these specimens showed sufficient evidence to suit strong-column weak-beam concept. The orientation of additional diagonal bars added strength in favor of members they were oriented to. That is, additional bars along beam added strength towards the beam ends and additional bars along column added strength towards the column [20].

**Gupta and Agarwal, (2012)** presented the experimental work for evaluation of Exterior RC Beam Column Joint strengthened with FRP under cyclic load. Four RC T-joints with different detailing; two unconfined (according to IS: 456-2000) and the other two confined (according to IS: 13920-

1993) were tested. Materials used were M-20 concrete and Fe-415 steel. Length of the beam = 3000 mm, Height of the column = 1500 mm, Cross section of the beam = 275 * 275 mm, and Cross section of the column = 300 * 300 mm. GFRP wrapping is used for retrofitting of damaged joints with epoxy resin. Cyclic load has been applied using Quasi-static testing technique. In this technique, testing is conducted at a sufficiently slow rate such that strain-rate effects are insignificant. Both ends of the column are fixed. Horizontal load was applied at the top of the specimen at a height of 1300 mm from footing by servo-controlled hydraulic actuator. In this study, comparison of strength and ductility of undamaged and retrofitted specimen has been done. Also the behavior of confined specimen is compared with the unconfined one. Unconfined specimen experienced the first flexural crack at the middle of the beam during the third cycle and the number of cracks increased as the load was increased up to 53.7 kN. Cracks were also developed on the joints. Confined specimen experienced lesser number of cracks as compared to the unconfined model but the behavior of all the four models was almost same, with initial flexural cracks in the beam and then shear cracks in the joints and then failure and spalling of joint and nearby region. In unconfined model the maximum load attained was 53.7 kN at 20 mm displacement. The unconfined model was repaired and retrofitted with GFRP wrapping in critical damaged region around joint, it restrained the strength upto 68 % and the maximum load attained was 36.4 kN at 20.5 mm displacement. In confined model the maximum load attained was 61.7 kN at 25 mm displacement. After retrofitting the confined model with GFRP wrapping the strength upto 85 % was restored with maximum strength as 52.2 kN with 35mm displacement. The effect of wrapping was seen in holding the strength of the model after its damage. After attaining its maximum load the fibers hold the strength of the specimen for some time. It was observed that GFRP wrapping retrofitting of RC beam column joint was effective with restoring its lateral load carrying capacity up to a significant amount and increasing its ductility. The GFRP wrapping acts as an anchor sheet at the time of earthquake as it does not allow the concrete to spall from the joints [10].

**Choudhury .A.M. et al., (2012)** examined on energy dissipation with emphasize on size effect for plain and Retrofitted Beam-Column joint under cyclic loading. In this study, a typical full scale residential building with floor to floor height as 3.3 meters and the beam of 3.0 meters effective span was considered. Two categories of specimens, viz. beam-column joint with beam weak in shear and beam-column joint with column weak in shear along with their corresponding retrofitted

specimens were considered. In each type, three geometrically similar specimens of full scaled, two third scaled and one third scaled sizes were tested. Thus, total twelve specimens covering two different types and three different scales were tested under cyclic loading. Cyclic displacement was applied to all the specimens with the help of hydraulic dynamic actuators. Displacement controlled load with a frequency of 0.025Hz was applied to the test specimens. Amplitude of the displacement histories were scaled down for two-third and one-third models. The load carrying capacity of the retrofitted specimen increased in comparison to control specimen. The ultimate load carrying capacity for all the specimens increased due to retrofitting and it was similar for column weak in shear specimens. Also the gain in energy dissipation due to retrofitting was 33.08% at failure stage for beam weak in shear large specimen. The gain in energy dissipation due to retrofitting was 85.7% at failure stage for beam weak in shear medium specimen and the same is 97.7% for small specimen. Energy dissipation for all the specimens increased due to retrofitting and it was similar for column weak in shear specimens also. In this paper it was observed that energy dissipation and ultimate load carrying capacity due to retrofitting increases as the specimen size decreases. Both energy dissipation and ultimate load carrying capacity followed the principle of size effect for both control and retrofitted specimens. Energy dissipation per unit volume also increased as the specimen size decreased [7].

**Patil S.S et al., (2013)** examined analytically the R. C. C. Beam Column Junction subjected to Quasi-Static (Monotonic) loading by nonlinear finite element analysis using ANSYS software for nonlinear analysis of reinforced concrete structures. The exterior beam-column joint is modelled and a monotonic loading of is applied at the tip of the beam till the failure of the beam had takes place. Model construction was done by defining geometrical joints and lines. The joint was fully restrained at the column ends. It was inferred from the paper that as load increases displacement, minimum stress and maximum stress also increases. Also because stiffness of the structure changes the displacement, minimum stress and maximum stress changes w. r t .loading [24].

## 2.3 GAPS IN RESEARCH AREA

Many experimental and analytical works has been done by many researchers in the area of strengthening and retrofitting the structural members with composite materials. The concept of retrofitting the structural members is rapidly growing due to enable the early identification of

damage and provides warning for unsafe condition. Some researchers have also investigated or work on the area of the failure mode of the FRP strengthened structural members and some are work on the strengthening of the structural members with different FRP materials.

This research is concerned with the finite element modelling of the retrofitted the RC beam using the GFRP. The use of GFRP sheets for retrofitting and the strengthening of the reinforced concrete structural have been studied extensively in previous studies. However, many researchers performed experimentally and analytically the strengthening of the beams but limited work is done on the study of RC beam column joints and in the field of stressed/damaged retrofitted structural members.

## 2.4 CLOSURE

The literature review has suggested that use of a finite element modelling of the RC beam column joint and retrofitted RCC frame is indeed feasible. So it has been decided to use ATENA for the FE modelling. With the help of this software study of RC beam column joint has been done. ATENA also helps in FE modelling and meshing inside the surface of element. It gives the load deflection curve and gives the values of stresses and strains, crack width of the elements of the joint at every step. A reinforced concrete beam column joint with reinforcing steel modelled discretely will be developed with results compared to the experimental work done by Gupta and Agarwal (2012). The load- deflection curve of the experimental work will be compared to analytical predictions to calibrate the FE model for further use.

# Chapter 3 FE MODELLING OF RC BEAM COLUMN JOINT

## 3.1 GENERAL

Modelling of beam-column joint presented in this chapter refers to the joint detail, material properties and loading conditions as taken in the experimental study conducted by **GUPTA AND AGGARWAL, (2012)**. The control specimen both confined and unconfined under monotonic and cyclic excitation was taken and analyzed by finite element method (FEM) using the commercial available software **ATENA**. Then, the same specimens were retrofitted with fiber reinforced polymer (FRP) and analyzed using the same software. The damaged retrofitted beam column joint (stressed to 90% and 75%) is also analyzed.

This chapter also discusses the theory related to ATENA and information about finite elements currently implemented in ATENA in its second part. All the necessary steps to create these models are explained in detail and the steps taken to generate the analytical load-deformation response of the model are discussed.

## 3.2 GENERAL DESCRIPTION OF STRUCTURE

In the experimental program conducted by GUPTA AND AGGARWAL, (2012), behavior of confined and unconfined external RC beam-column joint (T-joint) under cyclic excitation is studied. Same specimens after the tests were retrofitted with FRP sheets in the damage area to restore their strength. Four RC T-joints were constructed with different detailing; two were unconfined (according to IS: 456-2000) and the other two confined (according to IS: 13920-1993). The cyclic load has been applied using Quasi-static testing technique. GFRP wrapping is used for retrofitting of damaged joints with epoxy resin.

### 3.2.1 Material properties

The material used for construction is Reinforced concrete with M-20 grade concrete and fe-415 grade reinforcing steel. The RC T-joints were constructed with different detailing

Unconfined (according to IS:456-2000)

Confined (according to IS:13920-1993).

### 3.2.2 Model Geometry

Length of the beam = 3000mm

Height of the column = 1500mm

Cross section of the beam = 275*275mm

Cross section of the column = 300*300mm

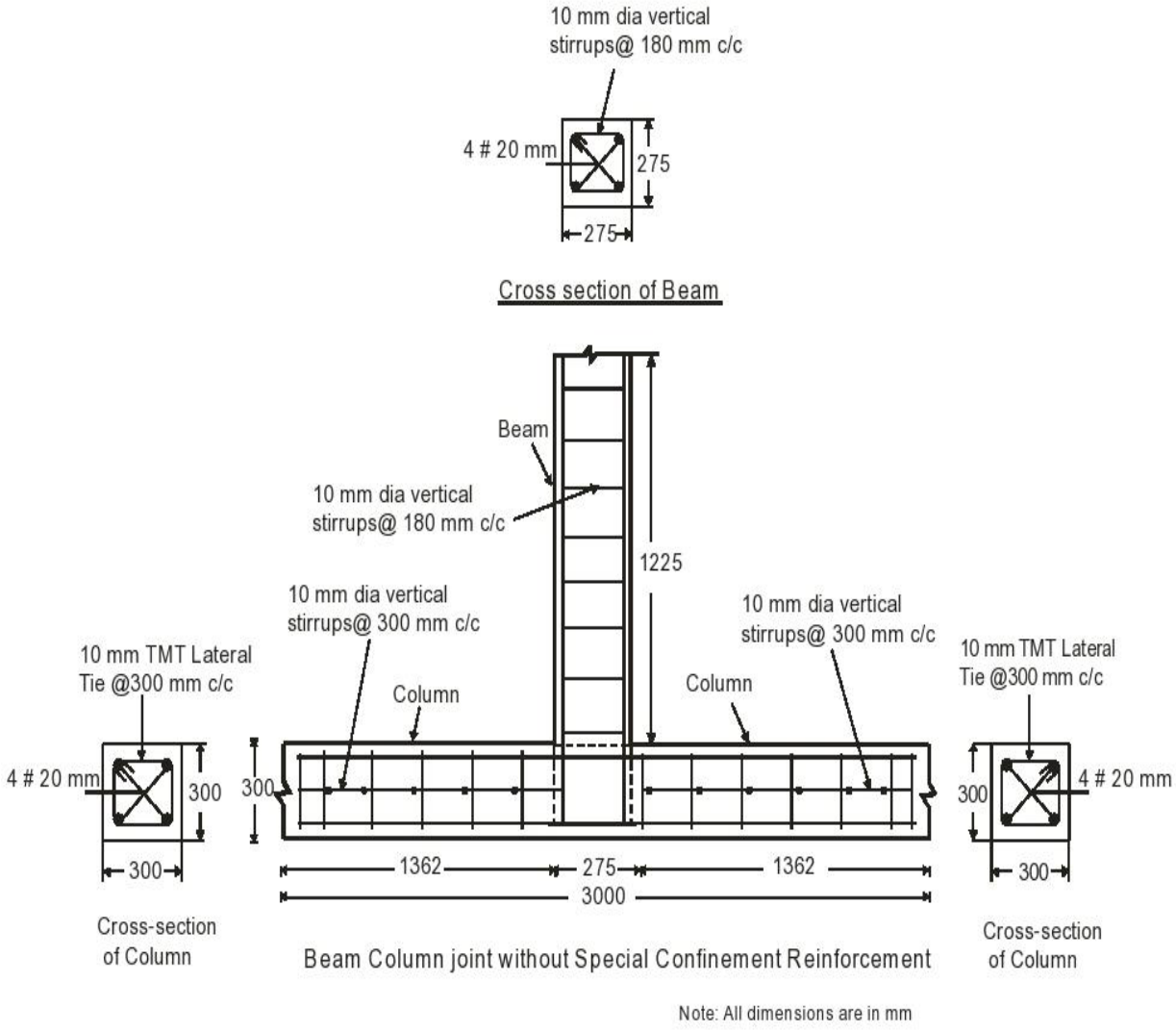


**Figure 3.1 Reinforcement detailing and cross section details of unconfined specimen[10]**

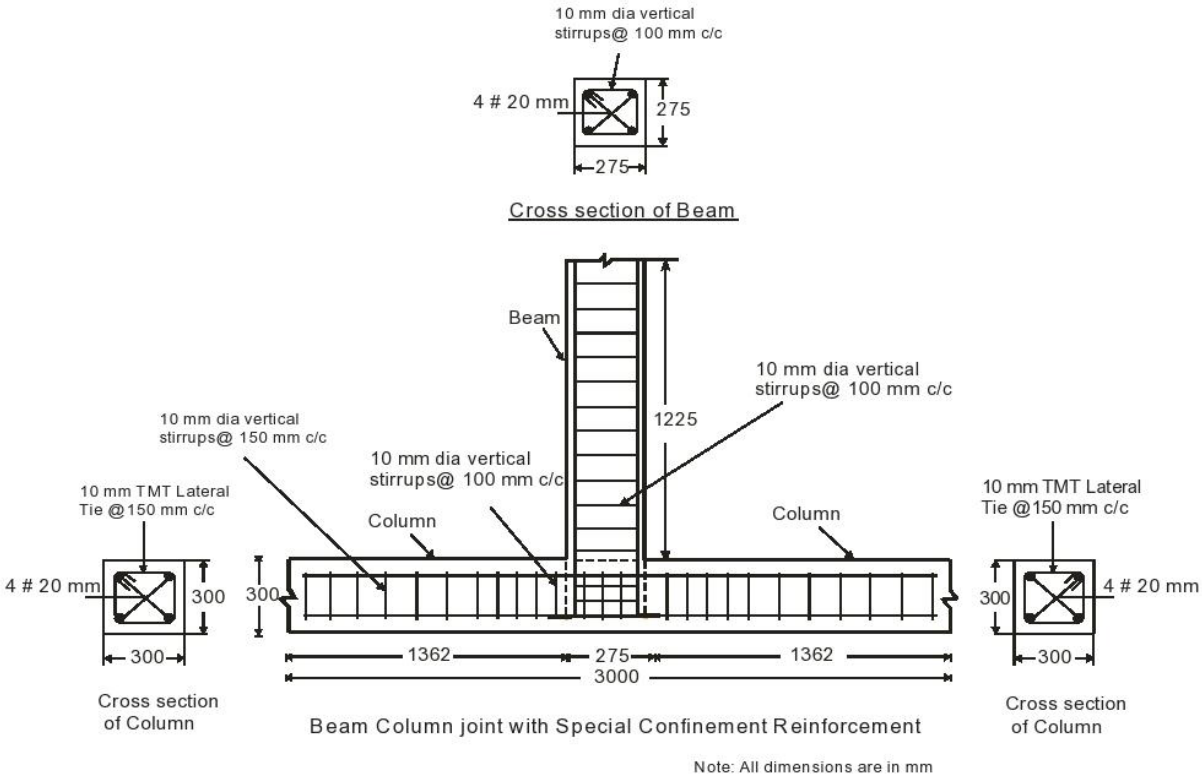


**Figure 3.2 Reinforcement detailing and cross section details of confined specimen [10]**

## 3.3 INTRODUCTION TO FE MODELLING

### 3.3.1 Finite Element Method

FEM is a numerical technique to find approximate solutions for boundary value problems, for partial differential equations and also for integral equations. These differential equations are solved by either eliminating the differential equations completely or by rendering these differential equations into ordinary differential equations which are then numerically integrated using standard techniques. Finite Element Method is a good choice for solving partial differential equations over complex domains.

How does FE Method works:

1. Discretize the Continuum.
2. Select Interpolation Functions.

3. Find the material properties.
4. Assemble the material Properties to Obtain the System Equations.
5. Impose the Boundary Conditions.
6. Solve the System Equations.
7. Make Additional Computations if desired.

### 3.3.2 Applications of Finite Element Method

1. FEM allows detailed visualization of where structures bend or twist, and indicates the distribution of stresses and displacements.
2. FEM can readily handle very complex geometry.
3. FEM can also handle complex loading.
4. FEM allows entire designs to be constructed, refined, and optimized before the design is manufactured.
5. FEM provides stiffness and strength visualizations.
6. FEM also provides a wide range of simulation options for controlling the complexity of both modelling and analysis of a system.

## 3.4 FINITE ELEMENT MODELLING

The finite element method (FEM) is the dominant discretization technique in structural mechanics. The concept of FEM modelling is the division of mathematical model into non-overlapping components of simple geometry. The response of each element is expressed in terms of a finite number of degrees of freedom characterized as the value of an unknown function.

The finite element method is well suited for superimposition of material models for the constituent parts of a composite material. Advanced constitutive models implemented in the finite element system ATENA serve as rational tools to explain the behaviour of connection between steel and concrete. Nonlinear simulation using the models in ATENA can be efficiently used to support and extend experimental investigations and to predict behaviour of structures and structural details.

Several constitutive models covering these effects are implemented in the computer code ATENA, which is a finite element package designed for computer simulation of concrete structures. The graphical user interface in ATENA provides an efficient and powerful environment for solving many anchoring problems. ATENA enables virtual testing of structures using computers, which is

the present trend in the research and development world. Utilization of ATENA for simulation of connections between steel and concrete is good. In ATENA, concrete is represented by solid brick element, reinforcement by bar elements and FRP by shell elements. Material properties play an important role in modeling of a structure.

## 3.5 MATERIAL MODELS

The program ATENA offers a variety of material models for different materials and purposes. The most important material models in ATENA for RCC structure are concrete and reinforcement. These advanced models considers all the important aspects of real material behaviour in tension and compression. GFRP material modelling is also considered.

### 3.5.1 MODELLING OF CONCRETE [3]

#### 1) Geometry of the Concrete

Element geometric modelling of concrete has been done using 3D solid brick element with 8 up to 20 nodes in ATENA, shown in Figure 3.3

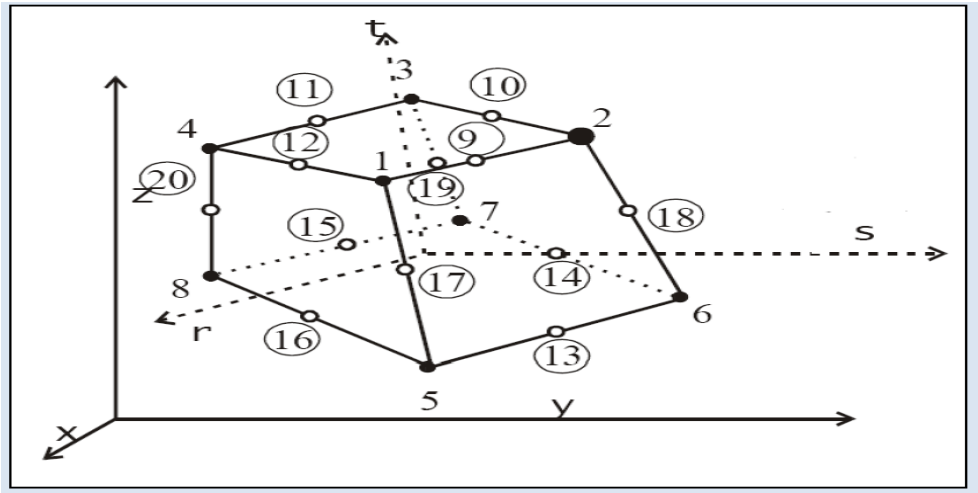


**Figure 3.3 Geometry of Brick elements [3]**

#### 2) Element Properties

3D solid brick element having three degree of freedom at each node: translations in the nodal x, y and z directions. This is an isoparametric elements integrated by Gauss integration at integration points. This element is capable of plastic deformation, cracking in three orthogonal directions, and

crushing. The most important aspect of this element is the treatment of non-linear material properties.

**3) Element Interpolation function**

3D solid brick element interpolation functions for all variants of the elements are given below:

N1= (1/8) (1+r) (1+s) (1+t) N2= (1/8) (1-r) (1+s) (1+t)

N3= (1/8) (1-r) (1-s) (1+t) N4= (1/8) (1+r) (1-s) (1+t)

N5= (1/8) (1+r) (1+s) (1-t) N6= (1/8) (1-r) (1+s) (1-t)

N7= (1/8) (1-r) (1-s) (1-t) N8= (1/8) (1+r) (1-s) (1-t)

### 3.5.2 MODELLING OF REINFORCEMENT [3]

**1) Geometry of the reinforcement**

Reinforcement modelling could be discrete or smeared. In our work, a discrete modelling of reinforcement has been done. The reinforcement has been modelled using bar elements in ATENA.

**2) Element Properties**

Reinforcement steel is a 3D bar element, which has three degrees of freedom at each node; translations in the nodal x, y and z direction. Bar element is a uniaxial tension-compression element. The stress is assumed to be uniform over the entire element. Also plasticity, creep, swelling, large deflection and stress-stiffening capabilities are included in the element.

**3) Element Shape Functions**

The shape functions in natural co-ordinate system for the three dimensional bar element without rotational degrees of freedom.

N1= (1/2) (1+s) N2= (1/2) (1-s)

### 3.5.3 MODELLING OF FRP [4]

The FRP modelling can be done as a 3D shell element in ATENA. The Ahmad shell element implemented in ATENA, described in ATENA theory manual. The present Ahmad element belongs to group of shell element formulation that is based on 3D elements concept. It can be

used to model thin as well as thick shell or plate structures.

**1. Geometry of the FRP**

The FRP can be modelled as a shell element in ATENA. The Ahmad shell element used the 20 nodes isoparametric brick element as shown in Figure 3.4. This is needed, in order to be able to use the same pre and post-processors support for the shell and native 3D brick element. After the 1st step of the analysis, the input geometry will automatically change to the external geometry from Figure 3.4. As nodes 17 and 18 contain only so called bubble function, the element is post- processed in the same way is it would be the isoparametric brick element. Internally, all element's vectors and matrices are derived based on the internal geometry as depicted in Figure 3.4.

**2. Element property of the FRP**

FRP is a Ahmad shell element. In the following general shell element theory concept, every node of element has five degree of freedom, e.g. three displacements and two rotations in planes normal to mid surface of element. In order to facilitate a simple connection of this element with other true 3D elements, the (original) five degrees o f freedom are transformed into x, y, z displacement of a top node and x, y displacement of a bottom node degrees of freedom. The two nodes are located on the normal to mid-surface passing thru the original mid-surface element's node.

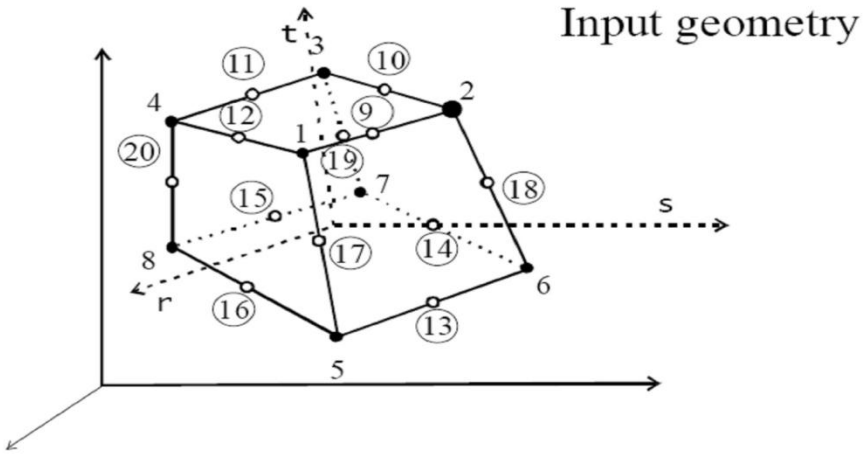

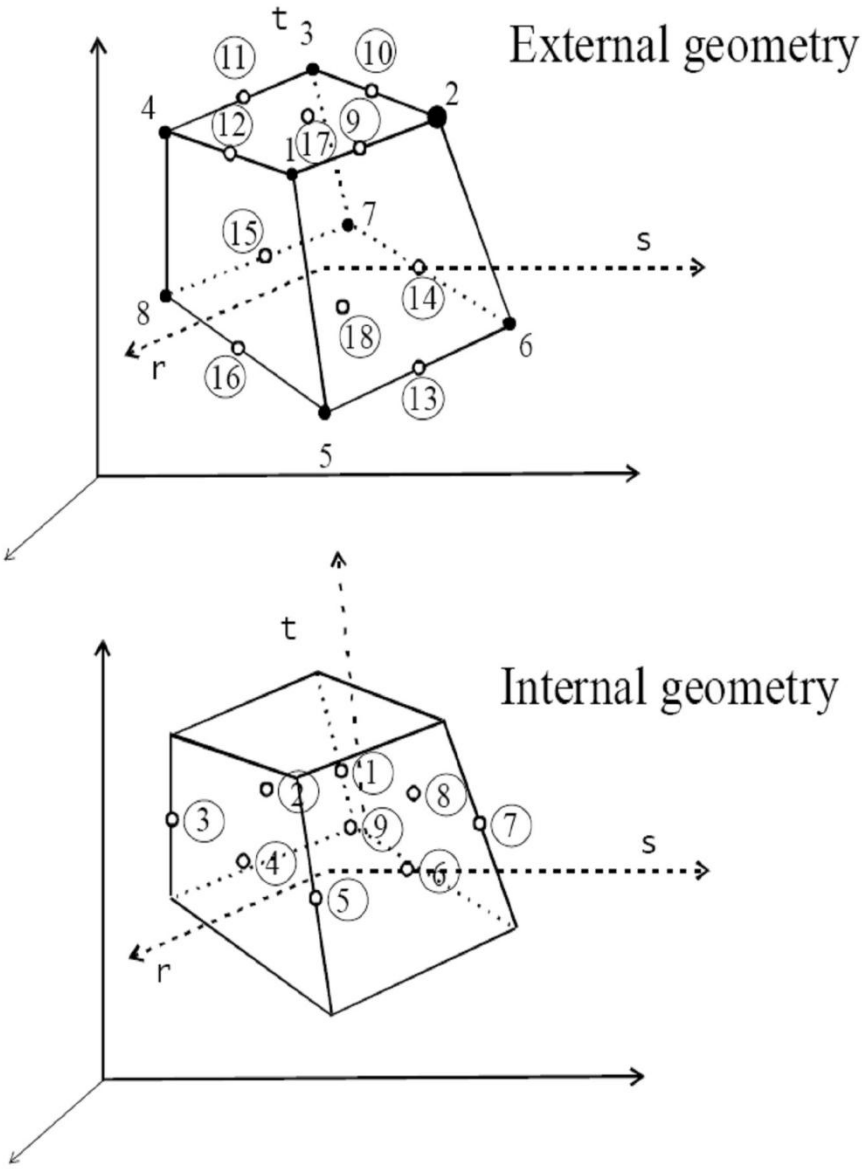


**Figure 3.4 Geometry of the FRP [4]**

## 3.6 STRESS - STRAIN RELATIONS FOR CONCRETE [3]

Concrete exhibits a large number of micro-cracks, especially, at the interface between coarser aggregates and mortar, even before subjected to any load. The presence of these micro-cracks has a great effect on the mechanical behaviour of concrete, since their propagation during loading contributes to the nonlinear behaviour at low stress levels and causes volume expansion near failure. Many of these micro-cracks are caused by segregation, shrinkage or thermal expansion of the mortar. Some micro-cracks may develop during loading because of the difference in stiffness

between aggregates and mortar. Since the aggregate-mortar interface has a significantly lower tensile strength than mortar, it constitutes the weakest link in the composite system. This is the primary reason for the low tensile strength of concrete.

The response of a structure under load depends to a large extent on the stress-strain relation of the constituent materials and the magnitude of stress. Since concrete is used mostly in compression, the stress-strain relation in compression is of primary interest [3].

### 3.6.1 EQUIVALENT UNIAXIAL LAW

The nonlinear behavior of concrete in the biaxial stress state is described by means of the so called effective stress $\sigma_c^{ef}$, and the equivalent uni-axial strain $\varepsilon^{eq}$. The effective stress is in most cases a principal stress. The equivalent uni-axial strain is introduced in order to eliminate the Poisson's effect in the plane stress state.

$$\boldsymbol{\varepsilon^{eq} = \sigma_{ci} / E_{ci}}$$

The equivalent uni-axial strain can be considered as the strain, that would be produced by the stress $\sigma_{ci}$ in a uni-axial test with modulus associated $E_{ci}$ with the direction i. Within this assumption, the nonlinearity representing damage is caused only by the governing stress $\sigma_{ci}$. The complete equivalent uni-axial stress-strain diagram for concrete is shown in Figure3.5.

The numbers of the diagram parts in Figure 3.5 (material state numbers) are used in the results of the analysis to indicate the state of damage of concrete.

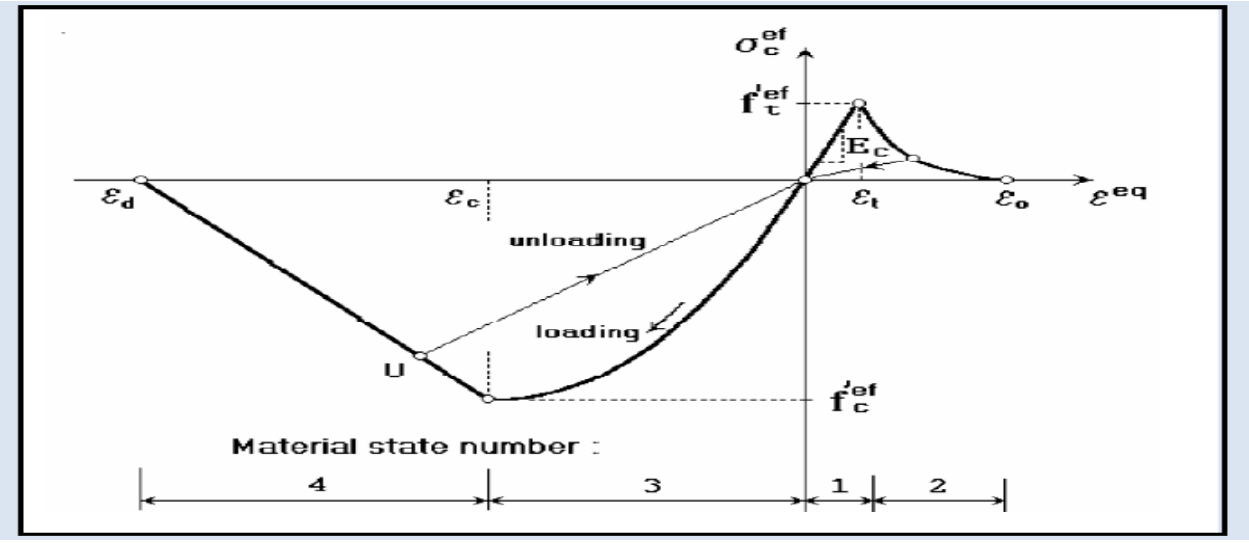


**Figure 3.5 Uniaxial stress-strain law for concrete [3]**

Unloading is a linear function to the origin. An example of the unloading point U is shown in Figure 3.5. Thus, the relation between stress $\sigma_c^{ef}$ and strain $\varepsilon^{eq}$ is not unique and depends on a load history. A change from loading to unloading occurs, when the increment of the effective strain changes the sign. If subsequent reloading occurs the linear unloading path is followed until the last loading point U is reached again. Then, the loading function is resumed.

The peak values of stress in compression $f_c^{ef}$ and in tension $f_t^{ef}$ are calculated according to the biaxial stress state. Thus, the equivalent uni-axial stress-strain law reflects the biaxial stress state.

### 3.6.2 BIAXIAL STRESS FAILURE CRITERION OF CONCRETE

**1) Compressive Failure**

A biaxial stress failure criterion according to KUPFER et al. (1969) is used as shown in Figure3.6. In the compression-compression stress state the failure function is

$$\mathbf{f'^{ef}_c = [(1+3.65a)/(1+a)2]f'_c;\ \ a = (\sigma_{c1}/\sigma_{c2})}$$

Where $\sigma_{c1}$, $\sigma_{c2}$ are the principal stresses in concrete and $f_c$ is the uni-axial cylinder strength. In the biaxial stress state, the strength of concrete is predicted under the assumption of a proportional stress path.

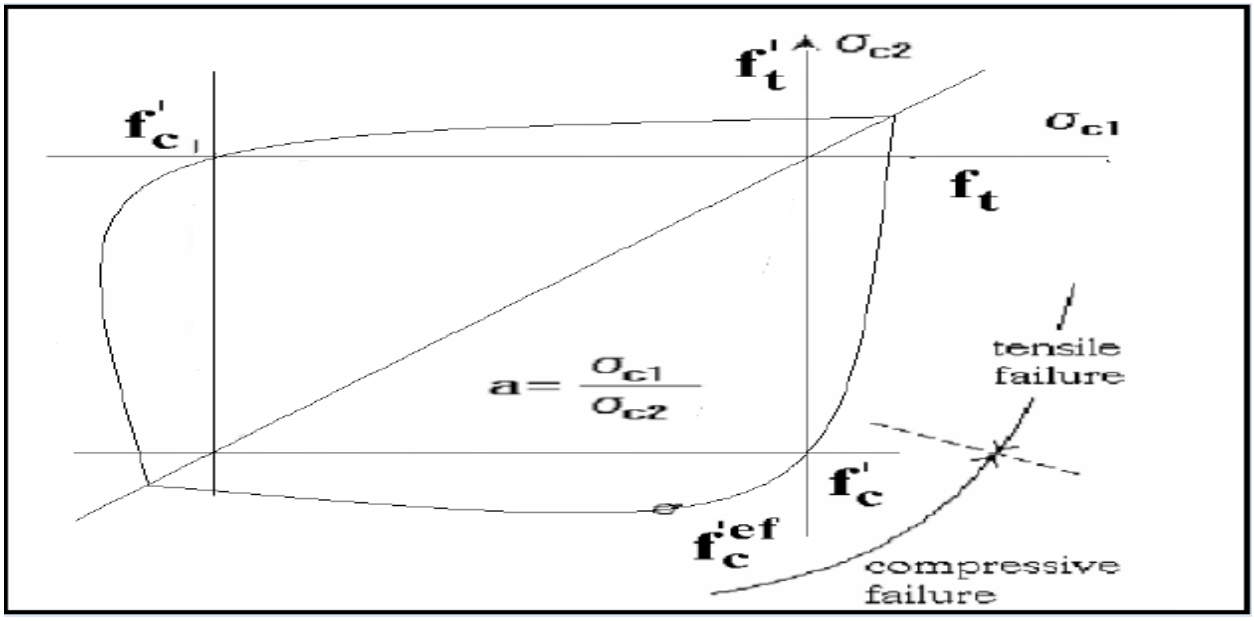


**Figure 3.6 Biaxial failure functions for concrete [3]**

In the tension-compression state, the failure function continues linearly from the point $\sigma_{c1} = 0$, $\sigma_{c2} = f'_c$, into the tension-compression region with the linearly decreasing strength:

$$\mathbf{f'^{ef}_c = f'_c\, r_{ec}}, \qquad \mathbf{r_{ec} = [1 + 5.3278(\sigma_{c1}/\, f'_c)]} \tag{3.2}$$

Where $r_{ec}$ is the reduction factor of the compressive strength in the principal direction 2 due to the tensile stress in the principal direction 1.

**2) Tensile failures**

In the tension-tension state, the tensile strength is constant and equal to the uniaxial tensile strength $f'_t$. In the tension-compression state, the tensile strength is reduced by the relation:

$$\mathbf{f'^{ef}_t = f'_t\, r_{et}} \tag{3.3}$$

Where $r_{et}$ is the reduction factor of the tensile strength in the direction 1 due to the compressive stress in the direction 2. The reduction function has one of the following forms.

$$\mathbf{r_{et} = 1 - 0.8\,(\sigma_{c2}/\, f'_c)} \tag{3.4}$$

$$\mathbf{r_{et} = [A + (A - 1)\,B]/\, AB;\ B = Kx + A;\ x = \sigma_{c2}/\, f'_c} \tag{3.5}$$

The relation in eq. (3.4) represents the linear decrease of the tensile strength and eq. (3.5) represents the hyperbolic decrease.

Two predefined shapes of the hyperbola are given by the position of an intermediate point r, x.

Constants K and A define the shape of the hyperbola. The values of the constants for the two positions of the intermediate point are given in the following table.

| *Type* | *Point* | | *Parameters* | |
|---|---|---|---|---|
| | r | X | A | K |
| A | 0.5 | 0.4 | 0.75 | 1.125 |
| B | 0.5 | 0.2 | 1.0625 | 6.0208 |

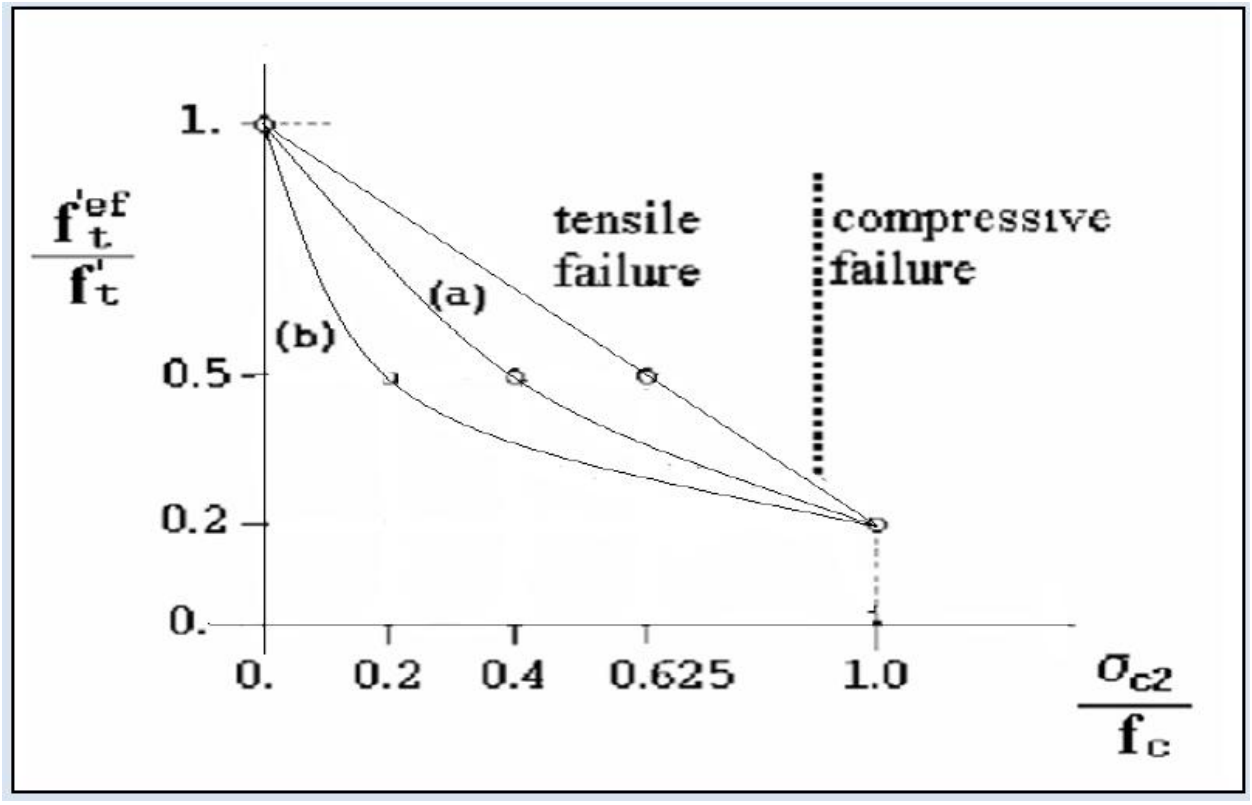


**Figure 3.7 Tension Compression failure function of concrete [3]**

### 3.6.3 TENSION BEFORE CRACKING

The behaviour of concrete in tension without cracks is assumed linear elastic. $E_c$ is the initial elastic modulus of concrete, $f'^{ef}_t$ is the effective tensile strength derived from the biaxial failure function already describe above.

$$\sigma_c^{ef} = E_c \, \varepsilon^{eq}, \; 0 < \sigma_c < f'^{ef}_t$$

### 3.6.4 TENSION AFTER CRACKING

A fictitious crack model is based on a crack-opening law and fracture energy. This formulation is suitable for modelling of crack propagation in concrete. It is used in combination with the crack band. It is a region (band) of material, which represents a discrete failure plane in the finite element analysis. In tension it is a crack, in compression it is a plane of crushing. In reality these failure regions have some dimension. However, since according to the experiments, the dimensions of the failure regions are independent on the structural size, they are assumed as fictitious planes. In case

of tensile cracks, this approach is known as rack the "crack band theory**", (BAZANT OH 1983).** Here is the same concept used also for the compression failure. The purpose of the failure band is to eliminate two deficiencies, which occur in connection with the application of the finite element model: element size effect and element orientation effect.

**1) Element size effect.**

The direction of the failure planes is assumed to be normal to the principal stresses in tension and compression, respectively. The failure bands (for tension $L_t$ and for compression $L_c$) are defined as projections of the finite element dimensions on the failure planes.

**2) Element Orientation Effect.**

The element orientation effect is reduced, by further increasing of the failure band for skew meshes, by the following formula (proposed by (**CERVENKA et al. 1995).**

$$\mathbf{L_t = \gamma L_t,\ L_c = \gamma L_c}$$

$$\gamma = 1 + (\gamma_{max} - 1)\ (\theta/ 45),\ \theta\ \varepsilon\ (0; 45) \qquad (3.6)$$

An angle $\theta$ is the minimal angle (min ($\theta_1$, $\theta_2$)) between the direction of the normal to the failure plane and element sides. In case of a general quadrilateral element the element sides' directions are calculated as average side directions for the two opposite edges. The above formula is a linear interpolation between the factor $\gamma$=1.0 for the direction parallel with element sides, and $\gamma=\gamma_{max}$, for the direction inclined at 45o. The recommended (and default) value of $\gamma_{max}$ =1.5.

## 3.7 BEHAVIOUR OF CRACKED CONCRETE [3]

### 3.7.1 Description of a Cracked Section

The nonlinear response of concrete is often dominated by progressive cracking which results in localized failure. The structural member has cracked at discrete locations where the concrete tensile strength is exceeded.

At the cracked section all tension is carried by the steel reinforcement. Tensile stresses are, however, present in the concrete between the cracks, since some tension is transferred from steel to concrete through bond. The magnitude and distribution of bond stresses between the cracks determines the distribution of tensile stresses in the concrete and the reinforcing steel between the cracks.

Additional cracks can form between the initial cracks, if the tensile stress exceeds the concrete tensile strength between previously formed cracks. The final cracking state is reached when a tensile force of sufficient magnitude to form an additional crack between two existing cracks can no longer be transferred by bond from steel to concrete.

As the concrete reaches its tensile strength, primary cracks form. The number and the extent of cracks are controlled by the size and placement of the reinforcing steel. At the primary cracks the concrete stress drops to zero and the steel carries the entire tensile force. The concrete between the cracks, however, still carries some tensile stress, which decreases with increasing load magnitude. This drop in concrete tensile stress with increasing load is associated with the breakdown of bond between reinforcing steel and concrete. At this stage a secondary system of internal cracks, called bond cracks, develops around the reinforcing steel, which begins to slip relative to the surrounding concrete.

Since cracking is the major source of material nonlinearity in the serviceability range of reinforced concrete structures, realistic cracking models need to be developed in order to accurately predict the load-deformation behaviour of reinforced concrete members. The selection of a cracking model depends on the purpose of the finite element analysis. If overall load-deflection behaviour is of primary interest, without much concern for crack patterns and estimation of local stresses, the "smeared" crack model is probably the best choice. If detailed local behaviour is of interest, the adoption of a "discrete" crack model might be necessary. Unless special connecting elements and double nodes are introduced in the finite element discretization of the structure, the well established smeared crack model results in perfect bond between steel and concrete, because of the inherent continuity of the displacement field.

### 3.7.2 Modeling of Cracks in Concrete

The process of crack formation can be divided into three stages as shown in Figure 3.8. The un-cracked stage is before a tensile strength is reached. The crack formation takes place in the process zone of a potential crack with decreasing tensile stress on a crack face due to a bridging effect. Finally, after a complete release of the stress, the crack opening continues without the stress.

The tension failure of concrete is characterized by a gradual growth of cracks, which join together and eventually disconnect larger parts of the structure. It is usually assumed that cracking formation is a brittle process and that the strength in tension loading direction abruptly goes to zero after such cracks have formed.

Therefore, the formation of cracks is undoubtedly one of the most important non-linear phenomenon, which governs the behaviour of the concrete structures. In the finite element analysis of concrete structures, two principally different approaches have been employed for crack modelling. These are (a) discrete crack modelling (b) smeared crack modeling.

The discrete approach is physically attractive but this approach suffers from few drawbacks, such as**,** it employs a continuous change in nodal connectivity, which does not fit in the nature of finite element displacement method; the crack is considered to follow a predefined path along the element edges and excessive computational efforts are required. The second approach is the smeared crack approach. In this approach the cracks are assumed to be smeared out in a continuous fashion.

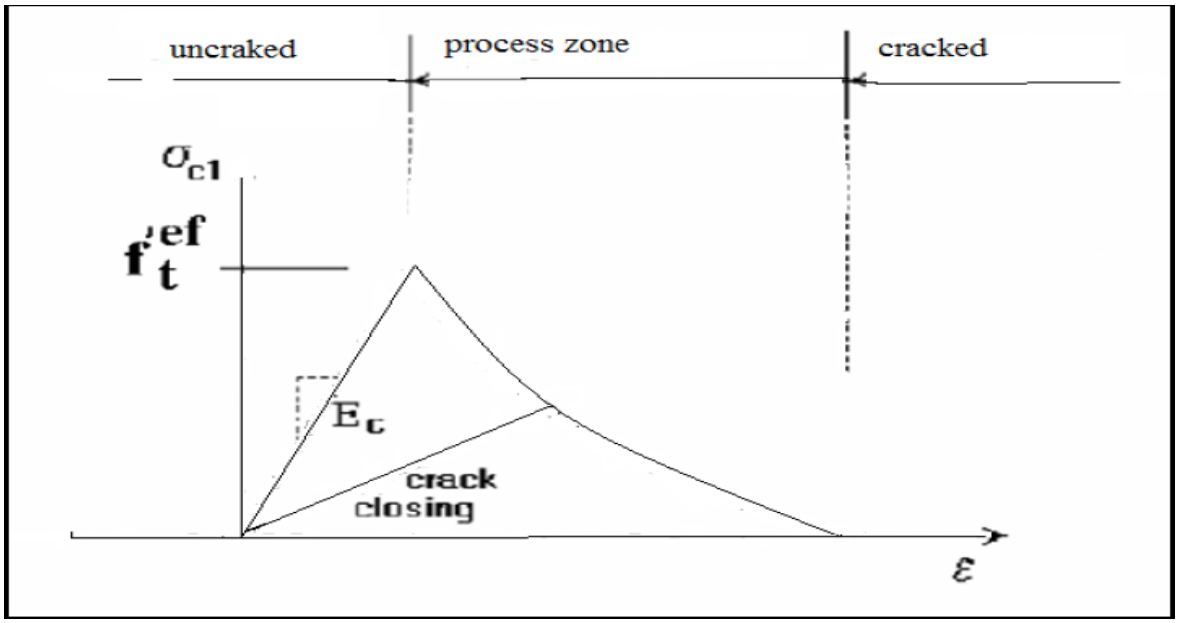


**Figure 3.8 Stages of Crack Opening [3]**

Within the smeared concept two options are available for crack models: the fixed crack model and the rotated crack model. In both models the crack is formed when the principal stress exceeds the tensile strength. It is assumed that the cracks are uniformly distributed within the material volume. This is reflected in the constitutive model by an introduction of orthotropy.

**1) Fixed Crack Model**

In the fixed crack model (**CERVENKA 1985, DARWIN 1974**) the crack direction is given by the principal stress direction at the moment of the crack initiation. During further loading this direction is fixed and represents the material axis of the orthotropy.

The principal stress and strain directions coincide in the un-cracked concrete, because of the assumption of isotropy in the concrete component. After cracking the orthotropy is introduced. The weak material axis $m_1$ is normal to the crack direction; the strong axis $m_2$ is parallel with the cracks. In a general case the principal strain axes $\varepsilon_1$ and $\varepsilon_2$ rotate and need not to coincide with the axes of the orthotropy $m_1$ and $m_2$. This produces a shear stress on the crack face as shown in Figure 3.9. The stress components $\sigma_{c1}$ and $\sigma_{c2}$ denote, respectively, the stresses normal and parallel to the crack plane and, due to shear stress, they are not the principal stresses.

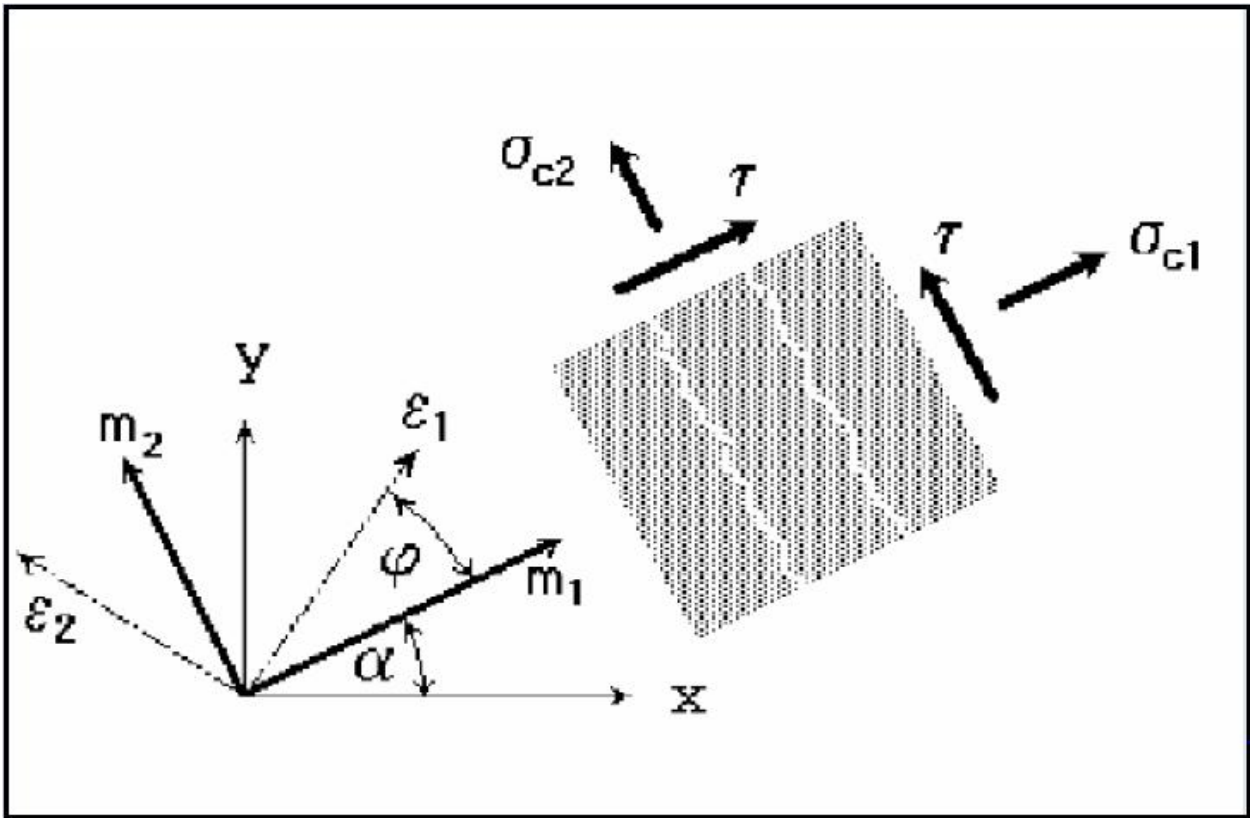


**Figure 3.9 Fixed crack model Stress and strain state [3]**

**2) Rotated Crack Model**

In the rotated crack model, the direction of the principal stress coincides with the direction of the principal strain. Thus, no shear strain occurs on the crack plane and only two normal stress components must be defined, as shown in Figure 3.10.

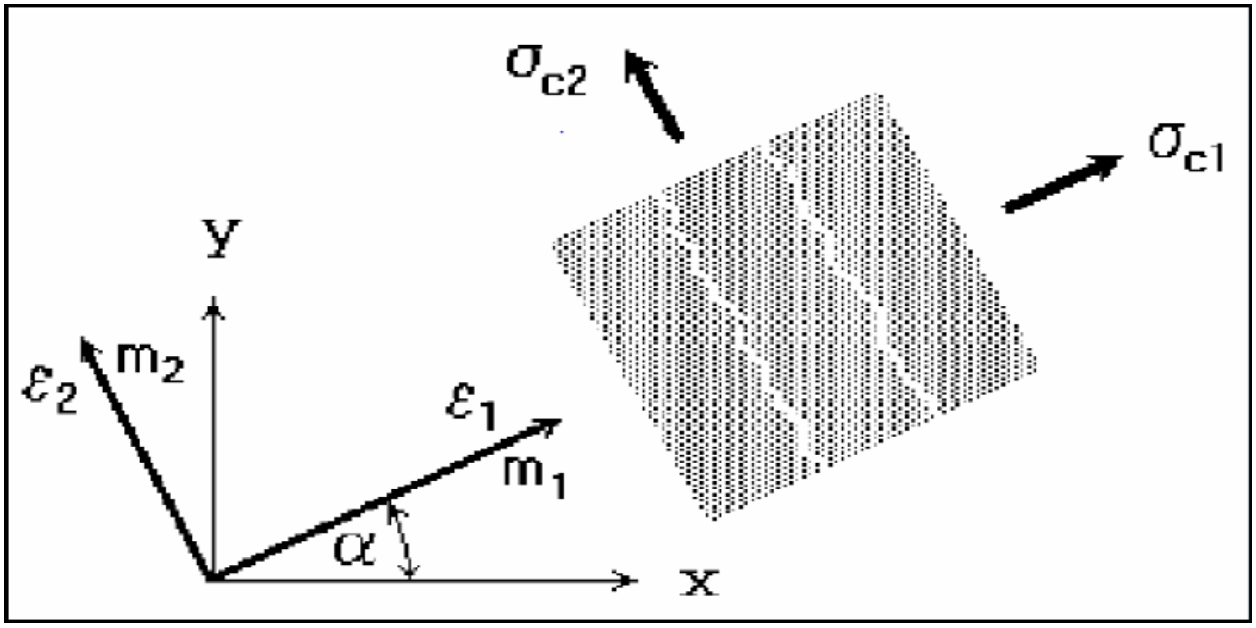


**Figure 3.10 Rotated crack model. Stress and strain state [3]**

If the principal strain axes rotate during the loading the direction of the cracks rotates, too. In order to ensure the co-axiality of the principal strain axes with the material axes the tangent shear modulus $G_t$ is calculated according to CRISFIELD 1989 as

$$G_t = (\sigma_{c1} - \sigma_{c2})/ 2\ (\varepsilon_1 - \varepsilon_2)$$

## 3.8 STRESS-STRAIN LAWS FOR REINFORCEMENT [3]

### 3.8.1 Introduction

Reinforcement can be modelled in two distinct forms: discrete and smeared. Discrete reinforcement is in form of reinforcing bars and is modelled by truss elements. The smeared reinforcement is a component of composite material and can be considered either as a single (only one-constituent) material in the element under consideration or as one of the more such constituents. The former case can be a special mesh element (layer), while the later can be an element with concrete containing one or more reinforcements. In both cases the state of uniaxial stress is assumed and the same formulation of stress-strain law is used in all types of reinforcement.

### 3.8.2 BILINEAR LAW

The bilinear law, elastic-perfectly plastic, is assumed as shown in Figure 3.14

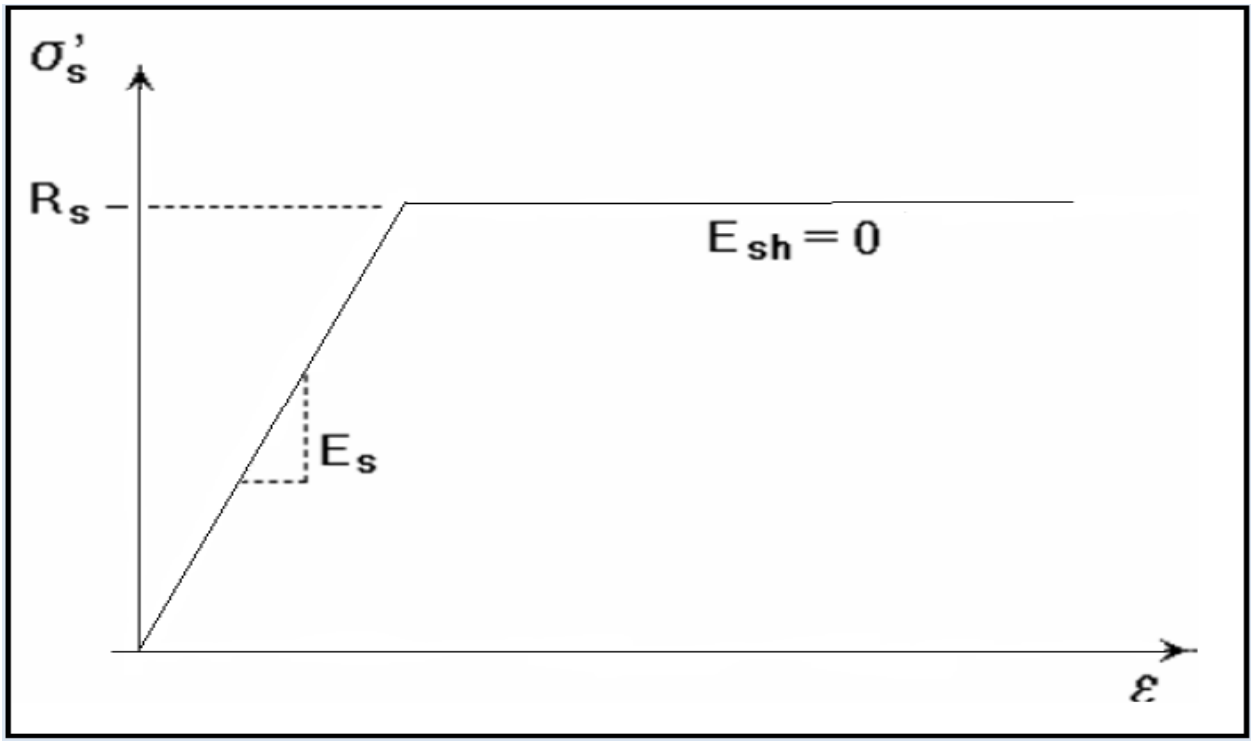


**Figure 3.11 The bilinear stress-strain law for reinforcement [3]**

The initial elastic part has the elastic modulus of steel $E_s$. The second line represents the plasticity of the steel with hardening and its slope is the hardening modulus $E_{sh}$. In case of perfect plasticity, $E_{sh}$ =0. Limit strain $\varepsilon_L$ represents limited ductility of steel.

### 3.8.3 MULTI-LINEAR LAW

The multi-linear law consists of four lines as shown in Figure 3.12**.** This law allows modelling of all four stages of steel behaviour: elastic state, yield plateau, hardening and fracture. The multi-line is defined by four points, which can be specified by input.

The above described stress-strain laws can be used for the discrete as well as the smeared reinforcement. The smeared reinforcement requires two additional parameters: the reinforcing ratio p and the direction angle β as shown in Figure 3.13.

Where ρ = (Area of steel/ Area of concrete)

The spacing s of the smeared reinforcement is assumed infinitely small. The stress in the smeared reinforcement is evaluated in the cracks; therefore it should include also a part of stress due to tension stiffening $\sigma_{scr} = \sigma_s + \sigma_{ts}$

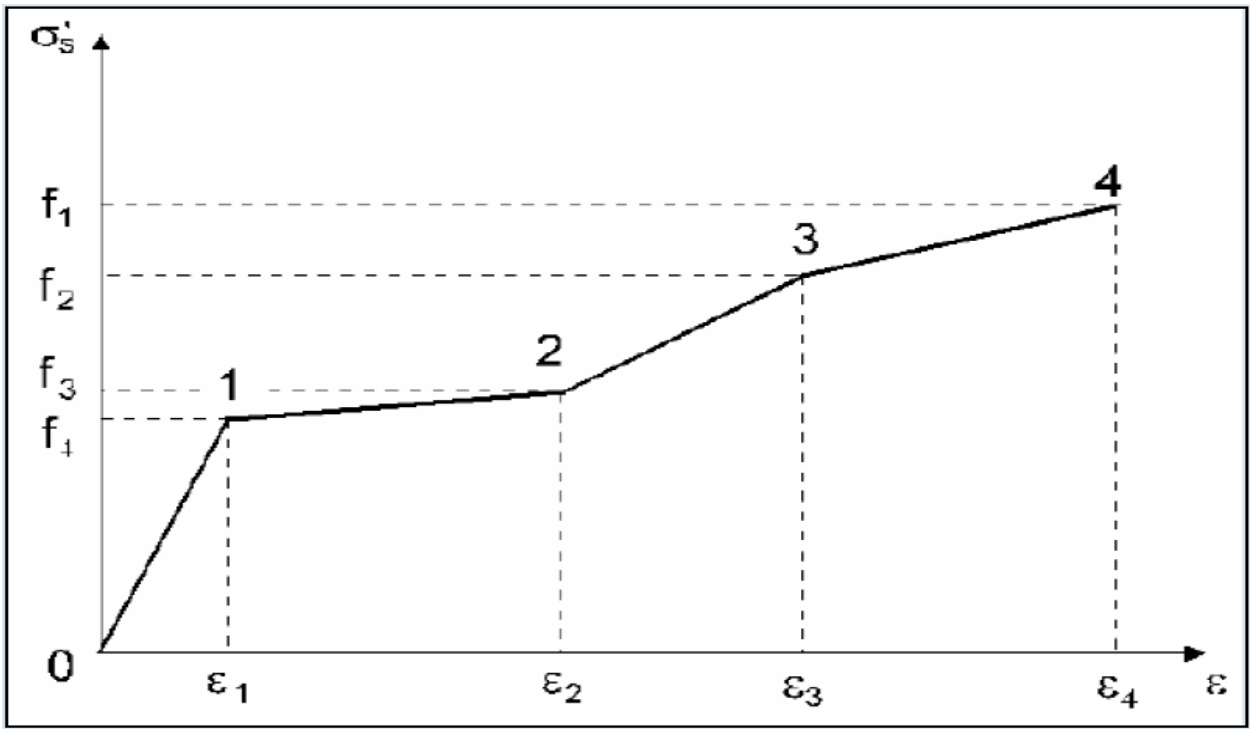


**Figure 3.12 The multi-linear stress-strain law for reinforcement [3]**

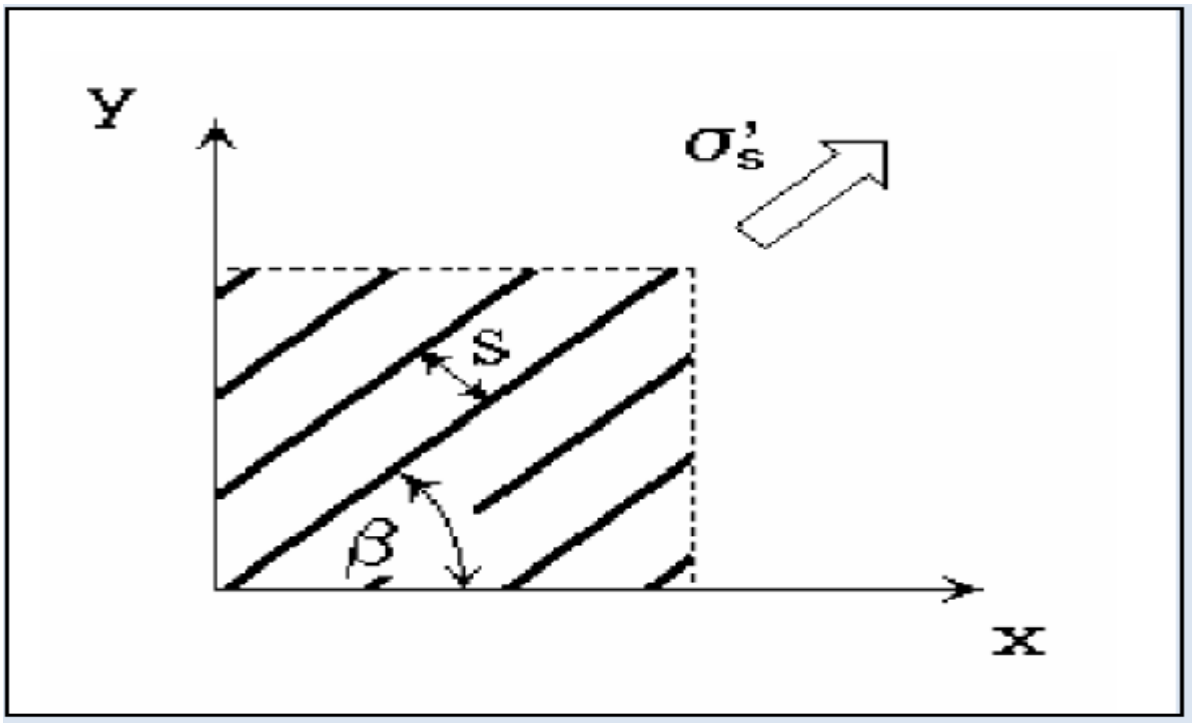


**Figure 3.13 Smeared reinforcement [3]**

where $\sigma_s$ is the steel stress between the cracks (the steel stress in smeared reinforcement),
$\sigma_{scr}$ is the steel stress in a crack. If no tension stiffening is specified $\sigma_{ts} = 0$ and $\sigma_{scr} = \sigma_s$. In case of the discrete reinforcement the steel stress is always $\sigma_s$.

Once we understand the finite element modelling, the next step is the analytical programming. In the analytical programming, first we select the materials and its properties and create geometry of the beam column joint. For this, confined and unconfined RC beam column joint (T-joint) under monotonic and cyclic excitation are created and done the FE modelling through automatic FE mesh generator in ATENA. Same specimens were retrofitted with FRP (stressed to 50% and 75%). All these specimens were tested up to its failure values and in between graphs. For modelling the control and retrofitted specimens in ATENA, concrete, reinforcement bars of different diameters, steel plates, epoxy and GFRP is used a material.

## 3.9 MATERIAL PROPERTIES

Concrete, reinforcement steel, steel plates, Epoxy and GFRP have been used to model the RC beam column joint. The specification and the properties of these materials are as under:

### 1) Concrete

In ATENA, concrete material is modelled as a 3D nonlinear cementitious2. The physical properties of 3D nonlinear cementitious2 material are given in **Table 3.1**. The values are calculated as per IS code 456:2000 and remaining are the default values.

### 2) Reinforcement Bars

HYSD steel of grade Fe-415 of 20mm diameter is used as main steel while 10mm diameter bars is used as shear reinforcement. The properties of these bars are shown in **Table 3.2**.

**Table 3.1 Material Properties of Concrete**

| Properties | Values |
|---|---|
| Elastic Modulus (Fresh concrete) | 22360 MPa |
| Elastic Modulus (75% stressed concrete) | 14534 MPa |

| | |
|---|---|
| Elastic Modulus (90% stressed concrete) | 11180 MPa |
| Poisson Ratio | 0.2 |
| Tensile Strength | 3.130 MPa |
| Compressive Strength | 20 MPa |
| Specific Fracture Energy | 4.421E-05 MN/m |
| Critical Compressive Displacement | 5E-04 |
| Plastic Strain at Compressive Strength | 6.681E-04 |
| Reduction of Compressive Strength | 0.8 |
| Fail Surface Eccentricity | 0.52 |
| Specific Material Weight | 0.023 MN/mE+3 |
| Coefficient of Thermal Expansion | 1.200E-05 1/K |
| Fixed Crack Model Coefficient | 1 |

**Table 3.2 Material Properties of Reinforcement**

| Properties | Values |
|---|---|
| Elastic modulus | 200000 MPa |
| Elastic modulus (75% stressed) | 160000 MPa |
| Elastic modulus (90% stressed) | 160000 MPa |
| Yield Strength | 415 MPa |
| Specific Material weight | 0.0785 MN/mE+3 |
| Coefficient of Thermal Expansion | 1.2E-05 1/K |

**3) Steel Plate**

The function of the steel plate in the ATENA is for support and for loading. Here, the property of steel plate is same as the reinforcement bar except its yield strength. The HYSD steel of grade Fe-415 was used for steel plate.

**4. Epoxy**

Mbrace saturant was used as a epoxy in the analysis. The material properties are taken from the "Watson Bowman Acme corp." company paper. The material properties of epoxy are shown inTable 3.3.

**Table 3.3 Material Properties of Epoxy**

| Properties | Values |
|---|---|
| Elastic Modulus | 3035 MPa |
| Poisson Ratio | 0.4 |
| Yield Strength | 54 MPa |
| Specific Material Weight | 0.000008 MN/mE+3 |
| Coefficient of Thermal Expansion | 1.200E-05 1/K |

**5. Glass Fibre Reinforcement Polymer**

Mbrace G sheet EU-900 unidirectional Glass fibre sheet is used in retrofitting. The properties which are used in the modelling are taken from the Mbrace Product Data, shown in the table 3.4.

**Table 3.4 Material Properties of GFRP**

| Properties | Values |
|---|---|
| Strain, stress | (0,0); (0.005,390); (0.01,690) MPa |
| Specific Material Weight | 7.85E-02 MN/mE+3 |
| Coefficient of Thermal Expansion | 1.200E-05 1/K |

## 3.10 FE MODELLING OF RC BEAM COLUMN JOINT IN ATENA

The ATENA program, which is determined for nonlinear finite element analysis of structures, offers tools specially designed for computer simulation of concrete and reinforced concrete structural behavior.

ATENA program system consists of a solution core and several user interfaces. The solution core offers capabilities for variety of structural analysis tasks, such as: stress and failure analysis, transport of heat and humidity, time dependent problems (creep, dynamics), and their interactions. Solution core offers a wide range of 2D and 3D continuum models, libraries of

finite elements, material models and solution methods. User interfaces are specialized on certain functions and thus one user interface need not necessarily provide access to all features of ATENA solution core. This limitation is made on order to maintain a transparent and user friendly user environment in all specific applications of ATENA.

ATENA 3D program is designed for 3D nonlinear analysis of solids with special tools for reinforced concrete structures. However, structures from other materials, such as soils, metals etc. can be treated as well. The program has three main functions:

A. Pre-processing

B. Run

C. Post-processing

A. **Pre-processing:** Input of geometrical objects (concrete, reinforcement, interfaces, etc.), loading and boundary conditions, meshing and solution parameters.

B. **Analysis:** It makes possible a real time monitoring of results during calculations.

C**. Post-processing:** Access to a wide range of graphical and numerical results.

**Procedure:**

In pre-processing window following steps are performed:-

**Step1**: Geometry of FE model is created .It has been presented in Figure 3.14 & 3.15.

**Step2**: Material properties are assigned to the various elements of the RC slab specimen.

**Step3**: Structural element, various supports, loadings, FRP and monitoring points are defined. (Figure 3.16 & 3.17)

**Step4**: Finite element meshing parameters are given and meshing of the model is generated accordingly. (Figure 3.16)

**Step5**: Various analysis steps are defined. The FE non-linear analysis is done in Run window. The FE non-linear static analysis calculates the effects of steady loading conditions on a structure. A static analysis can, however, include steady inertia loads (such as gravity and rotational velocity), and time-varying loads that can be approximated as static equivalent. Static analysis is used to determine the displacements, stresses, strains, and forces in structures or components by loads.

**Step6**: When the FE non linear static analysis is completed the, the results are shown in third part of the ATENA ie. Post processing. The stress- strain values at every step, crack pattern and cracks propagation at every step shown help in to analyze the behaviour of the elements at every step of load deflection.

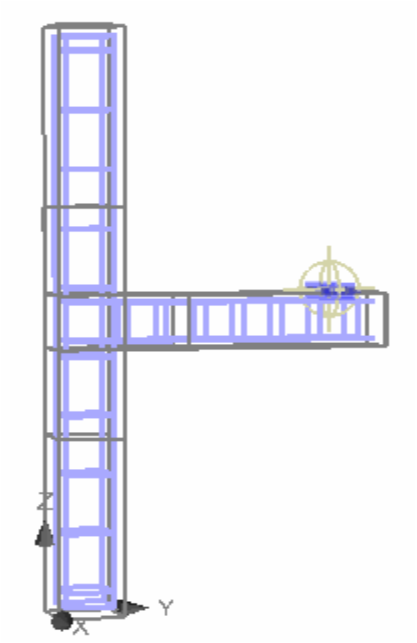

**Figure3.14 Modelling of unconfined joint**

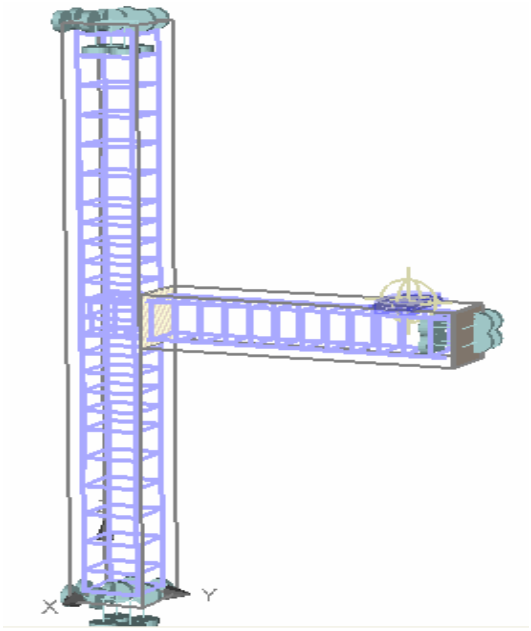

**Figure 3.15 Modelling of confined joint**

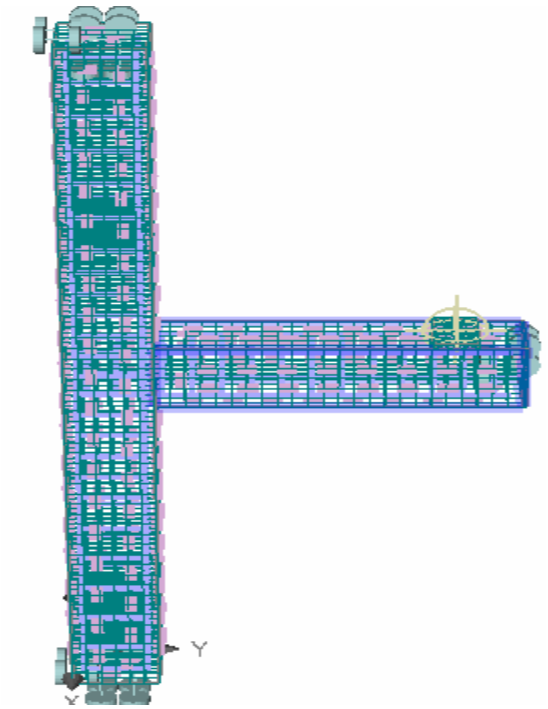

**Figure 3.16 Modelling of FE mesh and supports**

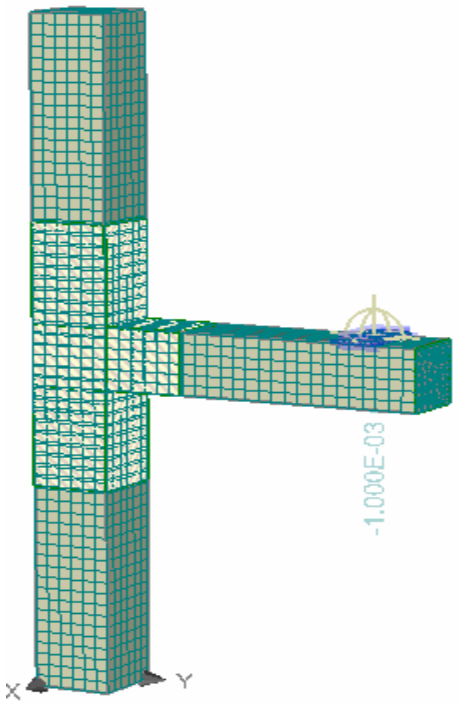

**Figure 3.17 Modelling of** FRP

## 3.11 METHODS FOR NON-LINEAR SOLUTION [3]

The best part of the ATENA is the simpler way of solving the non-linear structural behavior through finite element method and its incremental loading criteria. Different methods are available in ATENA for solving non-linear equations such as, linear method, Newton-Raphson Method, Modified Newton-Raphson method, Arc Length methods are used in ATENA.

Among these the Newton-Raphson Method and Modified Newton-Raphson Method are more commonly used methods. In our present study, Newton-Raphson method is used for solving the simultaneous equations. It is an iterative process of solving the non-linear equations.

One approach to non-linear solutions is to break the load into a series of load increments. The load increments can be applied either over several load steps or over several sub steps within a load step. At the completion of each incremental solution, the program adjusts the stiffness matrix to reflect the nonlinear changes in structural stiffness before proceeding to the next load increment. .

The ATENA program overcomes this difficulty by using Full Newton-Raphson method, or Modified Newton-Raphson method, which drive the solution to equilibrium convergence (within some tolerance limit) at the end of each load increment. In Full Newton-Raphson method, it obtains the following set of non-linear equations:

$$K(p)\,\Delta p = q - f(p)$$

where,

q is the vector of total applied joint loads,

f(p) is the vector of internal joint forces,

$\Delta p$ is the deformation increment due to loading increment,

p are the deformations of structure prior to load increment,

K(p) is the stiffness matrix, relating loading increments to deformation increments.

Figure 3.15 illustrates the use of Newton-Raphson equilibrium iterations in nonlinear analysis. Before each solution, the Newton-Raphson method evaluates the out-of -balance load vector, which is the difference between the restoring, forces (the loads corresponding to the element stresses) and the applied loads. The program then performs a linear solution, using the out-of - balance loads, and checks for convergence. If convergence criteria are not

satisfied, the out-of- balance load vector is re-evaluated, the stiffness matrix is updated, and a new solution is obtained. This iterative procedure continues until the problem converges. But sometimes, the most time consuming part of the Full Newton-Raphson method solution is the re-calculation of the stiffness matrix K (pi−1) at each iteration. In many cases this is not necessary and we can use matrix K ($p_0$) from the first iteration of the step. This is the basic idea of the so-called Modified Newton-Raphson method. It produces very significant time saving, but on the other hand, it also exhibits worse convergence of the solution procedure. The simplification adopted in the Modified Newton-Raphson method can be mathematically expressed by:

$$K(pi-1) = K(p_0)$$

The modified Newton-Raphson method is shown in Figure 3.17. Comparing Figure 3.16 and Figure 3.15, it is apparent that the Modified Newton-Raphson method converges more slowly than the original Full Newton-Raphson method. On the other hand, a single iteration costs less computing time, because it is necessary to assemble and eliminate the stiffness matrix only once. In practice a careful balance of the two methods is usually adopted in order to produce the best performance for a particular case. Usually, it is recommended to start a solution with the original Newton-Raphson method and later, i.e. near extreme points, switch to the modified procedure to avoid divergence.

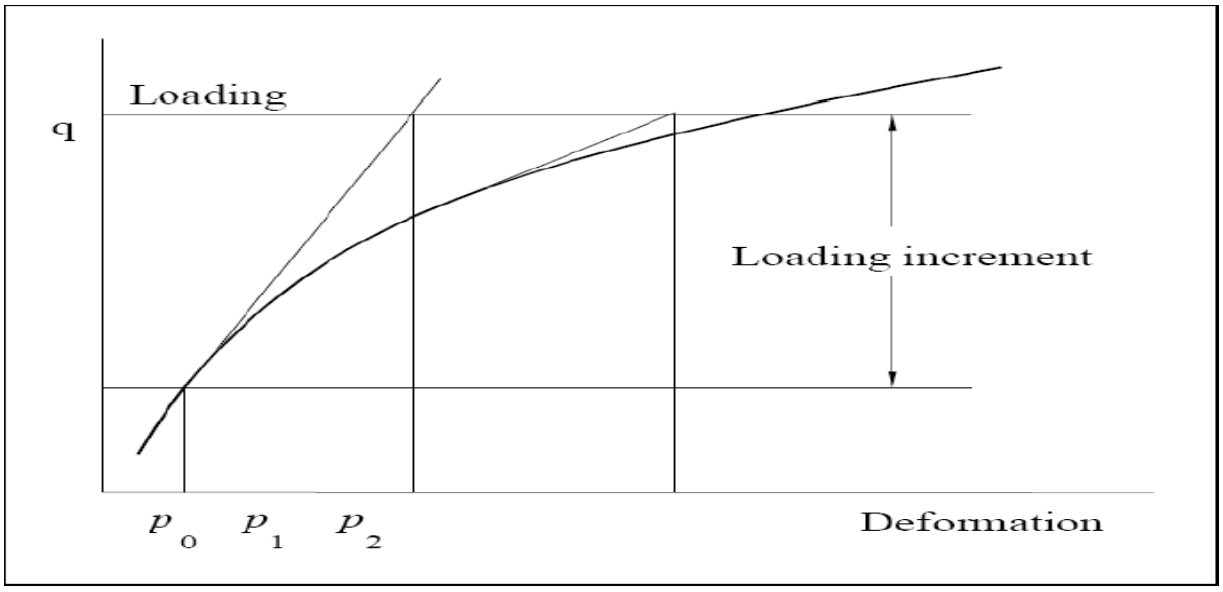


**Figure 3.18 Full Newton-Raphson Method [3]**

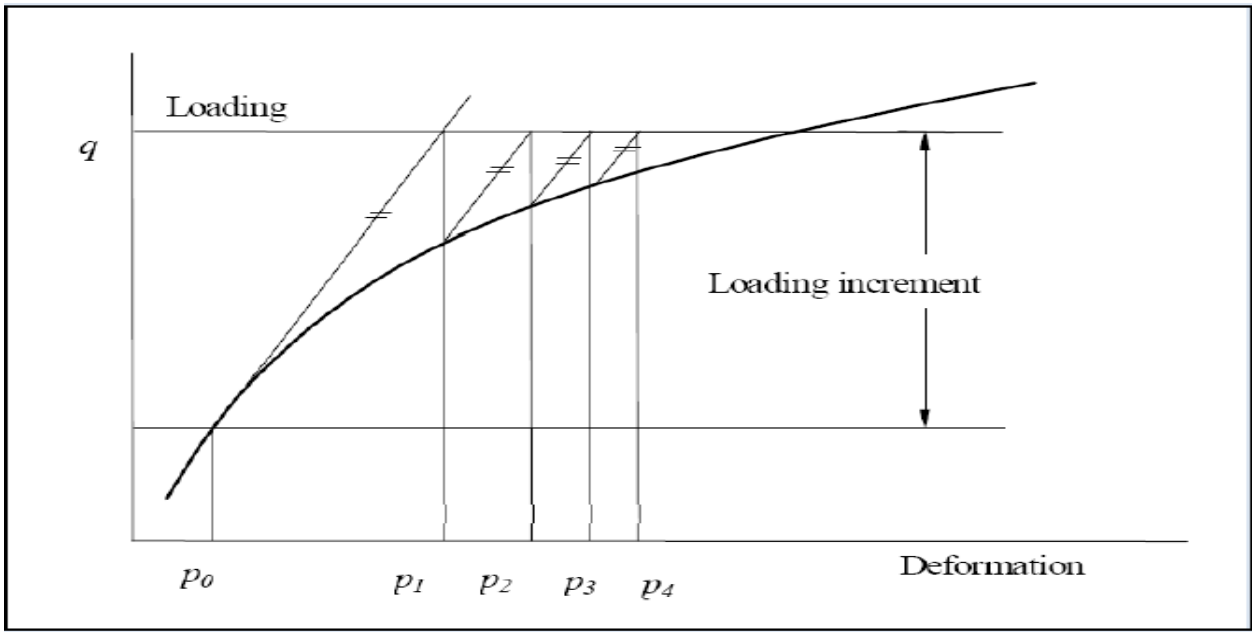


**Figure 3.19 Modified Newton-Raphson Method [3]**

# Chapter 4 RESULTS AND DISCUSSIONS

## 4.0 GENERAL

In the present study, non-linear response of RC beam column joint has been modeled as per details discussed in Chapter 3 (3.2 General Description of Structure) under the monotonic and cyclic loading. Results of confined and unconfined models have been compared. The objective of this study is to see the variation of load- displacement graph, the crack patterns, propagation of the cracks and the crack width at different values of the deflection

This chapter presents the results of Finite Element analysis of RC Beam column joint under both monotonic and cyclic load. Finite element analysis of RC beam column joint under the static incremental loads and dynamic load has been performed using ATENA software. This is followed by load deflection curve and the cracking behavior obtained from the analysis. In the end the results of confined and unconfined are also compared. The results obtained from the stressed retrofitted beam column joint have been discussed in the next chapter.

In the analysis, load has been applied in terms of prescribed deformation on the beam at distance of 1300mm from corner of the column and corresponding to the deformation, load taken by the joint are obtained. The load- deflection values at every step have been recorded, further the crack pattern and cracks propagation at every step has been studied. The load v/s deflection curves have been plotted for both confined and unconfined models under monotonic and cyclic loading**.** Subsequently these results are compared with experimental results of "Gupta and Agarwal (2012) ".

### 4.1 BEHAVIOR OF BEAM COLUMN JOINT UNDER MONOTONIC LOADING

Under monotonic loading, two RC beam column joints has been modeled; one unconfined (according to IS: 456-2000) and other confined (according to IS: 13920-1993). FE Modelling of the joint under the incremental loading has been carried out (discussed in detail in chapter 3). Load has been applied in terms of prescribed deformation on the beam at distance of 1300mm from corner of the column and corresponding to the deformation, load taken by the joint are obtained.

### 4.1.1 FE ANALYSIS OF UNCONFINED MODEL

Load deflection curve for unconfined joint has been plotted in Figure 4.1. It can be observed from figure 4.1 that the structure behaved linearly elastic up to the value of load around 30.06 KN at 1mm. At this point the minor cracks started to get generated at the joint. After this point there is a slight curvature in the plot and load started increasing with the deflection increments. When the load reached to the value of 80.85KN, the graph depicted non-linearity in its behavior and the maximum load taken by the joint is 86.43KN at deflection of 17mm. Subsequently deflection started increasing without any significant increment in load; it has reached to the value of 15mm with the load value around 86.1KN. As the analysis continued, the load carrying capacity decreased progressively. Further, the load has been found to be 53.32 KN at the deflection of 50mm.

The loads at joint for different displacements have been shown in Table 4.1

**Table 4.1 FE Results of unconfined joint under monotonic loading**

| DEFLECTION [mm] | LOAD [KN] |
|---|---|
| 2 | 36.97 |
| 5 | 53.02 |
| 10 | 74.75 |
| 15 | 86.1 |
| 20 | 85.35 |
| 25 | 82.33 |
| 30 | 66.62 |
| 35 | 56.62 |
| 40 | 50.79 |
| 45 | 47.81 |
| 50 | 44.78 |

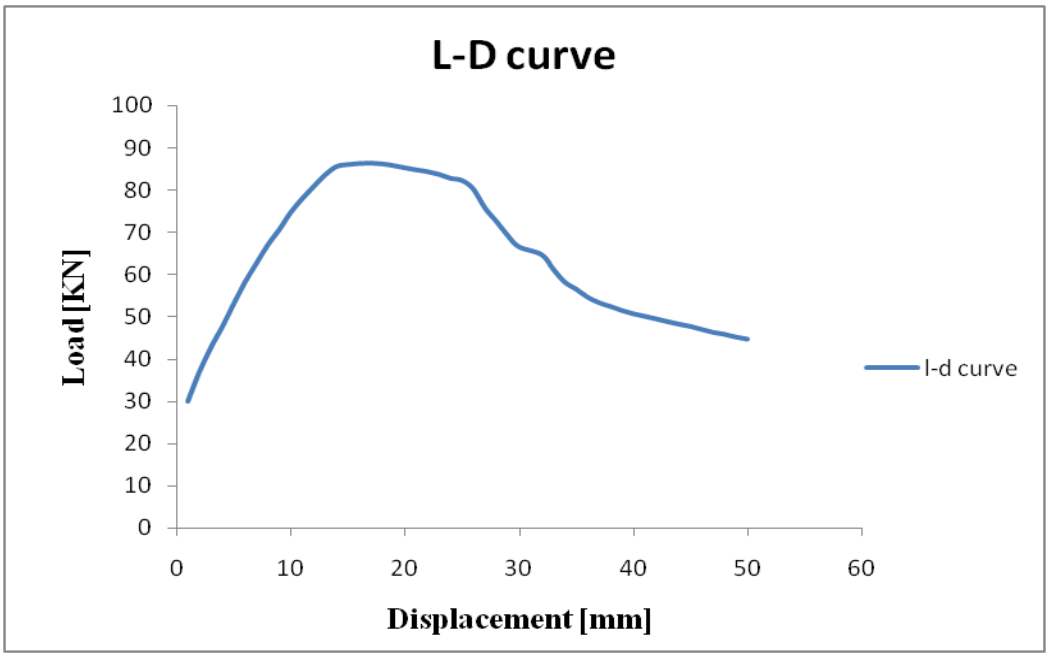


**Figure 4.1 load deflection curve for unconfined joint**

### 4.1.2 CRACK PATTERNS

The variations of crack pattern have been plotted in Figure 4.2 - 4.8. A discussion on crack pattern plotted here has been presented here. The shape of un-deformed and deformed structure has been shown in Figure 4.9.

It had been observed that micro-cracks appeared in the structure when the joint is in linear zone. The maximum width of crack at 10mm displacement was observed as 0.6mm. The first crack has been observed at 5mm at value of load 53.02 KN in the shape of shear crack as shown in Figure 4.2. This very small sized (actually invisible) crack appeared at beam-column joint.

The crack at 10mm displacement has been shown in Figure 4.3.

The maximum width of crack at 10mm displacement was observed as 0.6mm. The crack pattern at 17mm at load value of 86.43KN is presented in Figure 4.4. This is the ultimate load level of the joint. First flexural cracks have been observed near beam column joint, but at this step shear cracks along with flexural crack have been observed on the beam and columns. No visible shear cracks have been observed in linear zone. Crack at the joint and on the beam near to the joint joined with the flexural cracks were observed.

The cracks spread over the joint of beam column throughout at displacement ductility $\mu_{\Delta}$=4. The crack at 25mm displacement is shown in figure 4.5 with maximum width of crack as 2mm. The views showing the crack pattern with different crack size at 50mm taken from FE analysis at value of load 44.78 KN are presented in Figure 4.6 to Figure 4.8. The beam- column joint with flexural cracks in almost all the beam and around the joint in column can be visualized. The number of cracks increase as the load is increases upto 86.43 kN at a displacement of 17 mm. These cracks spread all over the joint at displacement 50mm Fewer crack have been seen at top and bottom of the column. Major damage has been noticed in the joint whereas beam experienced moderate damage and the column experienced minor damage

Maximum width of crack observed in FE analysis has been shown in Table 4.2

**Table 4.2 Maximum crack width at different values of load and displacement**

| Displacement [mm] | Load [KN] | Maximum width of crack [mm] |
|---|---|---|
| 5 | 53.02 | 0.1 |
| 10 | 74.75 | 0.6 |
| 17 | 86.43 | 1 |
| 25 | 82.33 | 2 |
| 50 | 44.78 | 6 |

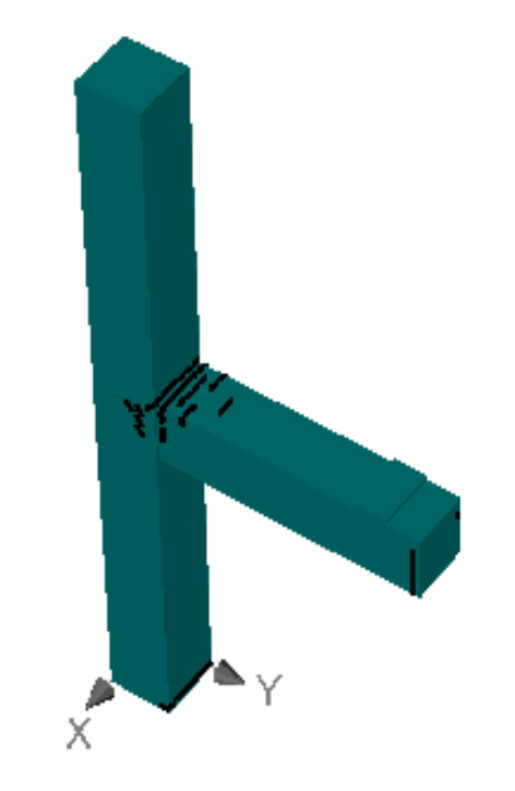


**Figure 4.2 First crack of 0.1 mm width at 5mm displacement**

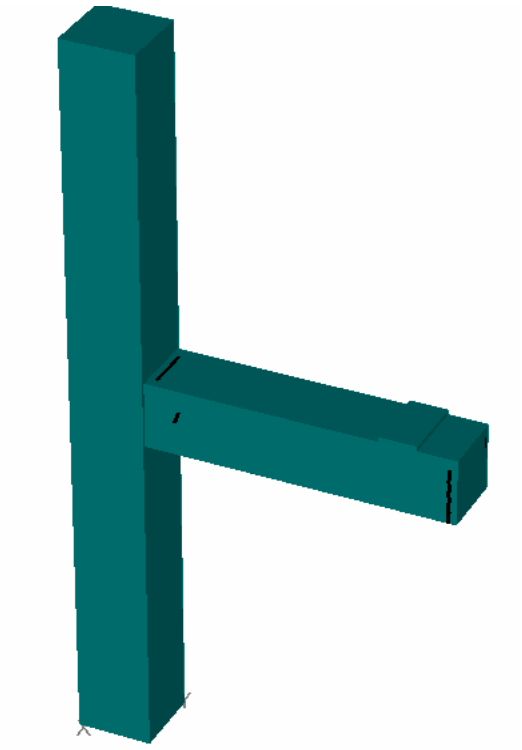

**Figure 4.3 Crack of 0.6mm width at 10mm displacement**

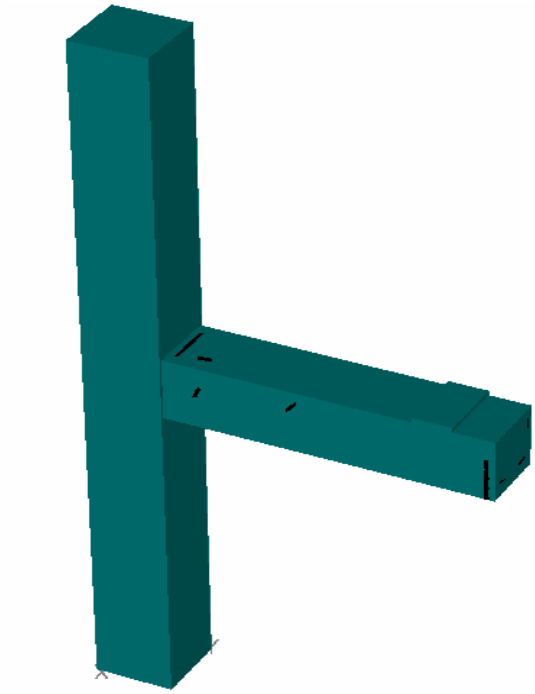

**Figure 4.4 Crack of 1mm width at 17mm displacement**

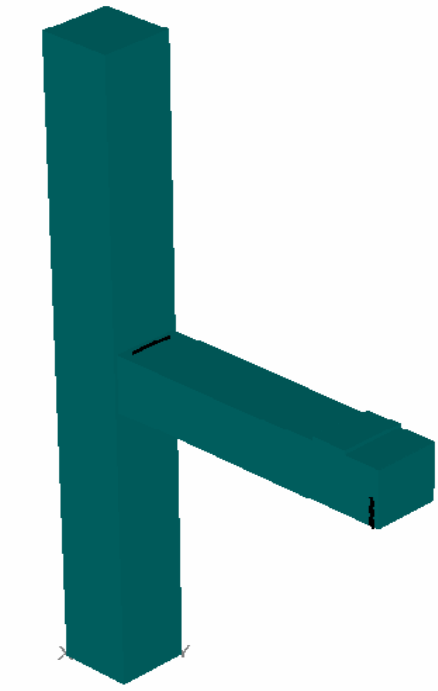

**Figure 4.5 Crack of 2mm width 25 mm displacement**

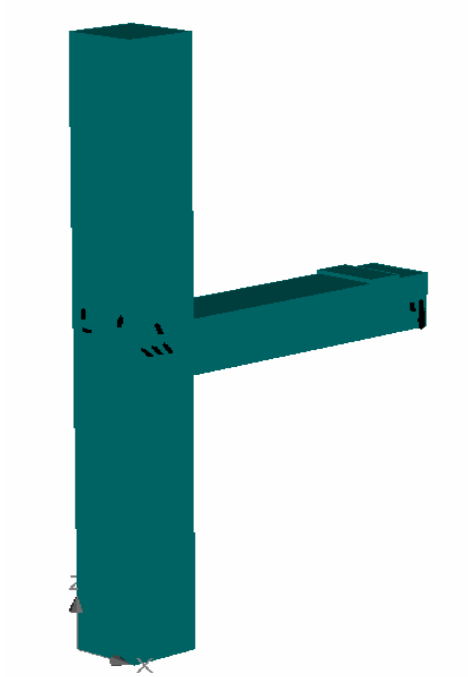

**Figure 4.6 Crack of 4mm width at 45mm displacement**

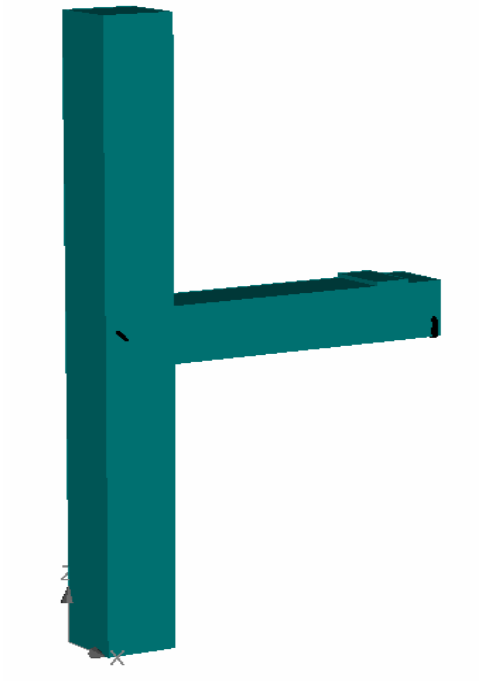

**Figure 4.7 Crack of 6mm width at 50mm displacement**

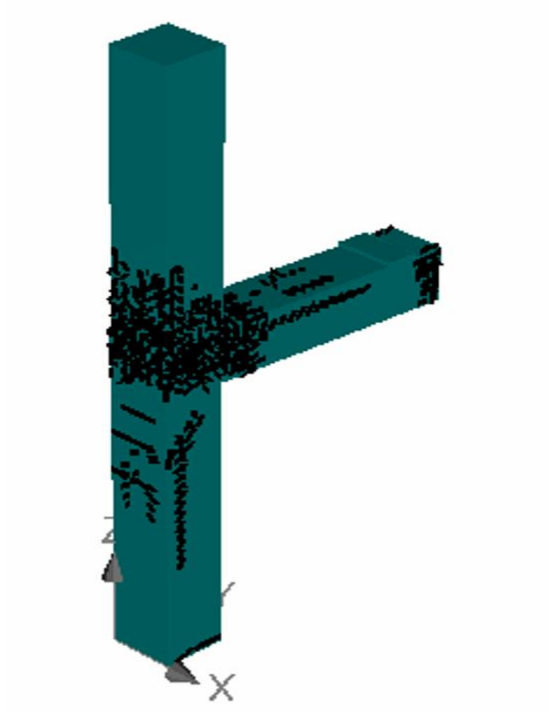

**Figure 4.8 Cracks of 0.1mm width at 50mm displacement**

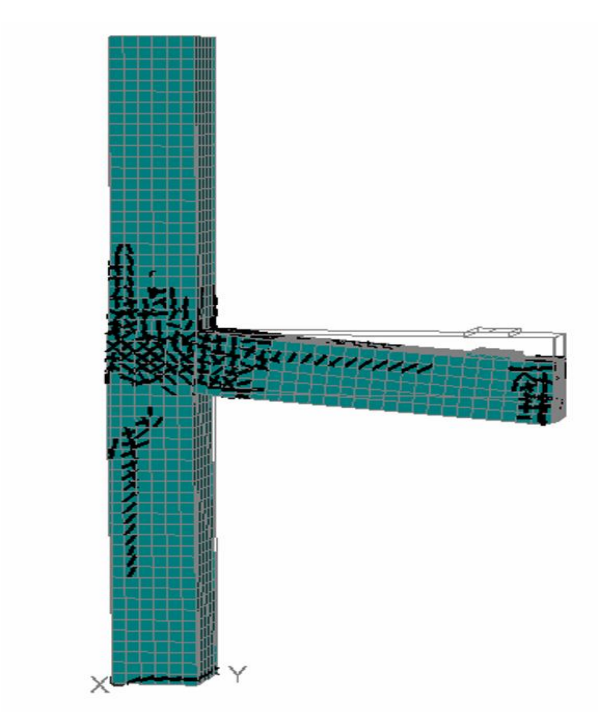

**Figure 4.9 Undeformed and deformed structure**

### 4.1.3 FE ANALYSIS OF CONFINED MODEL

The load and deflection for confined joint has been depicted through figure 4.7. It can be observed from this plot that the load-deformation behavior is same as of unconfined joint. The structure behaved linearly elastic up to the value of load around 31 KN at 1mm. At this point the minor cracks started to get generated at the joint. After this point there is a slight curvature in the plot and load started increasing with the deflection increments. When the load reached to the value of 92.1KN, the graph depicted non-linearity in its behavior with deflection of 16mm. Subsequently deflection started increasing without any significant increment in load; it has reached to the value of 33mm with the load value of 92.9KN. The maximum value of load has been observed to be 93.05KN at deflection of 35mm. Further, the load has been found to be 90.98 KN at the deflection of 50mm. There was 9% increase in ultimate load as compared to unconfined joint.

The loads at joint for different displacements have been shown in Table 4.3

**Table 4.3 FE Results of confined joint under monotonic loading**

| DEFLECTION [mm] | LOAD [KN] |
|---|---|
| 2 | 40.25 |
| 5 | 59.93 |
| 10 | 85.99 |
| 15 | 91.67 |
| 20 | 92.62 |
| 25 | 92.36 |
| 30 | 92.62 |
| 35 | 93.05 |
| 40 | 92.88 |
| 45 | 92.10 |
| 50 | 90.98 |

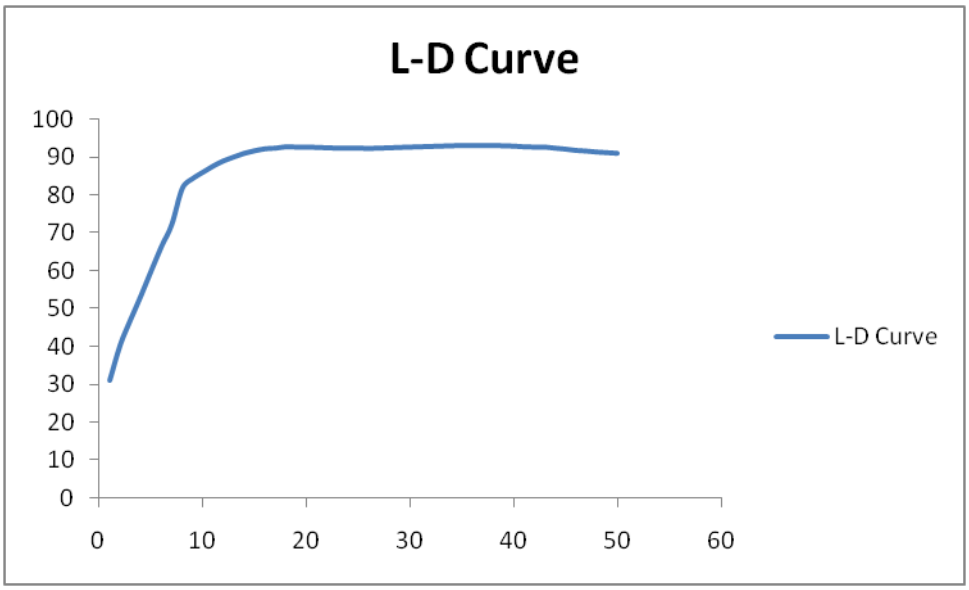


**Figure 4.10 Load deflection curve for confined joint**

## 4.1.4 CRACK PATTERNS

The variations of crack pattern with respect to size of crack and crack propagation have been plotted in Figure 4.11 - 4.16. A discussion on crack pattern plotted here has been presented here. The shape of un-deformed and deformed structure has been shown in Figure 4.17.

It had been observed that micro-cracks appeared in the structure when the joint is in linear zone. The first crack was observed at 6mm displacement at value of load 66.4 KN in the shape of shear crack as shown in Figure 4.11. This very small sized (actually invisible) crack appeared at beam-column joint.

The cracks spread over the joint of beam column throughout at displacement ductility $\mu_{\Delta}$=8.3. The crack at 17mm displacement has been shown in Figure 4.12.The maximum width of crack at 17mm displacement was observed as 2mm. The crack pattern at 35mm displacement with load value of 93.05KN is presented in Figure 4.13. The maximum width of crack at 35mm displacement has been observed as 5mm. This is the ultimate load level of the joint. First flexural cracks have been observed near beam column joint, but at this step shear cracks along with flexural crack have been observed on the beam and columns. No visible shear crack have been observed in linear zone, crack at the joint and on the beam near to the joint joined with the flexural cracks have been observed.

The number of cracks increase as the load is increases upto 93.05 kN at a displacement of 35 mm. These cracks spread all over the joint at displacement 50mm. It was observed that cracks have been propagating towards column. Maximum crack size at this level has been observed of 6mm width. The views showing the crack pattern with different crack size at 50mm displacement at load value of 90.98 KN are presented in Figure 4.15 & Figure 4.16. The beam- column joint with flexural cracks in almost all the beam and around the joint in column can be visualized. Fewer cracks have been seen at top and bottom of the column. Major damage has been noticed in the joint whereas beam experienced moderate damage and the column experienced minor damage.

Maximum width of crack observed in FE analysis has been shown in Table 4.4

**Table 4.4 Maximum crack width at different values of load and displacement**

| Displacement [mm] | Load [KN] | Maximum width of crack [mm] |
|---|---|---|
| 6 | 66.4 | 0.1 |
| 17 | 92.364 | 2 |
| 30 | 92.62 | 3 |
| 35 | 93.05 | 5 |
| 50 | 90.98 | 6 |

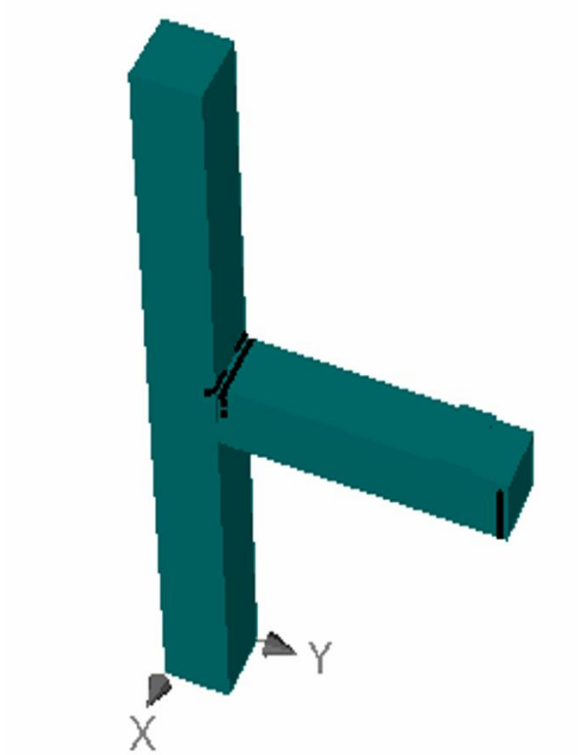


**Figure 4.11 First crack of 0.1 mm width at 6mm displacement**

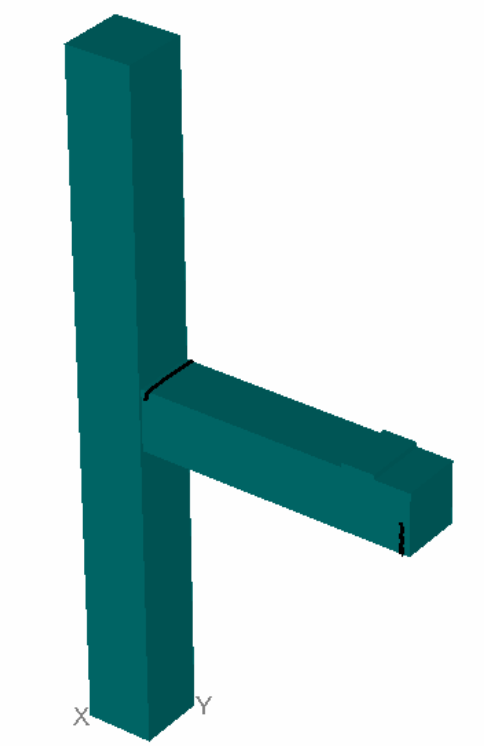


**Figure 4.12 Crack of 1mm width at 17mm displacement**

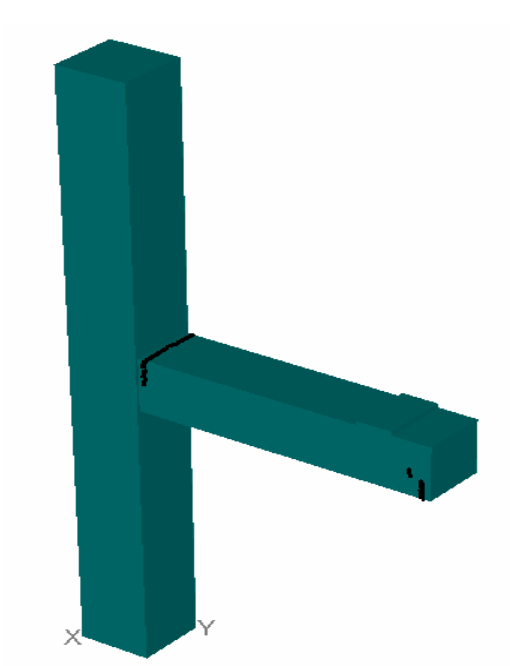


**Figure 4.13 Crack of 3mm width at 30mm displacement**

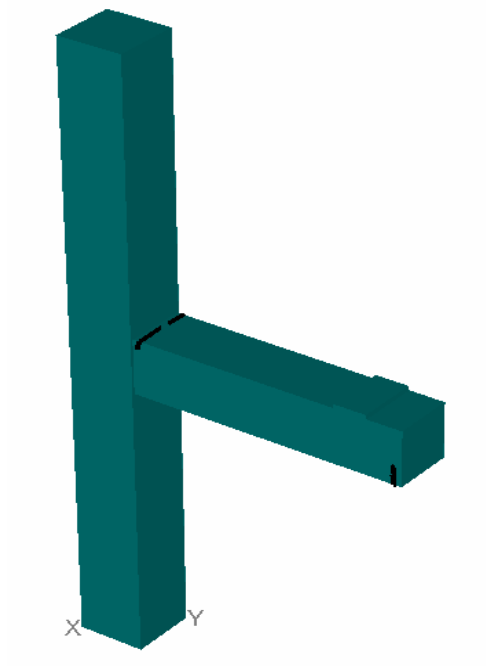


**Figure 4.14 Crack of 5mm width at 35mm displacement**


**Figure 4.15 Crack of 0.1 mm width at 50mm displacement**

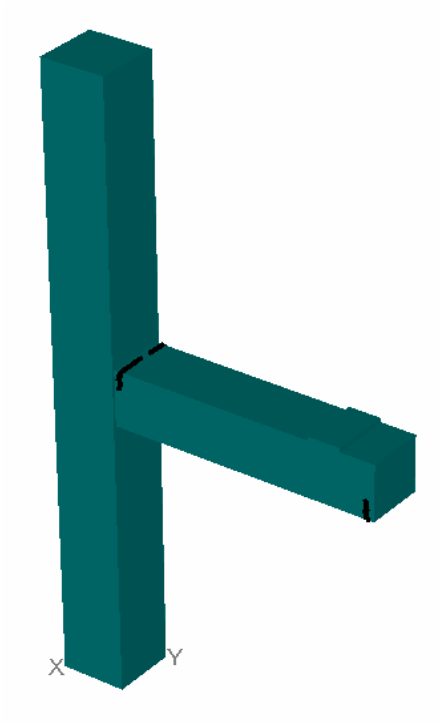


**Figure 4.16 Crack of 6mm width at 50mm displacement**


**Figure 4.17 Undeformed and deformed shape**

## 4.2 COMPARISON BETWEEN THE FE RESULTS OF UNCONFINED AND CONFINED JOINT UNDER MONOTONIC LOADING

Comparing the behavior of the confined and unconfined specimen it is observed that the load displacement envelop as shown in Figure 4.18 of confined joint is smoother and more stable as compared to unconfined joint. It has been depicted from figure that ultimate load carrying capacity of confined joint is 93.05KN at 35mm displacement and that of unconfined joint is 86.43KN at 17mm displacement with percentage increase of 9%. After the joint has taken the ultimate load, the load carrying capacity of confined joint remained almost same without any significant decrease, the load remained in the range of 91-93KN at displacement of 15-45mm whereas in unconfined joint the load carrying capacity decreased with increase in deflection after some value. Further the load taken by the confined and unconfined joint at 50mm displacement has been observed as 90.98 and 44.78 respectively. There was 47% increase in ductility in case of confined joint than unconfined joint.

The loads at joint for different displacements have been shown in Table 4.5

**Table 4.5 Comparison of FE Results of unconfined and confined joint under monotonic loading**

| DEFLECTION [mm] | LOAD [KN] | |
|---|---|---|
| | Unconfined | Confined |
| 2 | 36.97 | 40.25 |
| 5 | 53.02 | 59.93 |
| 10 | 74.75 | 85.99 |
| 15 | 86.1 | 91.67 |
| 20 | 85.35 | 92.62 |
| 25 | 82.33 | 92.36 |
| 30 | 66.62 | 92.62 |
| 35 | 56.62 | 93.05 |
| 40 | 50.79 | 92.88 |
| 45 | 47.81 | 92.10 |
| 50 | 44.78 | 90.98 |

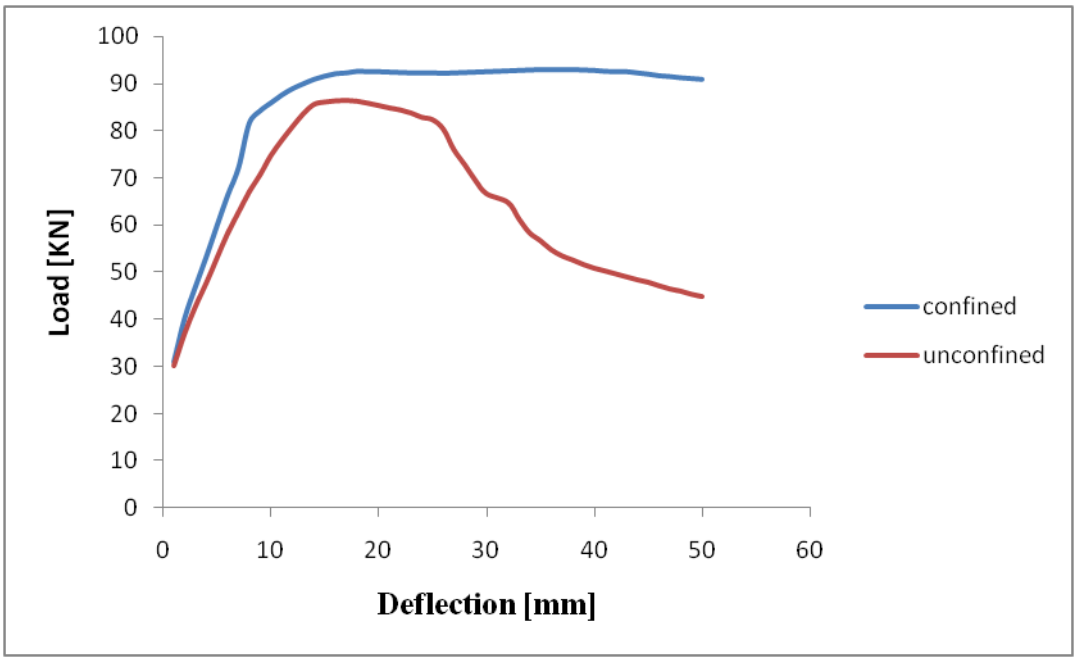


**Figure 4.18 Comparison of load deflection curves of confined and unconfined joint**

### 4.2.1 CRACK PATTERNS

The variations of crack pattern for both confined and unconfined joint have been plotted in Figure 4.19 - 4.22. A discussion on difference of crack pattern plotted here has been presented here.

The performance of confined joint in terms of initial cracks is better as fewer cracks are seen in confined joint. Figure 4.19 and 4.20 it has been observed that the confined joint experienced first crack at load value of 66.4 KN at 6mm displacement and unconfined joint at 53.02KN at 5mm displacement in the shape of shear crack but the behavior of T-joint remained almost same.

It was depicted that the shear cracks developed on joint face are lesser in confined joint than unconfined joint and intiated at higher load. The views showing the crack pattern with different crack size at 50mm displacement of the FE analysis at value of load 90.98 KN are presented in Figure 4.21 & Figure 4.22. It can be observed in Figure 4.21 & 4.22 that major damage has been noticed in the joint whereas beam experienced moderate damage and the column experienced minor damage in both cases. The cracks spread over the joint of beam column throughout at displacement ductility $\mu_{\Delta}$=4 in unconfined and $\mu_{\Delta}$=8.3 in confined joint.

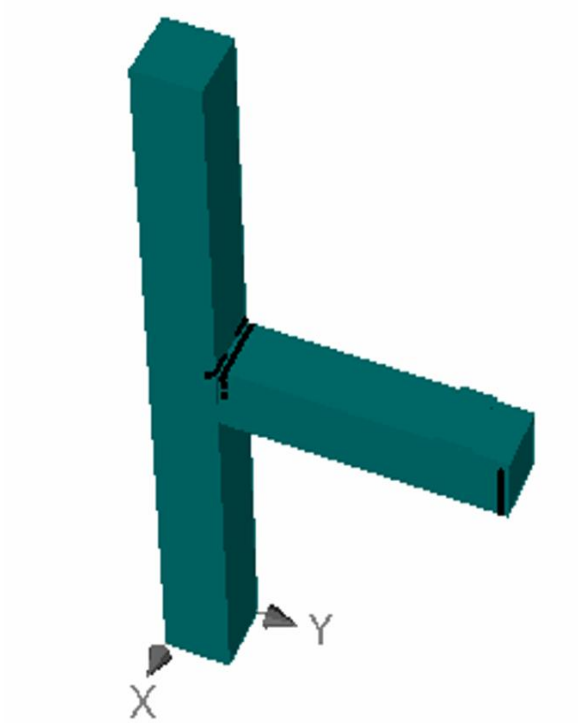


**Figure 4.19 First crack at 6mm of confined joint**

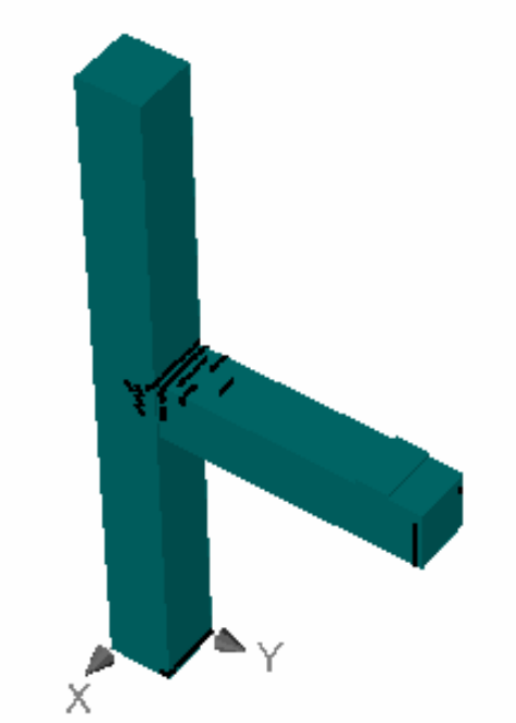


**Figure 4.20 First crack at 5mm of Unconfined joint**

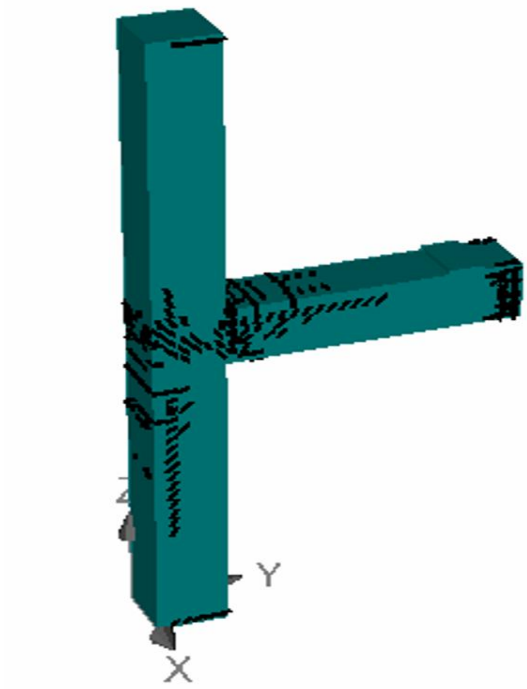


**Figure 4.21 All 0.1 mm crack of confined joint at 50mm displacement**

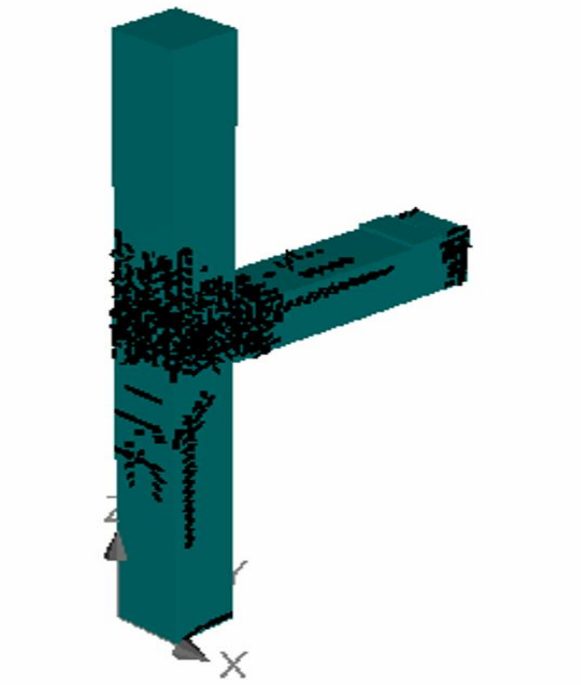


**Figure 4.22 All 0.1 mm crack of unconfined joint at 50mm displacement.**

## 4.3 BEHAVIOR OF BEAM COLUMN JOINT UNDER CYCLIC LOADING

Under cyclic loading, two RC T-joints has been modeled; one unconfined according to IS: 456-2000 and other confined according to IS: 13920-1993 (discussed in detail in chapter 3). Load has been applied in terms of prescribed deformation on the beam at distance of 1300mm from corner of the column and corresponding to the deformation, load taken by the joint are obtained.

### 4.3.1 FE ANALYSIS OF UNCONFINED MODEL

Hysteretic behavior obtained from FE analysis under cyclic load of the Unconfined Beam-Column Joint is shown in Figure 4.23. The joint is analyzed under displacement control and the loading is applied in terms of displacement in different number of cycles varies from 2 mm to 50 mm. The load increases upto 59.23 kN at a displacement of ± 10 mm. Load carrying capacity decreases to 43.45 kN at displacement of 15mm. As analysis continues, the load carrying capacity progressively decreases and the joint behave like a hinge at 9.693 kN load at 45mm displacement. The cracking with spalling of concrete at the joint and nearby places is also observed. The ultimate load taken by the joint is 59.23 kN at 10mm deflection. The loads at joint for different displacements have been shown in Table 4.6

**Table 4.6 FE Results of unconfined joint under cyclic loading**

| DEFLECTION [mm] | LOAD [KN] |
|---|---|
| 2 | 46.8 |
| 5 | 57.11 |
| 10 | 59.23 |
| 15 | 43.45 |
| 20 | 33.89 |
| 25 | 26.02 |
| 30 | 20.43 |
| 35 | 15.93 |
| 40 | 10.89 |
| 45 | 9.693 |
| 50 | 7.585 |

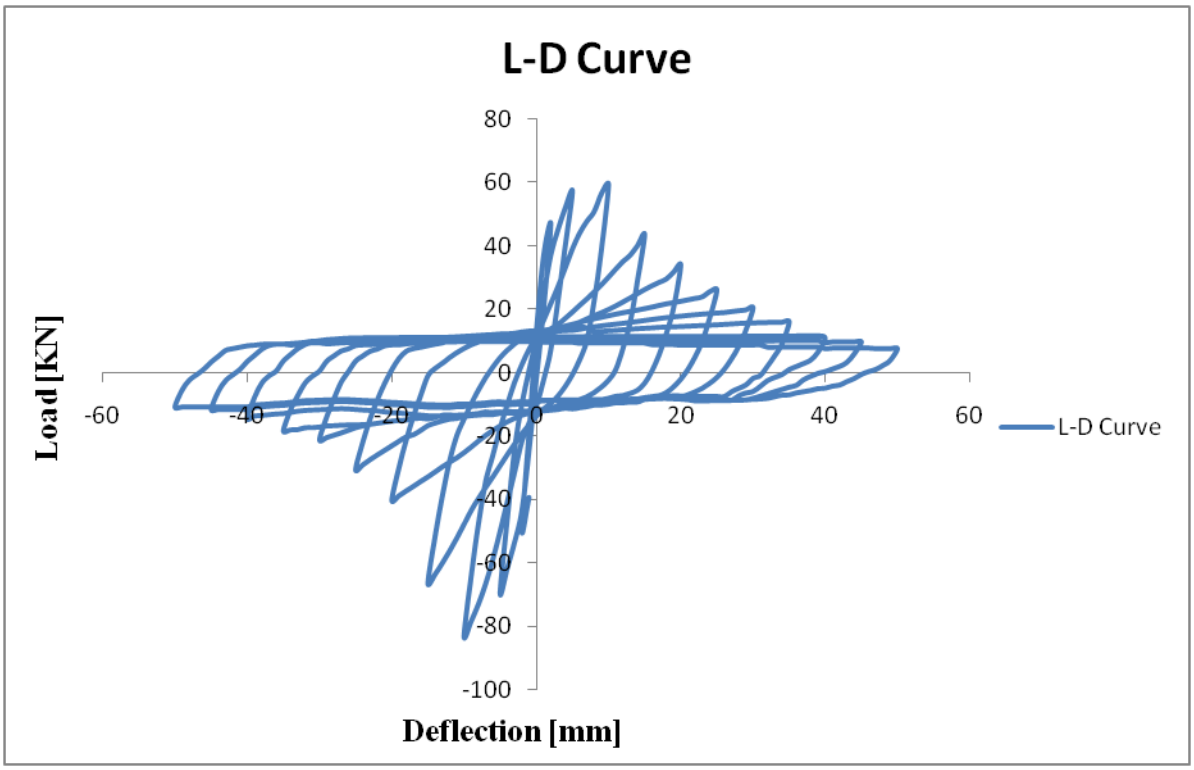


**Figure 4.23 Hysteresis behavior of unconfined joint**

### 4.3.2 CRACK PATTERNS

The variations of crack pattern with respect to size of crack and crack propagation have been plotted in Figure 4.24 - 4.30.

It had been observed that micro-cracks appeared in the structure when the joint is in linear zone. The first crack was observed at 2mm displacement at load value of 46.8 KN in the shape of flexural crack as shown in Figure 4.24. The maximum size of this crack depicted from FE analysis was 0.1mm. This very small sized (actually invisible) crack appeared at beam-column joint.

The crack at 10mm displacement has been shown in Figure 4.25.The maximum width of crack at 10mm displacement was observed as 1mm. This is the ultimate load level of the joint. Load carrying capacity of the joint decreases after 10 mm displacement. The number of cracks increases as the displacement increases up to 30 mm. Crack pattern at 15mm and 30mm displacement is presented in Figure 4.26 and Figure 4.27 respectively. The maximum width of

crack at 30mm displacement has been observed as 6mm. First flexural cracks have been observed near beam column joint, but at this step crack at the joint and on the beam near to the joint joined with the shear cracks have been observed. Crack pattern at 45mm displacement is presented in Figure 4.28.

These cracks spread all over the joint at displacement 50mm. It was observed that cracks have been propagating towards column. Maximum crack size at this level has been observed of 6mm width. The views showing the crack pattern with different crack size at 50mm displacement are presented in Figure 4.29 to Figure 4.31. The beam- column joint with flexural and shear cracks in almost all the beam and around the joint in column can be visualized. Fewer cracks have been seen at top and bottom of the column. Major damage has been noticed in the joint whereas beam experienced moderate damage and the column experienced minor damage.

Maximum width of crack observed in FE analysis has been shown in Table 4.7

**Table 4.7 Maximum crack width**

| Displacement | Load | Maximum crack width |
|---|---|---|
| 2 | 46.8 | 0.1 |
| 5 | 59.11 | 0.3 |
| 10 | 59.23 | 1 |
| 15 | 43.45 | 2 |
| 20 | 33.89 | 3.5 |
| 25 | 26.02 | 5 |
| 30 | 20.43 | 6 |
| 35 | 15.93 | 6 |
| 40 | 10.89 | 6 |
| 45 | 9.693 | 6 |
| 50 | 7.585 | 6.5 |

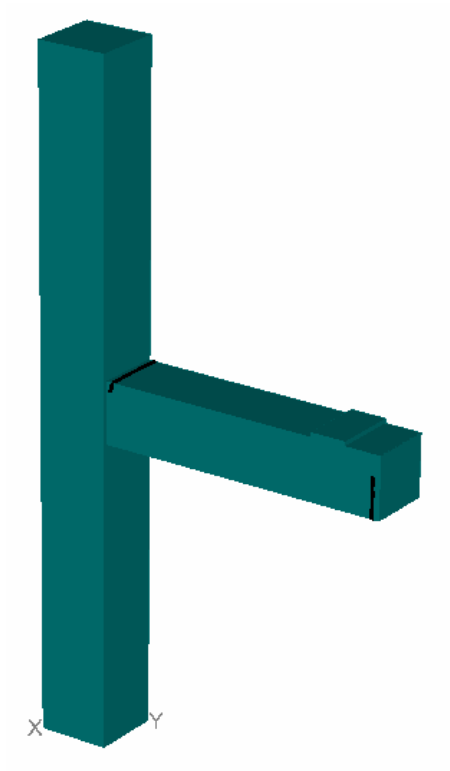

**Figure 4.24 0.1 mm crack at 2mm displacement**

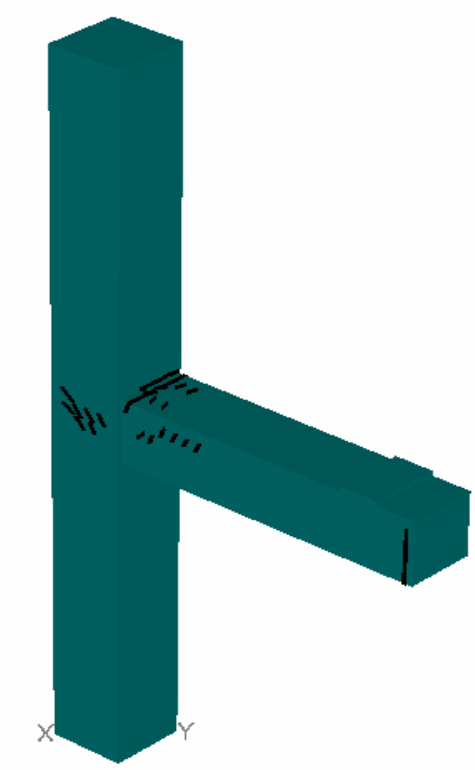

**Figure 4.25 1mm crack at 10mm displacement**

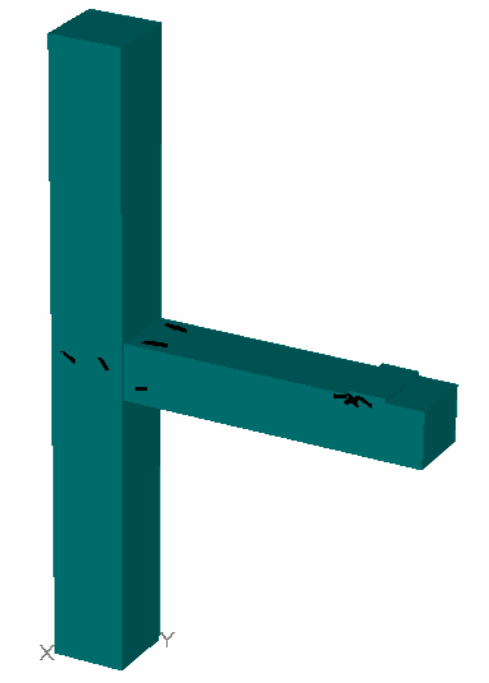

**Figure 4.26 6mm crack at 15 mm displacement**

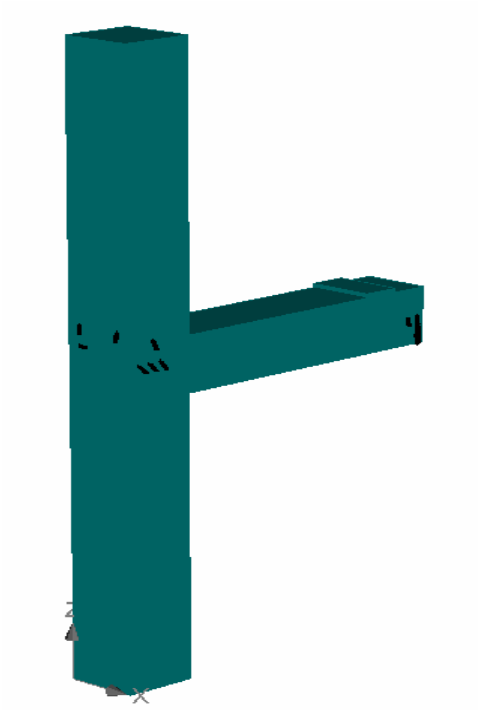

**Figure 4.27 6mm crack at 30mm displacement**

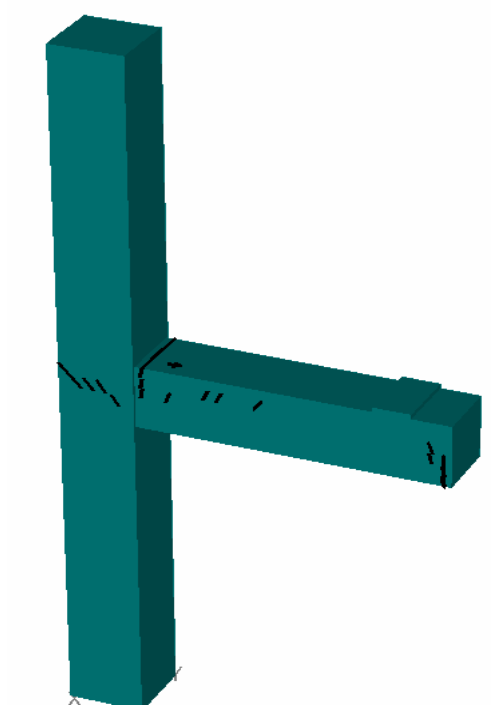

**Figure 4.28 6mm crack at 45mm displacement**

**Figure 4.29 6.5mm crack at 50mm dispacement**

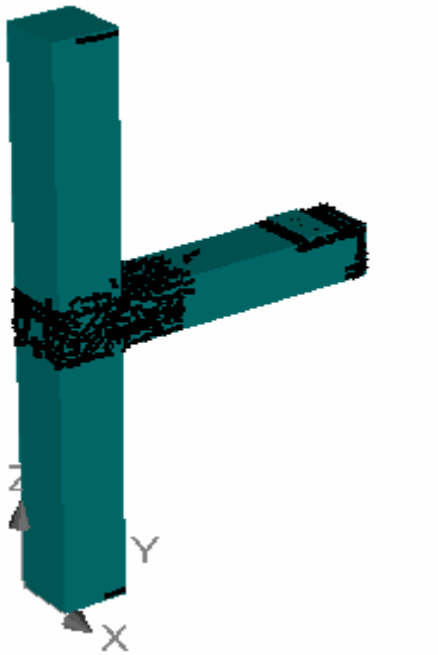


**Figure 4.30 0.1mm crack at 50mm displacement**

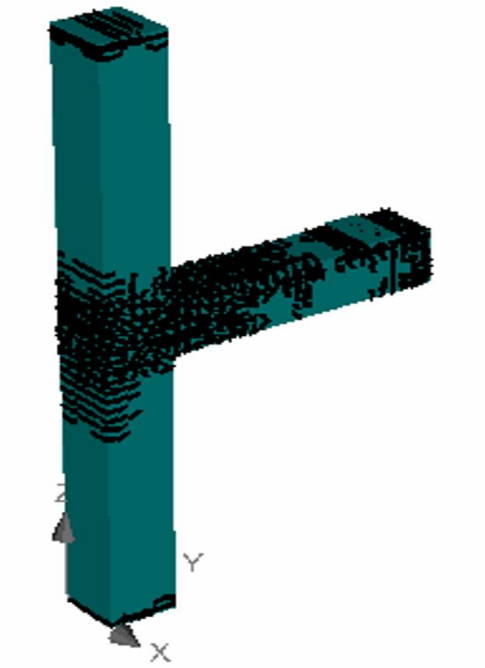


**Figure 4.31 all cracks at 50mm displacement**

### 4.3.3 FE ANALYSIS OF CONFINED MODEL

Hysteretic behavior obtained from FE analysis under cyclic load of the confined Beam-Column Joint is shown in Figure 4.32. The joint is analyzed under displacement control and the loading is applied in terms of displacement in different number of cycles varies from 2 mm to 50 mm. The load increases upto 63.72 kN at a displacement of ± 10 mm. Load carrying capacity decreases to 49.39 kN at displacement of 15mm. As analysis continues, the load carrying capacity progressively decreases and the joint behave like a hinge at 18.18 kN load at 45 mm displacement. The cracking with spalling of concrete at the joint and nearby places is also observed. The ultimate load taken by the joint is 63.72 kN at 10mm deflection. It was observed that there was 12% increase in ultimate load taken by confined joint than taken by unconfined. As expected, there was 54% increase in energy dissipation capacity in case of confined than unconfined joint. The loads at joint for different displacements have been shown in Table 4.8

**Table 4.8 FE Results of confined joint under cyclic loading**

| DEFLECTION [mm] | LOAD [KN] |
|---|---|
| 2 | 44.05 |
| 5 | 55.73 |
| 10 | 63.72 |
| 15 | 49.39 |
| 20 | 34.75 |
| 25 | 24.44 |
| 30 | 21.22 |
| 35 | 19.13 |
| 40 | 19.64 |
| 45 | 18.18 |
| 50 | 16.37 |

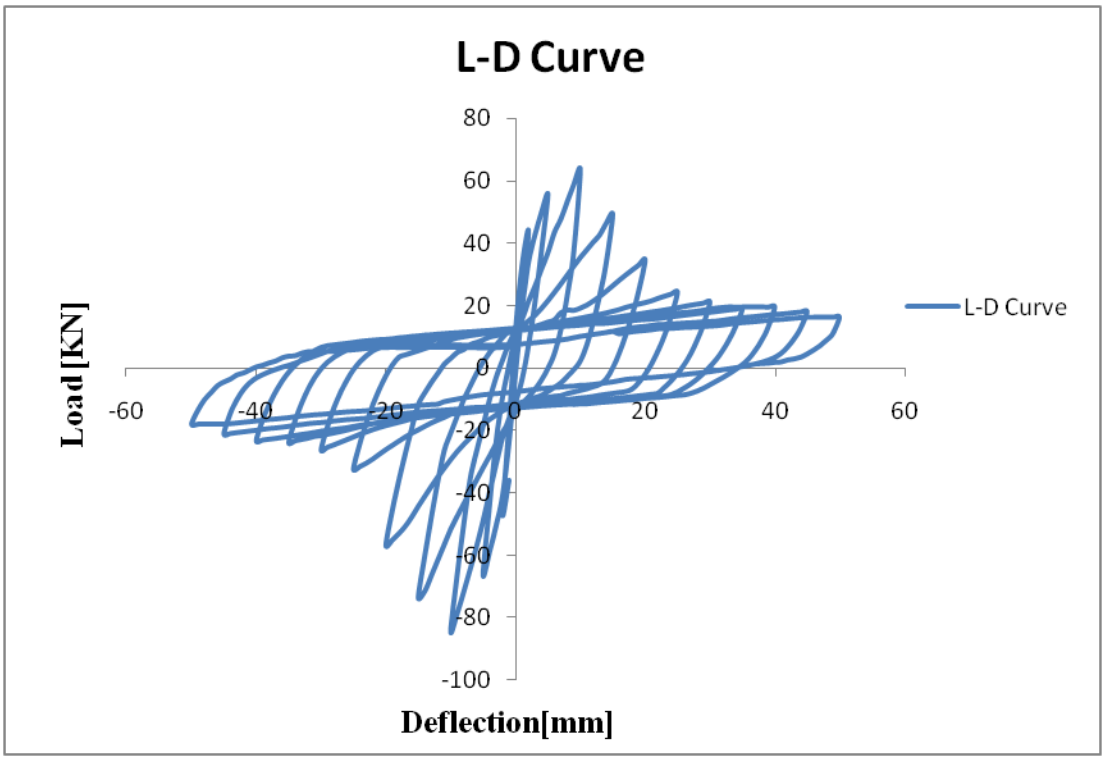


**Figure 4.32 Hysteresis behavior of confined joint**

### 4.3.4 CRACK PATTERNS

The variations of crack pattern with respect to size of crack and crack propagation have been plotted in Figure 4.33 - 4.40.

It had been observed that micro-cracks appeared in the structure when the joint is in linear zone. The first crack was observed at 2mm displacement at load value of 55.73 KN in the shape of flexural crack as shown in Figure 4.33. The maximum size of this crack depicted from FE analysis was 0.1mm. This very small sized (actually invisible) crack appeared at beam-column joint.

The crack at 10mm displacement has been shown in Figure 4.34.The maximum width of crack at 10mm displacement was observed as 1mm. This is the ultimate load level of the joint. Load carrying capacity of the joint decreases after 10 mm displacement. The number of cracks increases as the displacement increases up to 35 mm. Crack pattern at 15mm and 35mm displacement is presented in Figure 4.35 and figure 4.36 respectively. The maximum width of crack at 35mm displacement has been observed as 8mm. First flexural cracks have been

observed near beam column joint, but at this step crack at the joint and on the beam near to the joint joined with the shear cracks have been observed.

Crack pattern at 15mm and 35mm displacement is presented in Figure 4.37. These cracks spread all over the joint at displacement 50mm. It was observed that cracks have been propagating towards column. Maximum crack size at this level has been observed of 8mm width. The views showing the crack pattern with different crack size at 50mm displacement are presented in Figure 4.38 to Figure 4.40. The beam- column joint with flexural and shear cracks in almost all the beam and around the joint in column can be observed. Fewer cracks have been seen at top and bottom of the column. Major damage has been noticed in the joint whereas beam experienced moderate damage and the column experienced minor damage.

Maximum width of crack observed in FE analysis has been shown in Table 4.9

**Table 4.9 Maximum crack width**

| Displacement | Load | Maximum crack width |
|---|---|---|
| 2 | 44.05 | 0.1 |
| 5 | 55.73 | 0.2 |
| 10 | 63.72 | 1 |
| 15 | 49.39 | 2 |
| 20 | 34.75 | 3 |
| 25 | 24.44 | 5 |
| 30 | 21.22 | 6 |
| 35 | 19.13 | 6 |
| 40 | 19.64 | 7 |
| 45 | 18.18 | 7 |
| 50 | 16.37 | 8.5 |

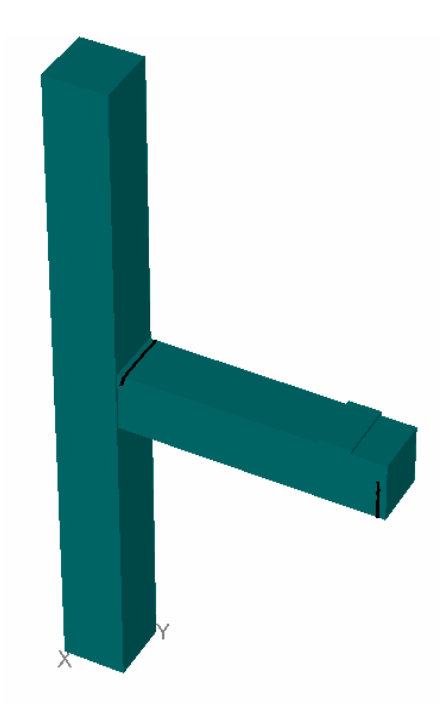

**Figure 4.33 0.1 mm crack at 2mm displacement**

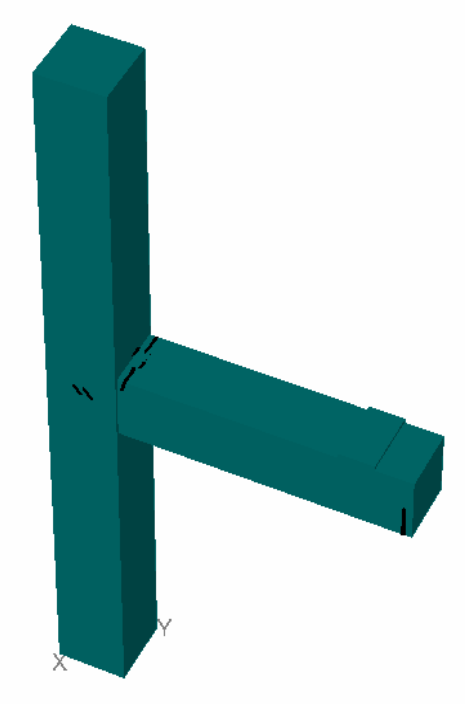

**Figure 4.34 1mm crack at 10mm displacement**

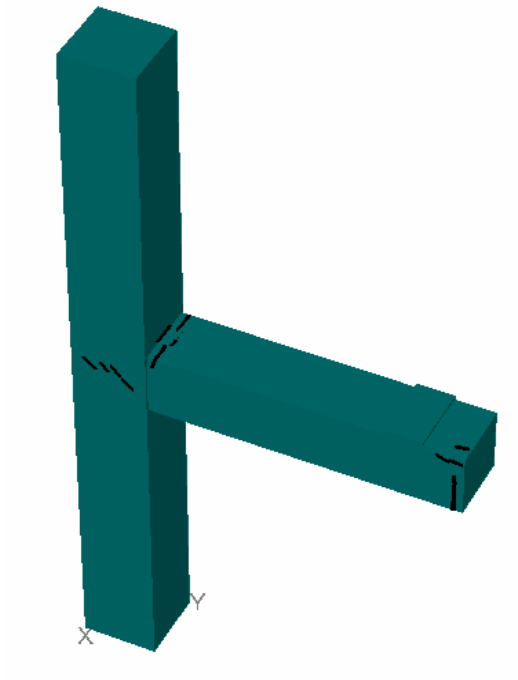

**Figure 4.35 2mm crack at 15 mm displacement**

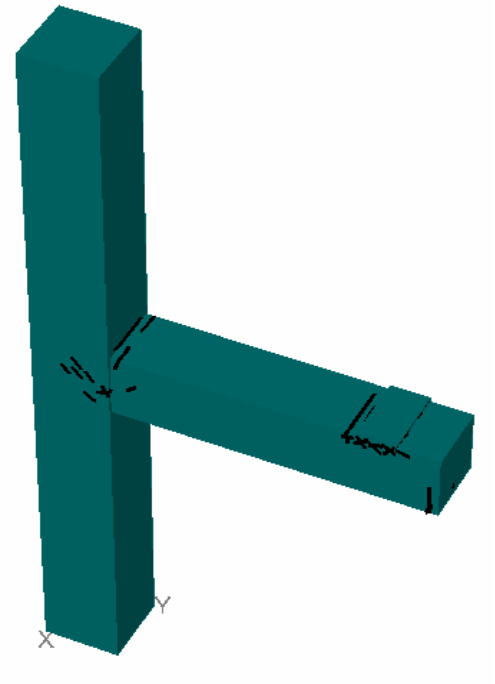

**Figure 4.36 6mm crack at 35mm displacement**

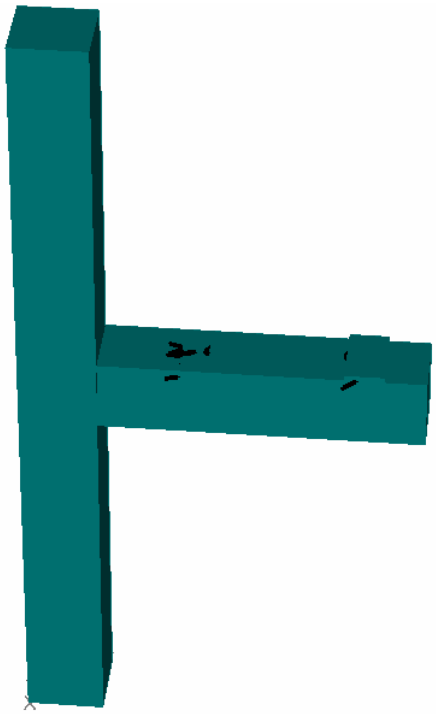

**Figure 4.37 7mm crack at 45mm displacement**

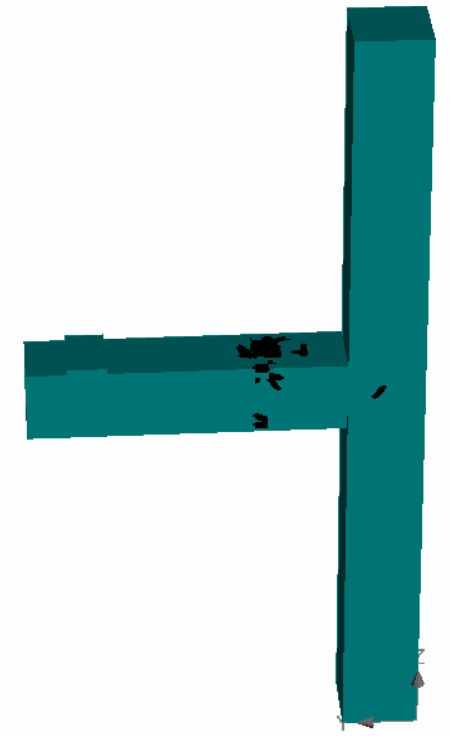

**Figure 4.38 7mm crack at 50mm dispacement**

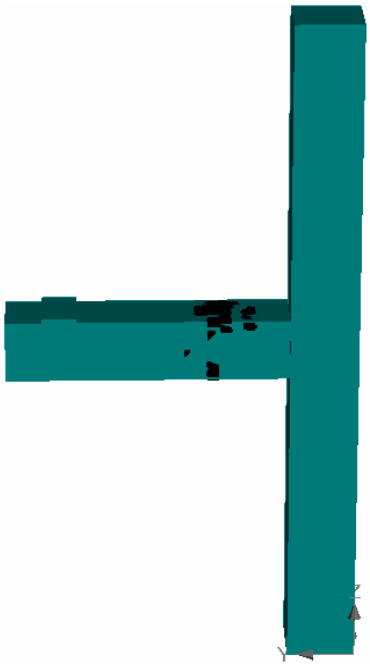

**Figure 4.39 8mm crack at 50mm displacement**

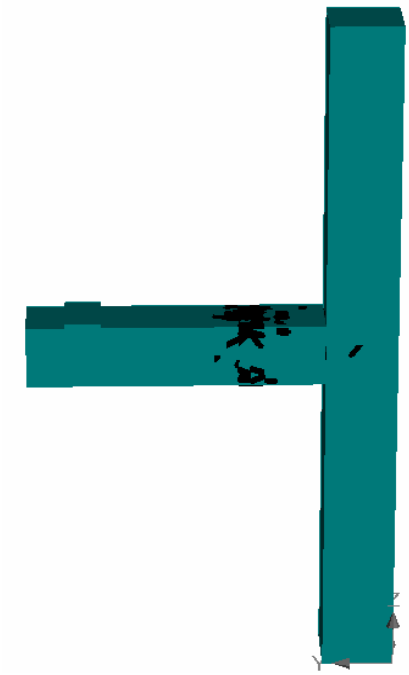

**Figure 4.40 8.5mm crack at 50mm dispacement**

## 4.4 COMPARISON BETWEEN THE FE MODEL AND THE EXPERIMENTAL RESULTS OF THE CONTROL JOINT

### 4.4.1 Comparison of results of unconfined joint

Results of analytical modeling are compared with Experimental Results of Unconfined Joint [4]. The maximum value of load at different displacement has been presented in Table 4.10.

**Table 4.10 Comparison of Experimental and FE Results of unconfined joint**

| DEFLECTION [mm] | LOAD [KN] | |
|---|---|---|
| | Experimental | Analytical |
| 2 | 11.3 | 46.8 |
| 5 | 23.9 | 57.11 |
| 10 | 39.3 | 59.23 |
| 15 | 49.4 | 43.45 |
| 20 | 53.7 | 33.89 |
| 25 | 52.8 | 26.02 |
| 30 | 45.7 | 20.43 |
| 35 | 39.3 | 15.93 |
| 40 | 31.9 | 10.89 |
| 45 | 30.8 | 9.69 |
| 50 | 28.3 | 7.585 |
| 60 | 28.6 | - |
| 75 | 30.3 | - |
| 90 | 22.9 | - |
| 100 | 25.5 | - |

When results of FE analysis are compared with the experimental results [4], the results vary but the behavior remains almost same. The analytical results vary due to actual experimental conditions and conditions of fixed end. The modeling parameters are constant for the analytical specimen but for actual specimen some parameters are different. The same model for concrete has been modeled but the actual behavior may not resemble exactly the same. Considerable increase in strength of around 11% was shown by analytical modeling. The maximum loads attained in experimental and analytical are 52.8KN and 59.23KN respectively. As expected, there was 54% increase in energy dissipation capacity in case of confined than unconfined joint. Hysteresis response of unconfined joint both experimentally and analytically is shown in figure 4.41 and figure 4.42.

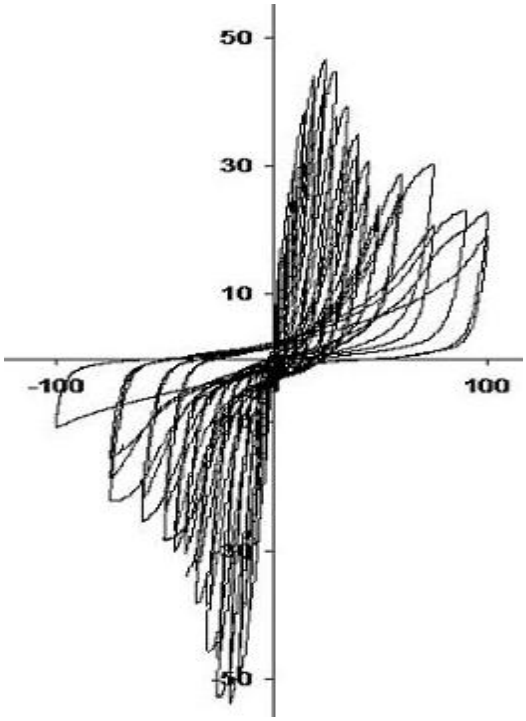


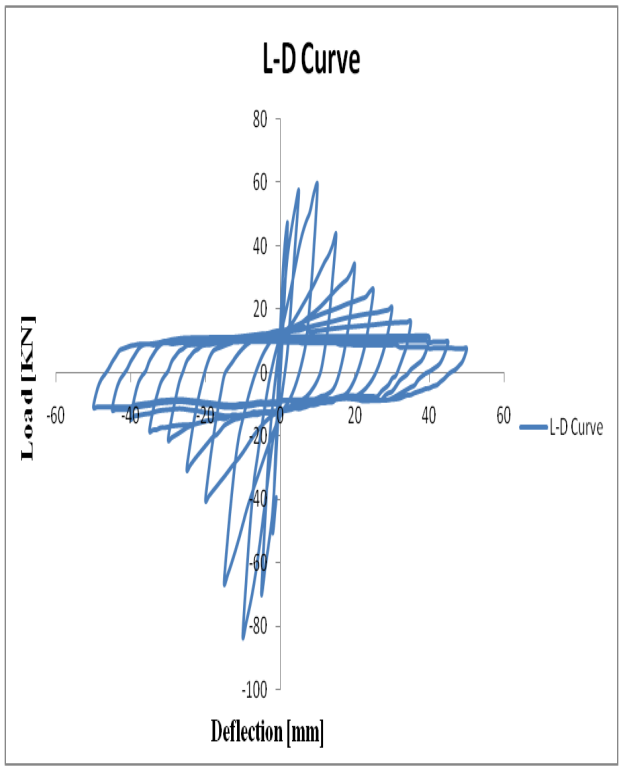


**Figure 4.41 Experimental hysteresis response** **Figure 4.42 Analytical hysteresis response**

### 4.4.2 Comparison of results of confined joint

Results of analytical modeling are compared with Experimental Results of confined Joint [4]. The maximum value of load at different displacement has been presented in Table 4.9.

**Table 4.11 Comparison of Experimental and FE Results of confined joint**

| DEFLECTION [mm] | LOAD [KN] | |
|---|---|---|
| | Experimental | Analytical |
| 2 | 11.9 | 44.05 |
| 5 | 24.6 | 55.73 |
| 10 | 42.4 | 63.72 |
| 15 | 54.7 | 49.39 |
| 20 | 59.8 | 34.75 |
| 25 | 61.7 | 24.44 |
| 30 | 61.6 | 21.22 |
| 35 | 61.5 | 19.13 |
| 40 | 61 | 19.64 |
| 45 | 56.4 | 18.18 |
| 50 | 47.7 | 16.37 |
| 60 | 43.9 | - |
| 75 | 39.2 | - |
| 90 | 36.2 | - |
| 100 | 34.4 | - |

When results of FE analysis are compared with the experimental results [4], the results vary but the behavior remains almost same. The analytical results vary due to actual experimental conditions and conditions of fixed end. The modeling parameters are constant for the analytical specimen but for actual specimen some parameters are different. The same model for concrete has been assumed but the actual behavior may not resemble exactly the same. Considerable increase in strength of around 4% was shown by analytical modeling. The maximum loads

attained in experimental and analytical are 61.6KN and 63.72KN respectively. Hysteresis response of unconfined joint both experimentally and analytically is shown in Figure 4.43 and Figure 4.44.

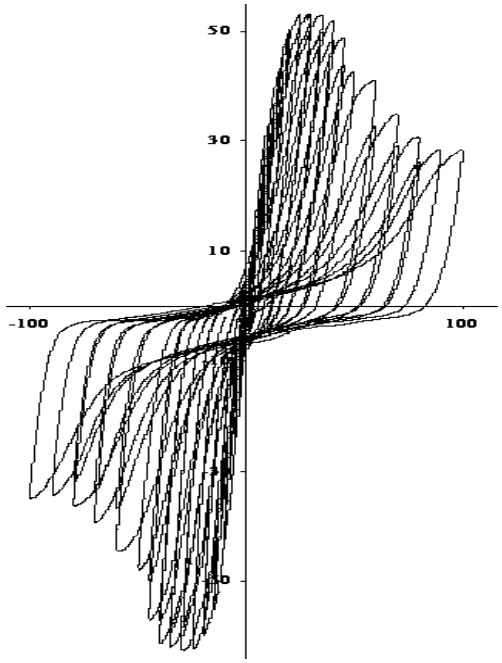


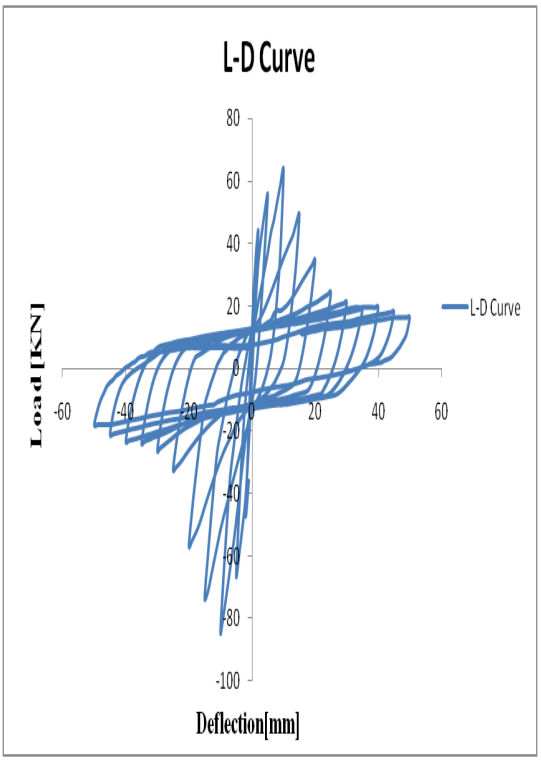


**Figure 4.43 Experimental hysteresis response**

**Figure 4.44 Analytical hysteresis response**

# Chapter 5 RESULTS AND DISCUSSIONS

## (Stressed Retrofitted Joint)

### 5.1 FE ANALYSIS OF 90% STRESSED UNCONFINED JOINT

Hysteretic behavior obtained from FE analysis under cyclic load of the 90% stressed retrofitted unconfined Beam-Column Joint is shown in Figure 5.1. The joint is analyzed under displacement control and the loading is applied in terms of displacement in different number of cycles varies from 2 mm to 50 mm. After strengthening with GFRP wrapping the joint showed the load of 45.12 kN at a displacement of ± 10 mm. Strengthened joint demonstrated significant performance in terms of restoring the original strength, yet original strength cannot be achieved. As analysis continues, the load carrying capacity progressively decreases to 36.8 kN at 15mm displacement and the joint behave like a hinge at 18.37 kN load at 45mm displacement. The ultimate load taken by the joint is 49.12 kN at 10mm deflection. Original strength was restored upto 82%. The loads at joint for different displacements have been shown in Table 5.1

**Table 5.1 FE Results of 90% stressed retrofitted unconfined joint under cyclic loading**

| DEFLECTION [mm] | LOAD [KN] |
|---|---|
| 2 | 38.98 |
| 5 | 43.86 |
| 10 | 45.12 |
| 15 | 36.8 |
| 20 | 29.96 |
| 25 | 24.87 |
| 30 | 22.97 |
| 35 | 22.21 |
| 40 | 20.04 |
| 45 | 18.37 |
| 50 | 16.87 |

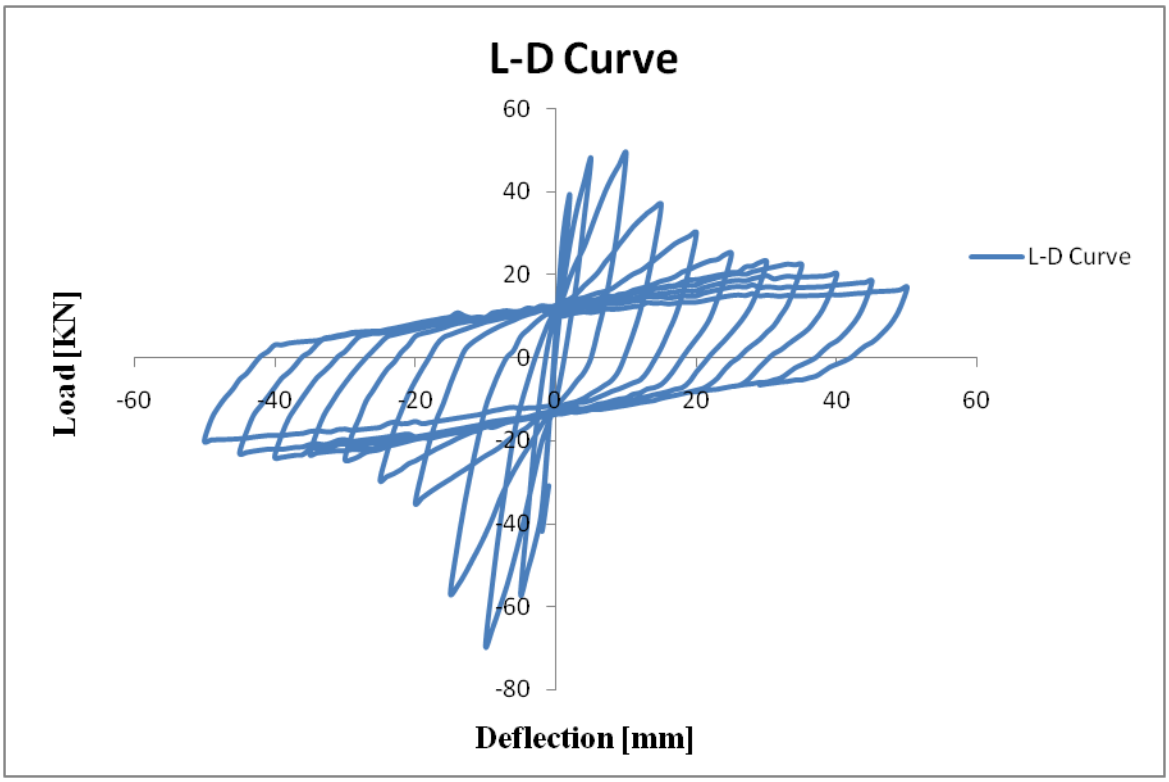


**Figure 5.1 Hysteresis behavior of 90% stressed retrofitted unconfined joint**

### 5.1.1 CRACK PATTERNS

The variations of crack pattern with respect to size of crack and crack propagation have been plotted in Figure 5.2 - 5.8.

It had been observed that micro-cracks appeared in the structure when the joint is in linear zone. After strengthening with GFRP wrapping, initially the flexural cracks were developed at the joint on the beam. The first crack was observed at 2mm displacement at load value of 38.98 KN in the shape of flexural crack as shown in Figure 5.2. The maximum size of this crack depicted from FE analysis was 0.1mm. This very small sized (actually invisible) crack appeared at beam-column joint.

The crack at 10mm displacement has been shown in Figure 5.3. The maximum width of crack at 10mm displacement was observed as 1mm. This is the ultimate load level of the joint. Load carrying capacity of the joint decreases after 10 mm displacement. The number of cracks increases as the displacement increases up to 35 mm. Crack pattern at 15mm and 35mm displacement is presented in Figure 5.4 and Figure 5.5 respectively. The maximum width of

crack at 35mm displacement has been observed as 5mm. First flexural cracks have been observed near beam column joint, but at this step crack at the joint and on the beam near to the joint joined with the shear cracks have been observed. Crack pattern at 45mm displacement is presented in Figure 5.6.

These cracks spread all over the joint at displacement 50mm. It was observed that cracks have been propagating towards column. Maximum crack size at this level has been observed of 6mm width. The views showing the crack pattern with different crack size at 50mm displacement are presented in Figure 5.7 to Figure 5.8. The beam- column joint with flexural and shear cracks in almost all the beam and around the joint in column can be visualized. Fewer cracks have been seen at top and bottom of the column. Major damage has been noticed in the joint whereas beam experienced moderate damage and the column experienced minor damage.

Maximum width of crack observed in FE analysis has been shown in Table 5.2.

**Table 5.2 Maximum crack width**

| Displacement | Load | Maximum crack width |
|---|---|---|
| 2 | 38.98 | 0.1 |
| 5 | 47.86 | 0.5 |
| 10 | 49.12 | 1 |
| 15 | 36.8 | 2 |
| 20 | 29.96 | 2.5 |
| 25 | 24.87 | 4 |
| 30 | 22.97 | 4.5 |
| 35 | 22.21 | 5 |
| 40 | 20.04 | 5 |
| 45 | 18.37 | 6 |
| 50 | 16.87 | 6 |

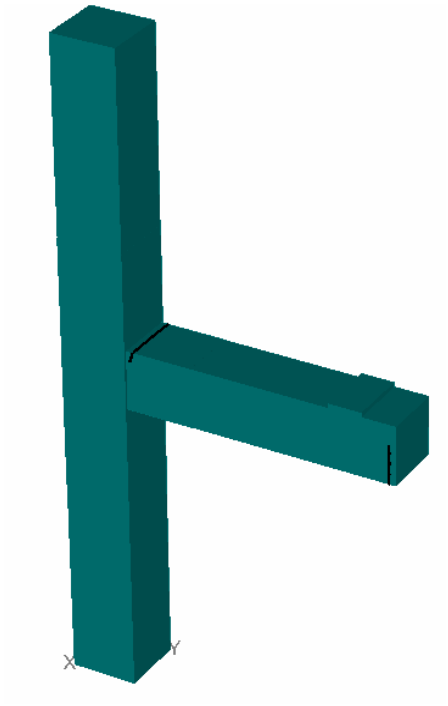

**Figure 5.2 0.1 mm crack at 2mm displacement**

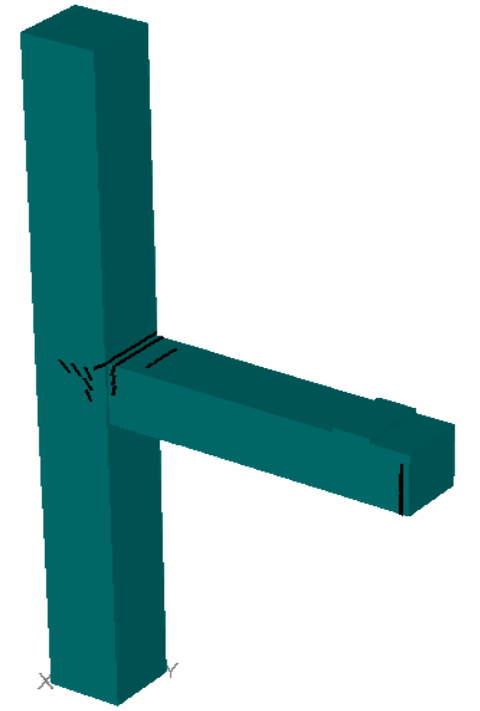

**Figure 5.3 1mm crack at 10mm displacement**

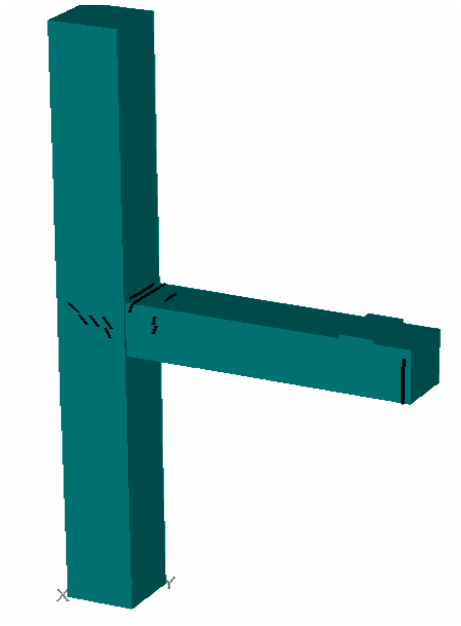

**Figure 5.4 2mm crack at 15mm displacement**

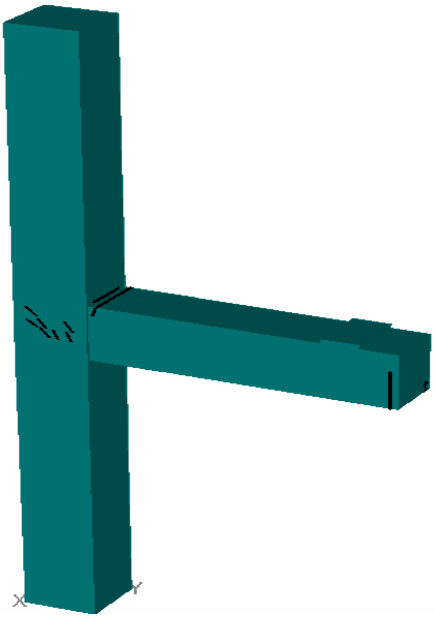

**Figure 5.5 5mm crack at 35mm displacement**

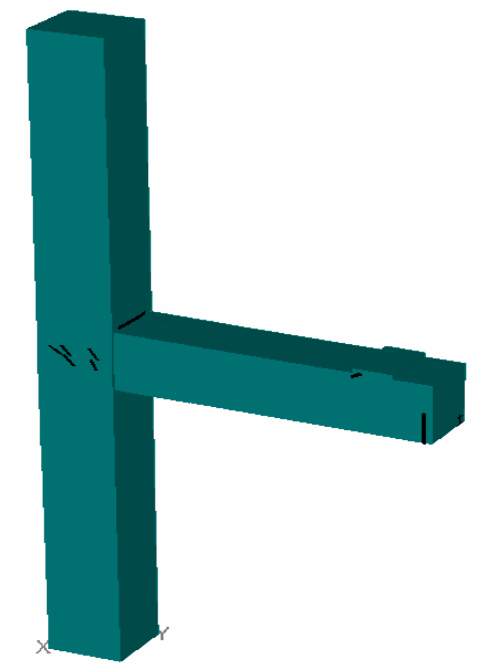

**Figure 5.6 6 mm crack at 40mm displacement**

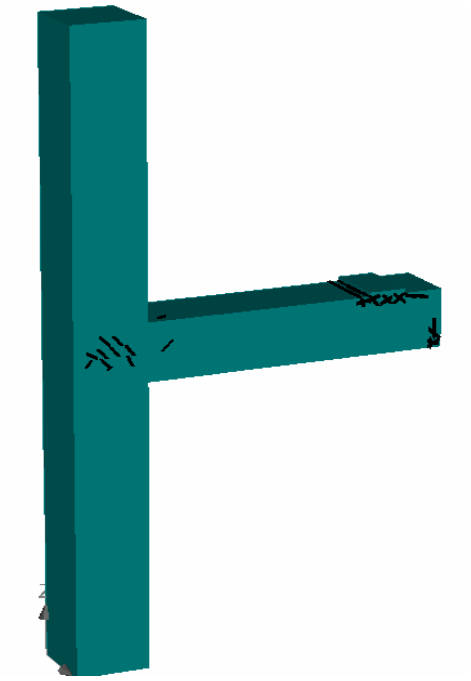

**Figure 5.7 6mm crack at 50mm displacement**

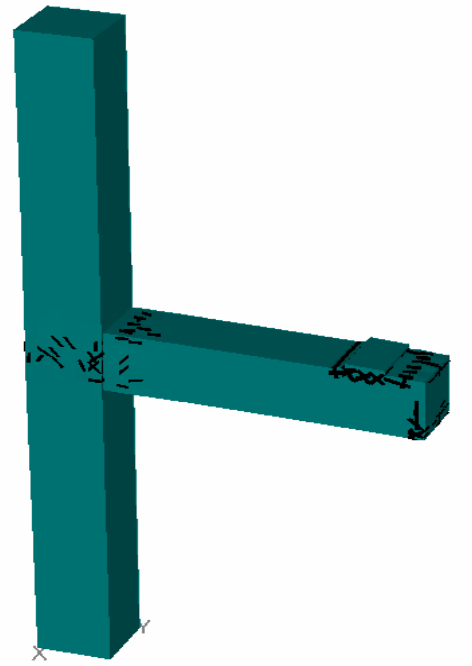

**Figure 5.8 1 mm crack at 50mm displacement**

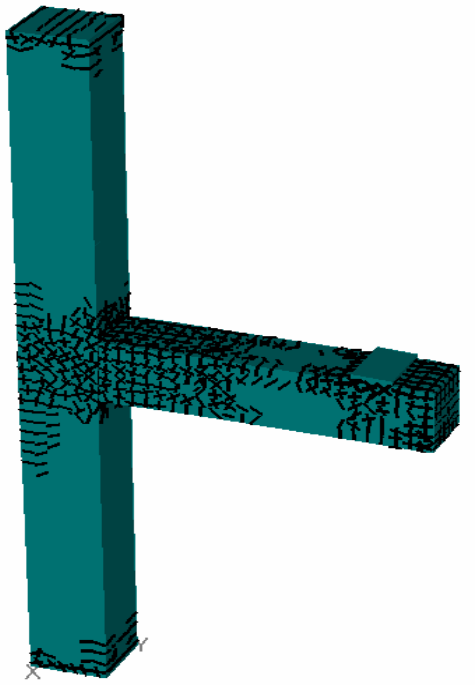

**Figure 5.9 All cracks at 50mm displacement**

## 5.2 FE ANALYSIS OF 90% STRESSED CONFINED JOINT

Hysteretic behavior obtained from FE analysis under cyclic load of the 90% stressed retrofitted confined Beam-Column Joint is shown in Figure 5.10. The joint is analyzed under displacement control and the loading is applied in terms of displacement in different number of cycles varies from 2 mm to 50 mm. After strengthening with GFRP wrapping the joint showed the load of 55.89 kN at a displacement of ± 10 mm. Strengthened joint demonstrated significant performance in terms of restoring the original strength, yet original strength cannot be achieved. As analysis continues, the load carrying capacity progressively decreases to 44.43 kN at 15mm displacement and the joint behave like a hinge at 17.85 kN load at 45mm displacement. The ultimate load taken by the joint is 55.89 kN at 10mm deflection. Original strength was restored upto 85%. There was no significant change in energy dissipation in confined joint than unconfined joint. The loads at joint for different displacements have been shown in Table 5.3

**Table 5.3 FE Results of 90% stressed retrofitted confined joint under cyclic loading**

| DEFLECTION [mm] | LOAD [KN] |
|---|---|
| 2 | 38.93 |
| 5 | 49.92 |
| 10 | 55.89 |
| 15 | 44.43 |
| 20 | 37.4 |
| 25 | 29.51 |
| 30 | 26.32 |
| 35 | 24.11 |
| 40 | 22.28 |
| 45 | 17.85 |
| 50 | 17.07 |

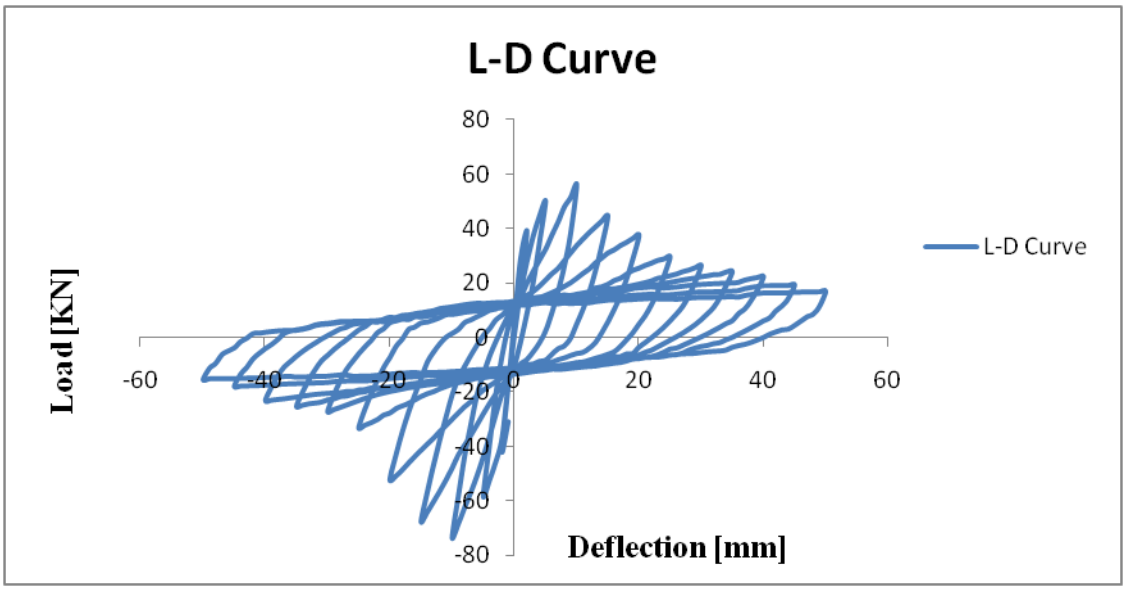


**Figure 5.10 Hysteresis behavior of 90% stressed retrofitted confined joint**

### 5.2.1 CRACK PATTERNS

The variations of crack pattern with respect to size of crack and crack propagation have been plotted in Figure 5.11 - 5.18.

It had been observed that micro-cracks appeared in the structure when the joint is in linear zone. After strengthening with GFRP wrapping, initially the flexural cracks were developed at the joint on the beam. The first crack was observed at 2mm displacement at load value of 38.98 KN in the shape of flexural crack as shown in Figure 5.11. The maximum size of this crack depicted from FE analysis was 0.1mm. This very small sized (actually invisible) crack appeared at beam-column joint.

The crack at 10mm displacement has been shown in Figure 5.12. The maximum width of crack at 10mm displacement was observed as 1mm. This is the ultimate load level of the joint. Load carrying capacity of the joint decreases after 10 mm displacement. The number of cracks increases as the displacement increases up to 35 mm. Crack pattern at 15mm and 35mm displacement is presented in Figure 5.13 and Figure 5.14 respectively. The maximum width of crack at 35mm displacement has been observed as 5mm. First flexural cracks have been observed near beam column joint, but at this step crack at the joint and on the beam near to the joint joined with the shear cracks have been observed. Crack pattern at 45mm displacement is

presented in Figure 5.15.

These cracks spread all over the joint at displacement 50mm. It was observed that cracks have been propagating towards column. Maximum crack size at this level has been observed of 6mm width. The views showing the crack pattern with different crack size at 50mm displacement are presented in Figure 5.16 to Figure 5.18. The beam- column joint with flexural and shear cracks in almost all the beam and around the joint in column can be visualized. Fewer cracks have been seen at top and bottom of the column. Major damage has been noticed in the joint whereas beam experienced moderate damage and the column experienced minor damage.

Maximum width of crack observed in FE analysis has been shown in Table 5.4

**Table 5.4 Maximum crack width**

| Displacement | Load | Maximum crack width |
|---|---|---|
| 2 | 38.93 | 0.1 |
| 5 | 49.92 | 0.5 |
| 10 | 55.89 | 1 |
| 15 | 44.43 | 1.5 |
| 20 | 37.4 | 2 |
| 25 | 29.51 | 2 |
| 30 | 26.32 | 3.5 |
| 35 | 24.11 | 5 |
| 40 | 22.28 | 5 |
| 45 | 17.85 | 5 |
| 50 | 17.07 | 5 |

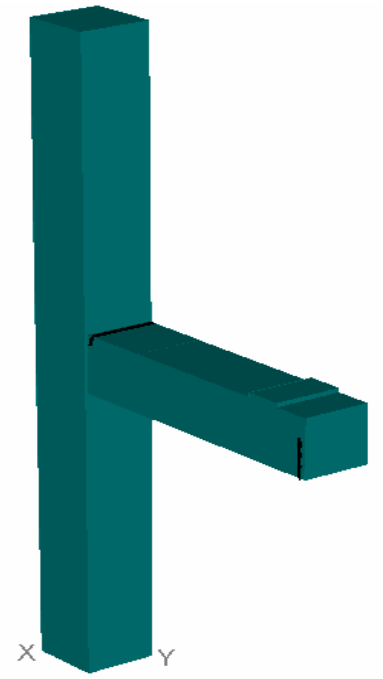


**Figure 5.11 0.1 mm crack at 2mm displacement**

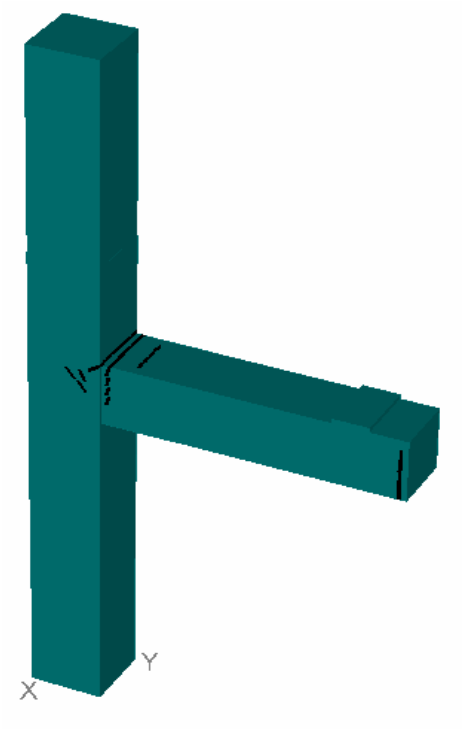


**Figure 5.12 1mm crack at 10mm displacement**

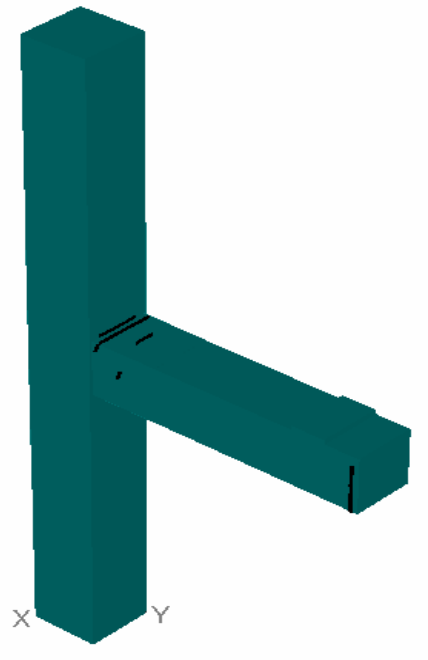


**Figure 5.13 1.5 mm crack at 15mm displacement**

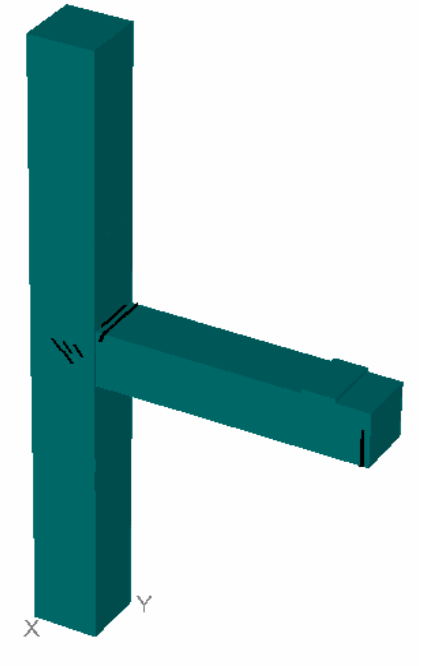


**Figure 5.14 5mm crack at 35mm displacement**

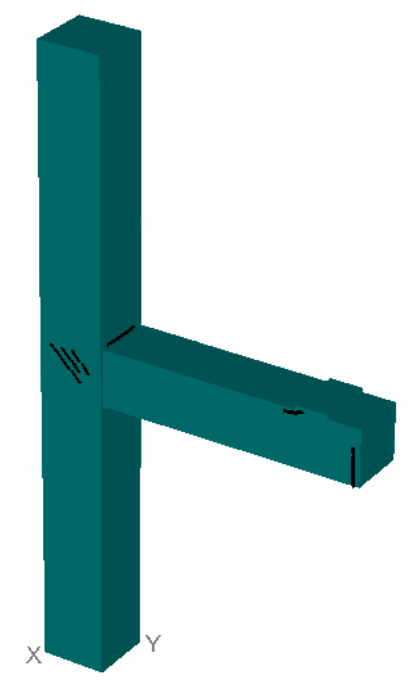


**Figure 5.15 5 mm crack at 45mm displacement**

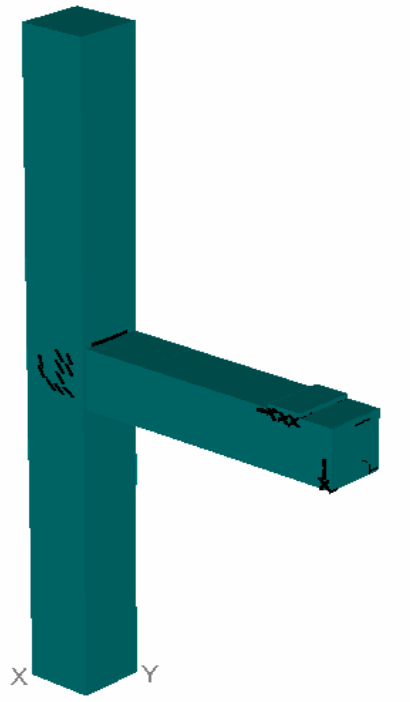


**Figure 5.16 5mm crack at 50mm displacement**

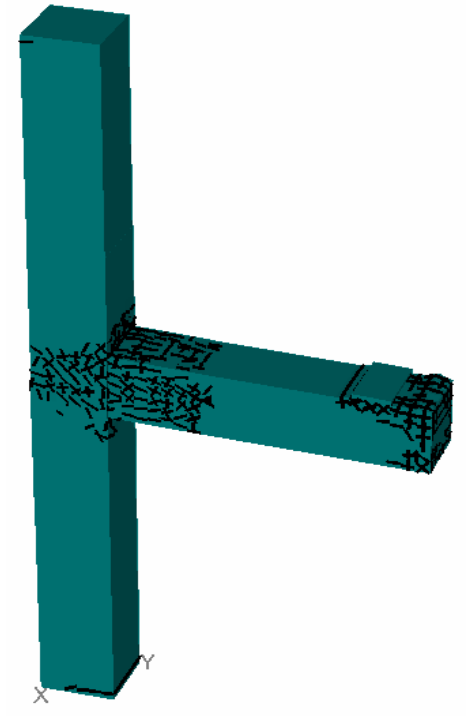


**Figure 5.17 0.1 mm crack at 50mm displacement**

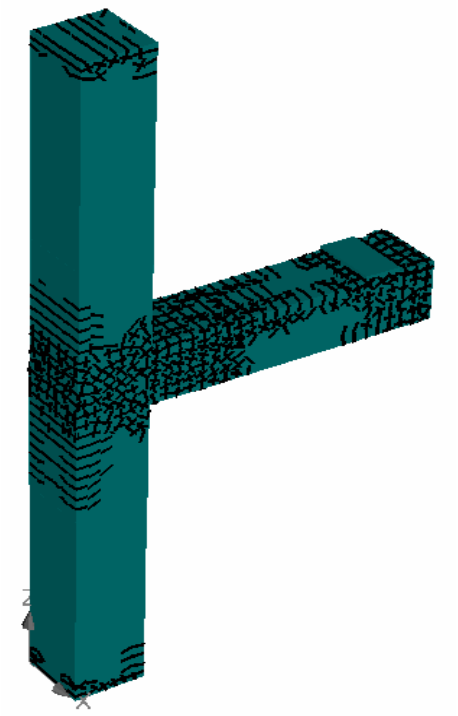

**Figure 5.18 All crack at 50mm displacement**

## 5.3 COMPARISON BETWEEN THE FE MODEL AND THE EXPERIMENTAL RESULTS OF THE STRESSED RETROFITTED JOINT

### 5.3.1 Comparison of results of (90% stressed) unconfined joint

Results of analytical modeling are compared with Experimental Results of Unconfined Joint [4]. The maximum value of load at different displacement has been presented in Table 5.5.

**Table 5.5 Comparison of Experimental and FE Results of unconfined joint**

| DEFLECTION [mm] | LOAD [KN] | |
|---|---|---|
| | Experimental | Analytical |
| 2 | 8.6 | 38.98 |
| 5 | 15.7 | 43.86 |
| 10 | 29.2 | 45.12 |
| 15 | 33.8 | 36.8 |
| 20 | 36.4 | 29.96 |
| 25 | 36.2 | 24.87 |
| 30 | 34 | 22.97 |
| 35 | 30 | 22.21 |
| 40 | 29.2 | 20.04 |
| 45 | 26.8 | 18.37 |
| 50 | 25.1 | 16.87 |
| 60 | 23.4 | - |
| 70 | 22.22 | - |
| 80 | 19.6 | - |
| 90 | 17.5 | - |
| 100 | 16.1 | - |

When results of FE analysis are compared with the experimental results [4], the results vary but the behavior remains almost same. The analytical results vary due to actual experimental conditions and conditions of fixed end. The modeling parameters are constant for the analytical specimen but for actual specimen some parameters are different. The same model for concrete has been assumed but the actual behavior may not resemble exactly the same. Considerable increase in strength of around 19% was shown by analytical modeling. The maximum loads attained in experimental and analytical are 36.4KN and 45.12KN respectively. Hysteresis response of unconfined joint both experimentally and analytically is shown in Figure 5.19 and figure 5.20.

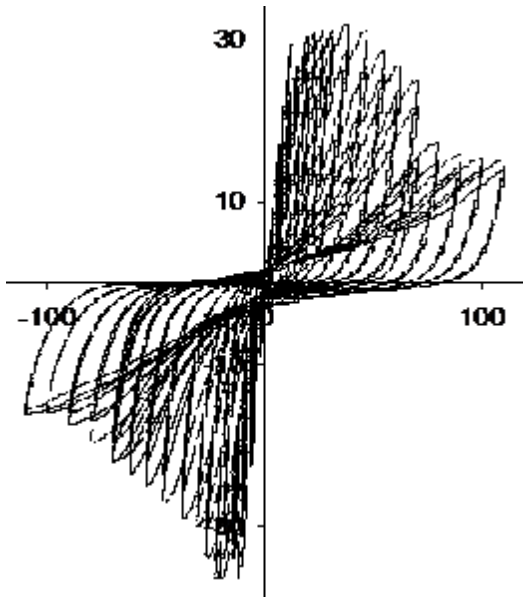


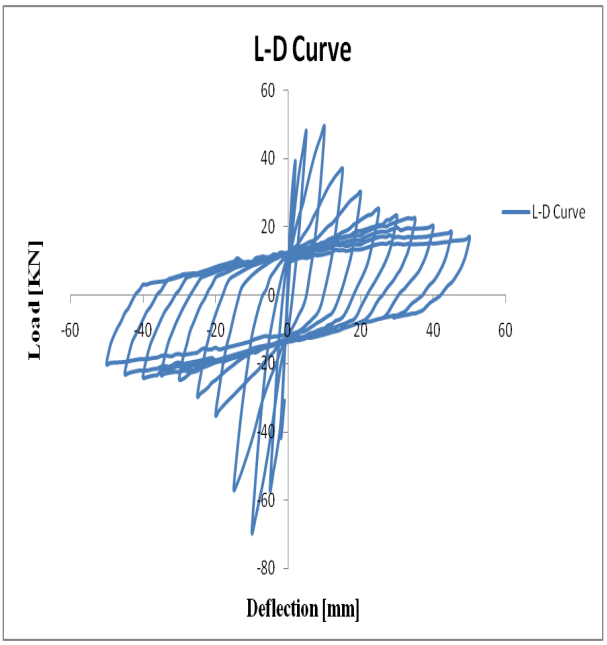


**Figure 5.19 Experimental hysteresis response** **Figure 5.20 Analytical hysteresis response**

### 5.3.2 Comparison of results of (90% stressed) confined joint

Results of analytical modeling are compared with Experimental Results of confined Joint [4]. The maximum value of load at different displacement has been presented in Table 5.6.

**Table 5.6 Comparison of Experimental and FE Results of confined joint**

| DEFLECTION [mm] | LOAD [KN] | |
|---|---|---|
| | Experimental | Analytical |
| 2 | 6.1 | 38.93 |
| 5 | 14.6 | 49.92 |
| 10 | 31.6 | 55.89 |
| 15 | 45.3 | 44.43 |
| 20 | 47.8 | 37.4 |
| 25 | 49.4 | 29.51 |
| 30 | 48.9 | 26.32 |
| 35 | 52.0 | 24.11 |
| 40 | 48.5 | 22.28 |
| 45 | 45.3 | 17.85 |
| 50 | 43.7 | 17.07 |
| 60 | 42.9 | - |
| 75 | 42.5 | - |
| 90 | 37.5 | - |
| 100 | 31.3 | - |

When results of FE analysis are compared with the experimental results [4], the results vary but the behavior remains almost same. The analytical results vary due to actual experimental conditions and conditions of fixed end. The modeling parameters are constant for the analytical specimen but for actual specimen some parameters are different. The same model for concrete has been assumed but the actual behavior may not resemble exactly the same. Considerable increase in strength of around 7% was shown by analytical modeling. The maximum loads attained in experimental and analytical are 52KN and 55.89KN respectively. Hysteresis response of unconfined joint both experimentally and analytically is shown in Figure 5.21 and Figure 5.22.

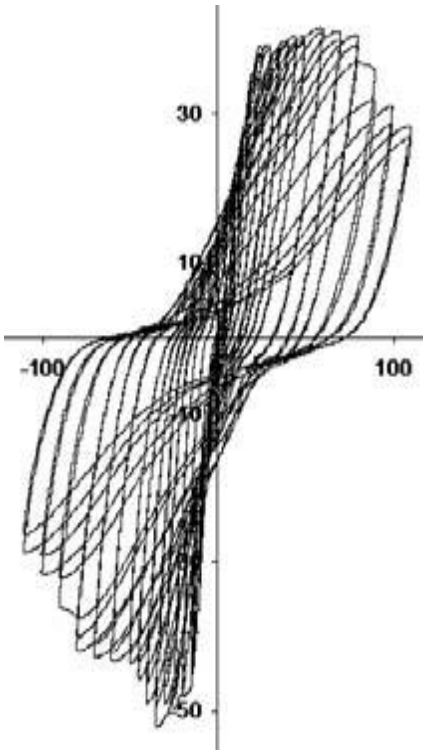


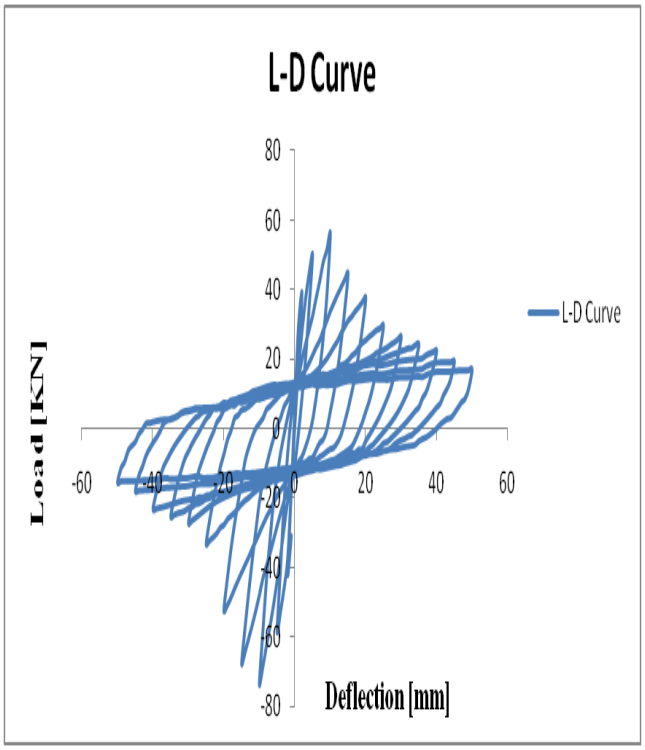


**Figure 5.21 Experimental hysteresis response** **Figure 5.22 Analytical hysteresis response**

## 5.4 FE ANALYSIS OF 75% STRESSED UNCONFINED JOINT

Hysteretic behavior obtained from FE analysis under cyclic load of the 75% stressed retrofitted unconfined Beam-Column Joint is shown in Figure 5.23. The joint is analyzed under displacement control and the loading is applied in terms of displacement in different number of cycles varies from 2 mm to 50 mm. After strengthening with GFRP wrapping the joint showed the load of 45.91 kN at a displacement of ± 10 mm. Strengthened joint demonstrated significant performance in terms of restoring the original strength, yet original strength cannot be achieved. As analysis continues, the load carrying capacity progressively decreases to 26.42 kN at 15mm displacement and the joint behave like a hinge at 18.02 kN load at 45mm displacement. The ultimate load taken by the joint is 45.91 kN at 10mm deflection. Original strength was restored upto 81%. The loads at joint for different displacements have been shown in Table 5.6

**Table 5.7 FE Results of 75% stressed reteofitted unconfined joint under cyclic loading**

| DEFLECTION [mm] | LOAD [KN] |
|---|---|
| 2 | 35.88 |
| 5 | 44.52 |
| 10 | 45.91 |
| 15 | 26.42 |
| 20 | 21.68 |
| 25 | 20.56 |
| 30 | 20.92 |
| 35 | 20.34 |
| 40 | 19.57 |
| 45 | 18.02 |
| 50 | 17.17 |

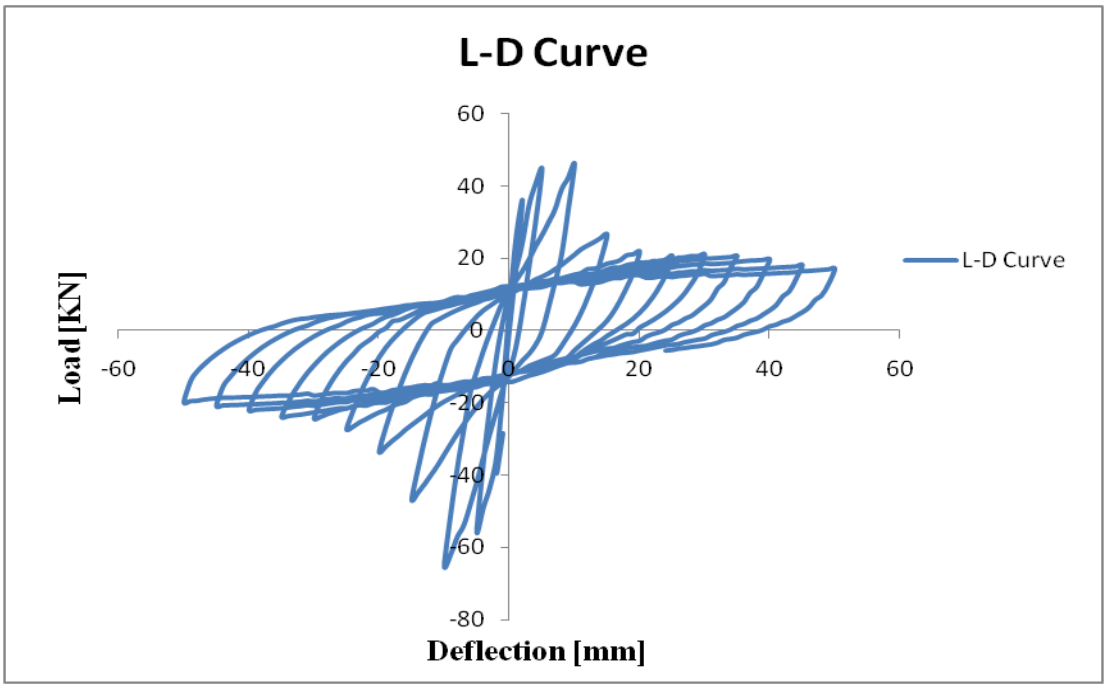


**Figure 5.23 Hysteresis behavior of 75% stressed retrofitted unconfined joint**

### 5.4.1 CRACK PATTERNS

The variations of crack pattern with respect to size of crack and crack propagation have been plotted in Figure 5.24 - 5.31.

It had been observed that micro-cracks appeared in the structure when the joint is in linear zone. After strengthening with GFRP wrapping, initially the flexural cracks were developed at the joint on the beam. The first crack was observed at 2mm displacement at load value of 38.98 KN in the shape of flexural crack as shown in Figure 5.24. The maximum size of this crack depicted from FE analysis was 0.1mm. This very small sized (actually invisible) crack appeared at beam-column joint.

The crack at 10mm displacement has been shown in Figure 5.25. The maximum width of crack at 10mm displacement was observed as 1mm. This is the ultimate load level of the joint. Load carrying capacity of the joint decreases after 10 mm displacement. The number of cracks increases as the displacement increases upto 35 mm. Crack pattern at 15mm and 35mm displacement is presented in Figure 5.26 and Figure 5.27 respectively. The maximum width of crack at 35mm displacement has been observed as 4mm. First flexural cracks have been observed near beam column joint, but at this step crack at the joint and on the beam near to the joint joined with the shear cracks have been observed. Crack pattern at 45mm displacement is presented in Figure 5.28.

These cracks spread all over the joint at displacement 50mm. It was observed that cracks have been propagating towards column. Maximum crack size at this level has been observed of 6mm width. The views showing the crack pattern with different crack size at 50mm displacement are presented in Figure 5.29 to Figure 5.31. The beam- column joint with flexural and shear cracks in almost all the beam and around the joint in column can be visualized. Fewer cracks have been seen at top and bottom of the column. Major damage has been noticed in the joint whereas beam experienced moderate damage and the column experienced minor damage.

Maximum width of crack observed in FE analysis has been shown in Table 5.8

**Table 5.8 Maximum crack width**

| Displacement | Load | Maximum crack width |
|---|---|---|
| 2 | 35.88 | 0.1 |
| 5 | 44.52 | 0.5 |
| 10 | 45.91 | 1 |
| 15 | 26.42 | 1 |
| 20 | 21.68 | 2 |
| 25 | 20.56 | 3 |
| 30 | 20.92 | 3 |
| 35 | 20.34 | 4 |
| 40 | 19.57 | 5 |
| 45 | 18.02 | 6 |
| 50 | 17.17 | 6 |

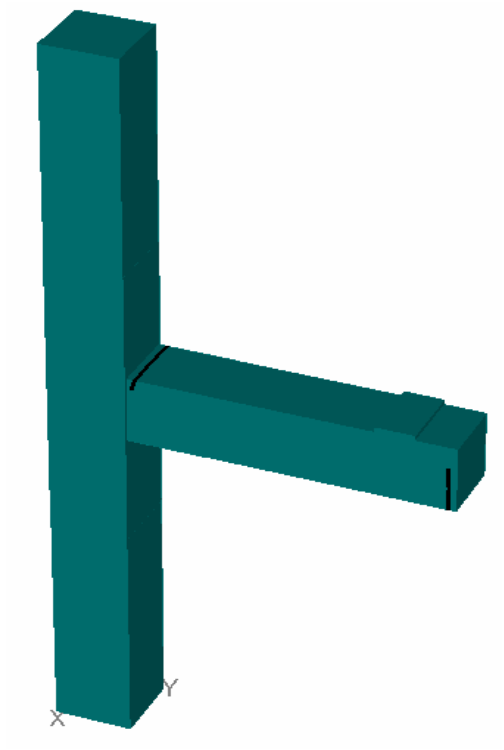

**Figure 5.24 0.1 mm crack at 2mm displacement**

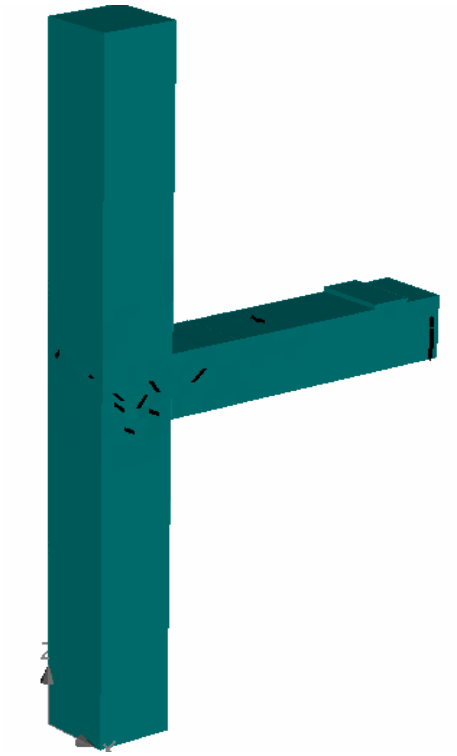

**Figure 5.25 1mm crack at 10mm displacement**

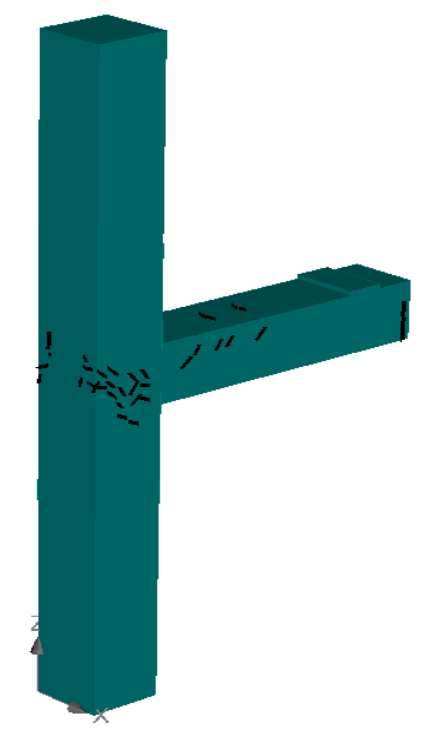

**Figure 5.26 1 mm crack at 15mm displacement**

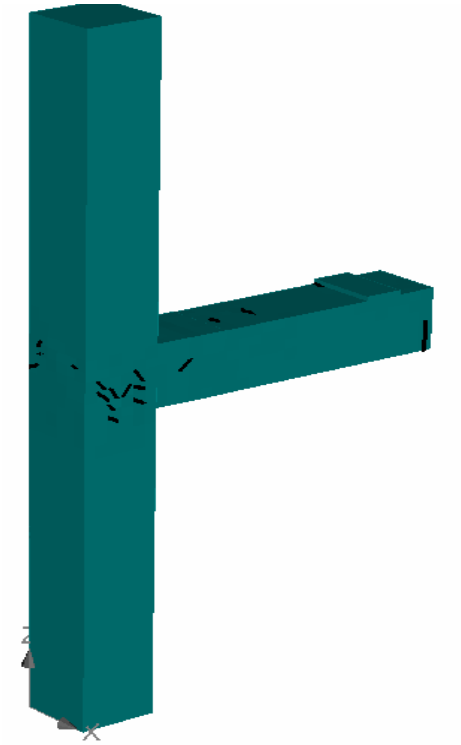

**Figure 5.27 4mm crack at 35mm displacement**

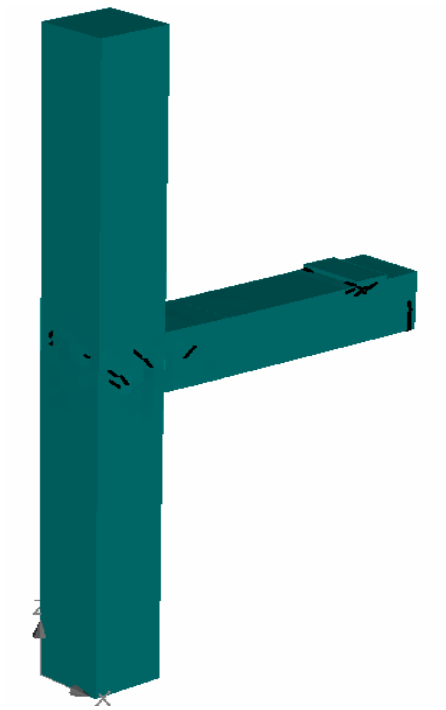

**Figure 5.28 6 mm crack at 45mm displacement**

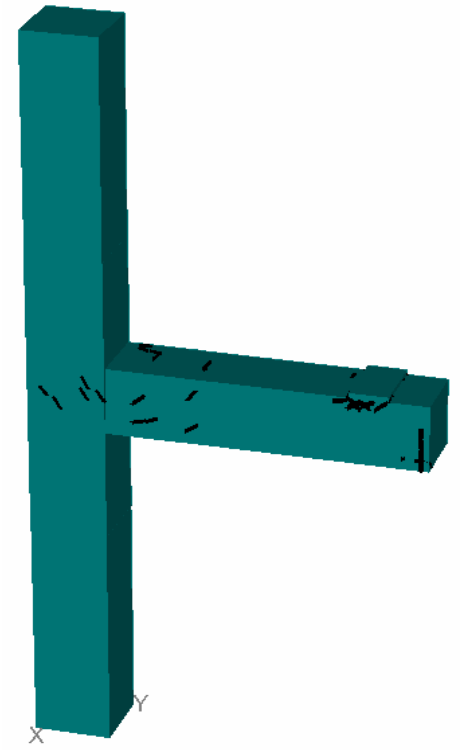

**Figure 5.29 6mm crack at 50mm displacement**

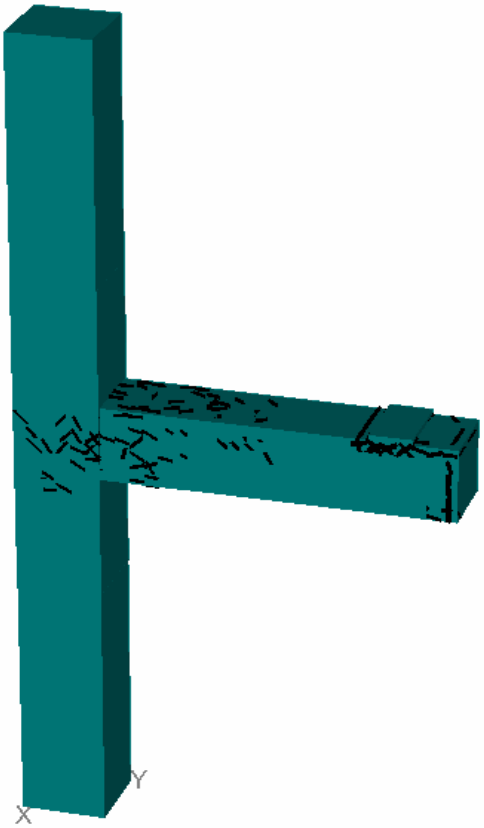


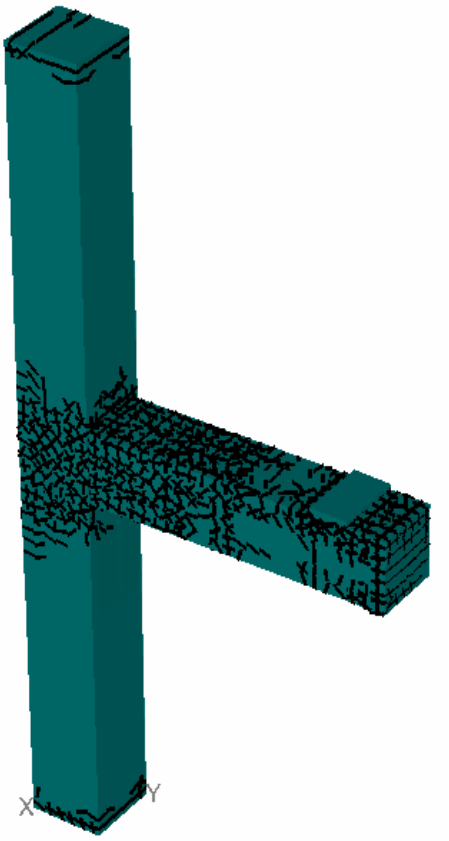


**Figure 5.30 1 mm crack at 50mm displacement** **Figure 5.31 All crack at 50mm displacement**

## 5.5 FE ANALYSIS OF 75% STRESSED CONFINED JOINT

Hysteretic behavior obtained from FE analysis under cyclic load of the 75% stressed retrofitted confined Beam-Column Joint is shown in Figure 5.32. The joint is analyzed under displacement control and the loading is applied in terms of displacement in different number of cycles varies from 2 mm to 50 mm. After strengthening with GFRP wrapping the joint showed the load of 55.89 kN at a displacement of ± 10 mm. Strengthened joint demonstrated significant performance in terms of restoring the original strength, yet original strength cannot be achieved. As analysis continues, the load carrying capacity progressively decreases to 44.43 kN at 15mm displacement and the joint behave like a hinge at 17.85 kN load at 45 mm displacement. The ultimate load taken by the joint is 55.89 kN at 10mm deflection. Original strength was restored upto 78%. There was no significant change in energy dissipation in confined joint than unconfined joint. The loads at joint for different displacements have been shown in Table 5.9

**Table 5.9 FE Results of 75% stressed retrofitted confined joint under cyclic loading**

| DEFLECTION [mm] | LOAD [KN] |
|---|---|
| 2 | 38.93 |
| 5 | 49.92 |
| 10 | 55.89 |
| 15 | 44.43 |
| 20 | 37.4 |
| 25 | 29.51 |
| 30 | 26.32 |
| 35 | 24.11 |
| 40 | 22.28 |
| 45 | 17.85 |
| 50 | 17.50 |

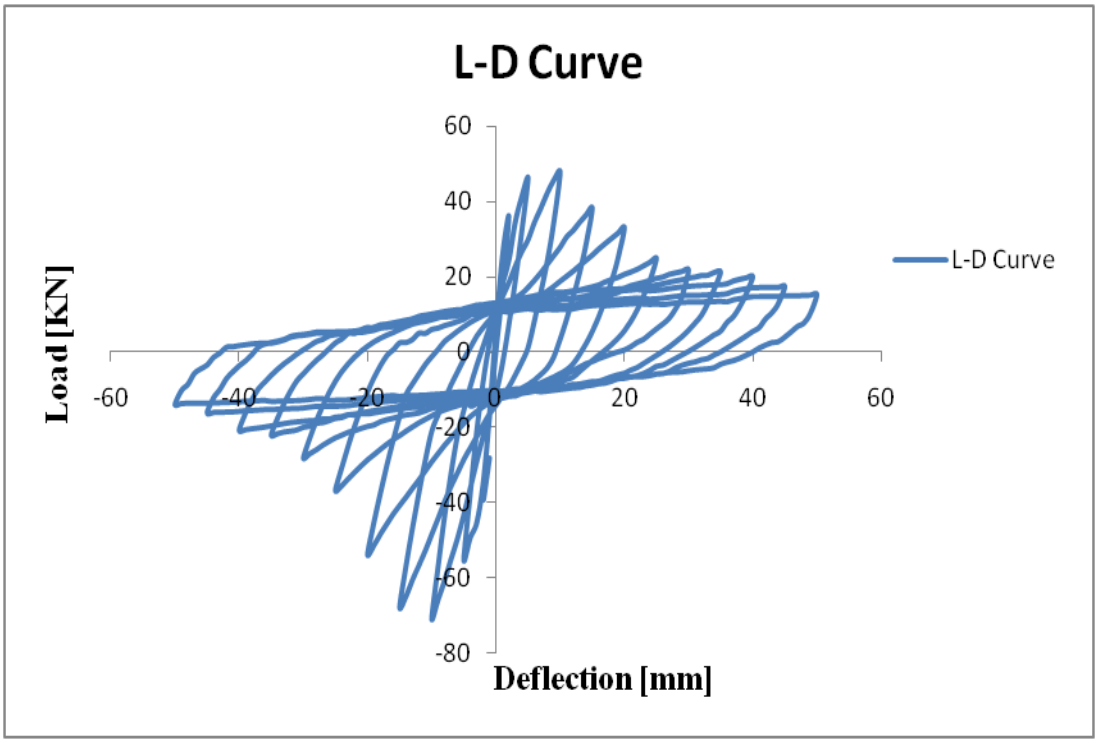


**Figure 5.32 Hysteresis behavior of 75% stressed retrofitted confined joint**

### 5.5.1 CRACK PATTERNS

The variations of crack pattern with respect to size of crack and crack propagation have been plotted in Figure 5.33 - 5.40.

It had been observed that micro-cracks appeared in the structure when the joint is in linear zone. After strengthening with GFRP wrapping, initially the flexural cracks were developed at the joint on the beam. The first crack was observed at 2mm displacement at load value of 35.94 KN in the shape of flexural crack as shown in Figure 5.33. The maximum size of this crack depicted from FE analysis was 0.1mm. This very small sized (actually invisible) crack appeared at beam-column joint.

The crack at 10mm displacement has been shown in Figure 5.34. The maximum width of crack at 10mm displacement was observed as 1mm. This is the ultimate load level of the joint. Load carrying capacity of the joint decreases after 10 mm displacement. The number of cracks increases as the displacement increases up to 35 mm. Crack pattern at 15mm and 35mm displacement is presented in Figure 5.35 and figure 5.36 respectively. The maximum width of crack at 35mm displacement has been observed as 4mm. First flexural cracks have been observed near beam column joint, but at this step crack at the joint and on the beam near to the joint joined with the shear cracks have been observed. Crack pattern at 45mm displacement is presented in Figure 5.37.

These cracks spread all over the joint at displacement 50mm. It was observed that cracks have been propagating towards column. Maximum crack size at this level has been observed of 6mm width. The views showing the crack pattern with different crack size at 50mm displacement are presented in Figure 5.38 to Figure 5.40. The beam- column joint with flexural and shear cracks in almost all the beam and around the joint in column can be visualized. Fewer cracks have been seen at top and bottom of the column. Major damage has been noticed in the joint whereas beam experienced moderate damage and the column experienced minor damage.

Maximum width of crack observed in FE analysis has been shown in Table 5.10

**Table 5.10 Maximum crack width**

| Displacement | Load | Maximum crack width |
|---|---|---|
| 2 | 38.93 | 0.1 |
| 5 | 49.92 | 0.5 |
| 10 | 55.89 | 1 |
| 15 | 44.43 | 1 |
| 20 | 37.4 | 2 |
| 25 | 29.51 | 2 |
| 30 | 26.32 | 3 |
| 35 | 24.11 | 4 |
| 40 | 22.28 | 4 |
| 45 | 17.85 | 5 |
| 50 | 17.50 | 6 |

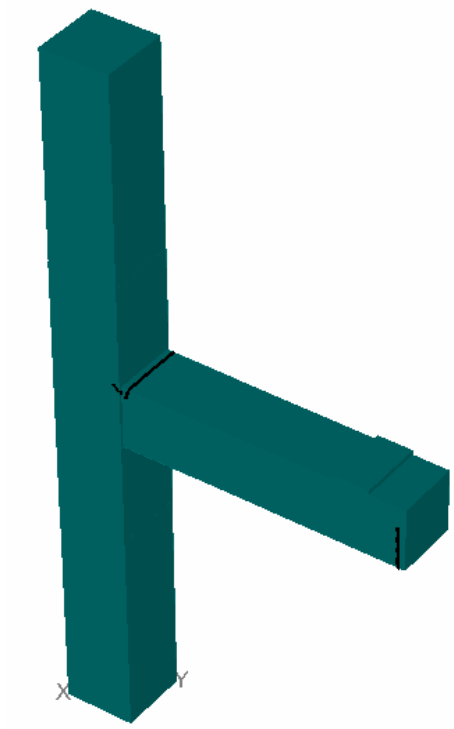

**Figure 5.33 0.1 mm crack at 2mm displacement**

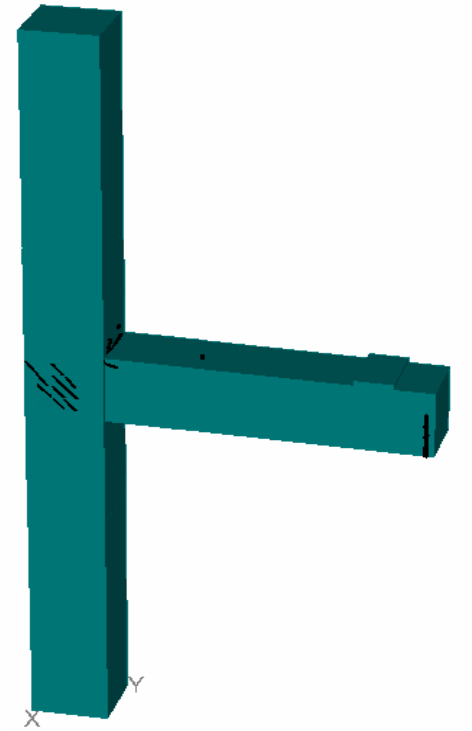

**Figure 5.34 1mm crack at 10mm displacement**

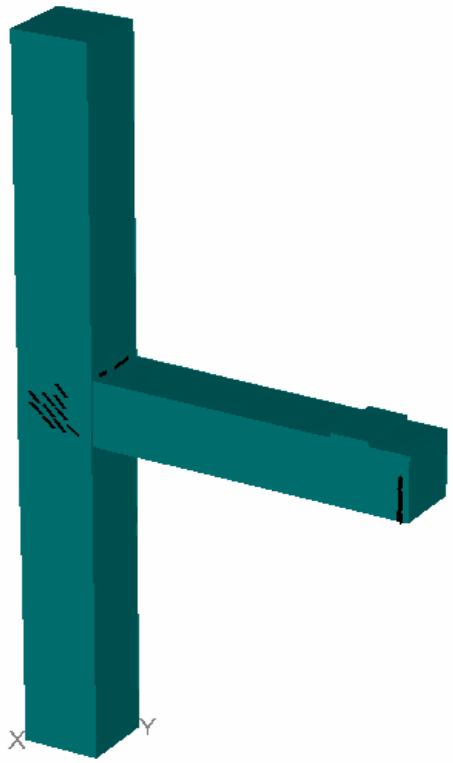


**Figure 5.35 1 mm crack at 15mm displacement**

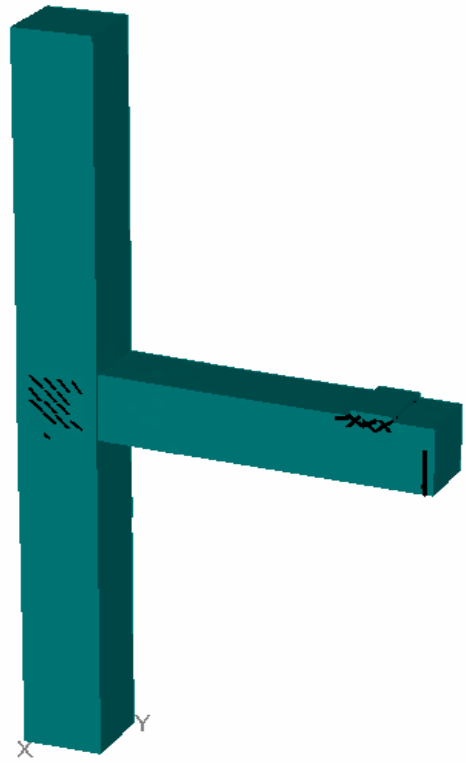


**Figure 5.36 4mm crack at 35mm displacement**

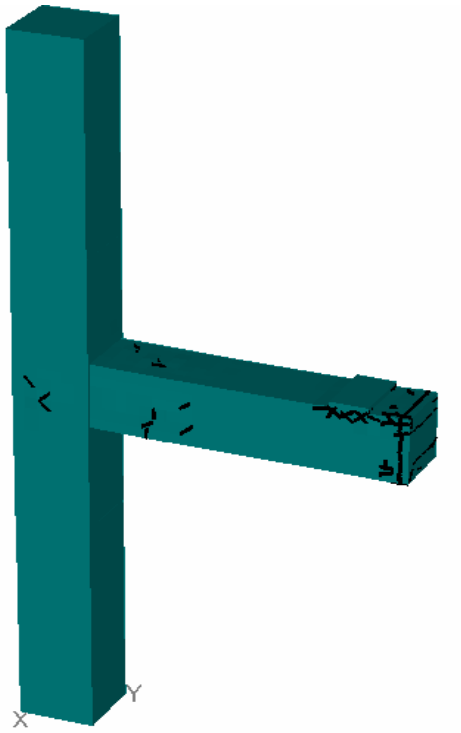


**Figure 5.37 5 mm crack at 45mm displacement**

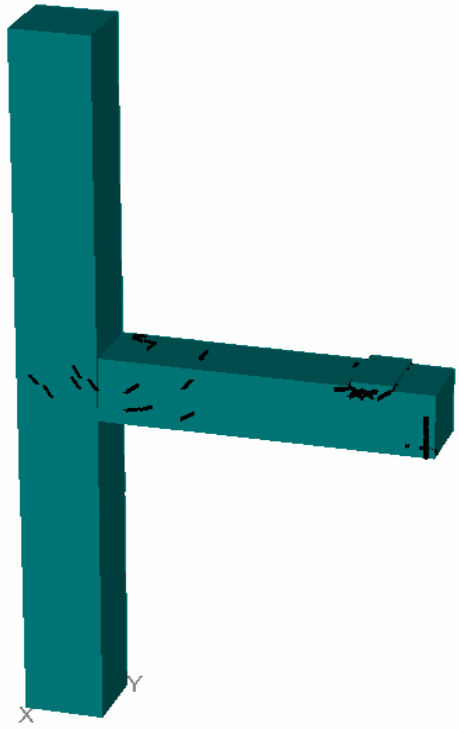


**Figure 5.38 6mm crack at 50mm displacement**

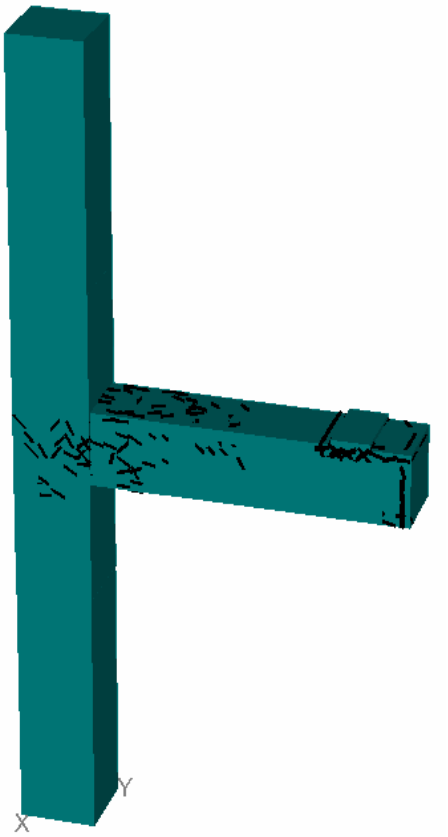

**Figure 5.39 1 mm crack at 50mm displacement**

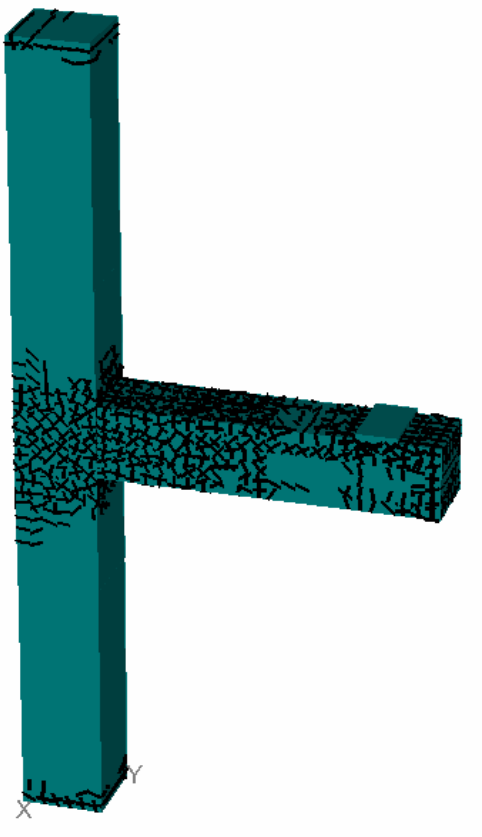

**Figure 5.40 All crack at 50mm displacement**

# Chapter 6 CONCLUSIONS & RECOMMENDATIONS

## 6.1 GENERAL

In the present study, the non-linear response of RC beam column joint under incremental loading and cyclic loading and the stressed (90% and 75%) retrofitted RC beam column joint using FE Modeling under the cyclic loading has been carried out with the intention to study the relative importance of several factors in the non-linear finite element analysis of RC beam column joint.

## 6.2 CONCLUSIONS

The main observations and conclusions drawn are summarized below:

- Analytical modeling results of both unconfined and confined joint showed the same behavior upto the elastic region with the intial flexural cracks in the beam and then shear cracks in the joint.
- Major damage has been noticed in the joint whereas beam experienced moderate damage and the column experienced minor damage in all the cases.
- Comparing the behavior of confined and unconfined joint under monotonic loading a significant gain in strength is noticed because of attribution of the reinforcement detailing. There was around 9% increase in ultimate load carrying capacity.
- Comparing the behavior of the confined and unconfined joint under cyclic loading, the load displacement envelop of confined joint is smoother and more stable as compared to unconfined joint. There is around 12% increase in strength and 54% increase in energy dissipation due to confinement.
- There was 47% increase in ductility in case of confined joint than unconfined joint under monotonic loading. The performance of confined joint in terms of intial cracks was better, as fewer cracks were seen in confined joint. The shear cracks developed on the joint face are lesser than unconfined joint and initiated at higher load.
- After retrofitting the damaged unconfined joint (90% stressed) with GFRP wrapping in critical damaged region around joint, the original strength was restored upto 66% as the

maximum load in case of unconfined joint and 87% in case of confined joint. There was no significant change in energy dissipation in confined joint than unconfined joint.

- In case of 75% damaged joint it was observed that after retrofitting the joint, the strength of damaged joint was restored upto 76% of the maximum load in case of unconfined and 82% in case of confined joint. There was no significant change in energy dissipation in confined joint than unconfined joint.
- After comparing experimental and FE Model Load v/s deflection curves of the joint, the FE model results can be said to be reasonably in close agreement with the experimental data from Gupta and Agarwal (2012). The analytical results were on little higher side due to actual experimental conditions and condition of fixed end. The modeling parameters are constant in case of analytical work but in actual some parameters are different.

## 6.3 FUTURE SCOPE

In the present study control RC T-joint has been studied under monotonic and cyclic loading. The joint can be studied under cyclic-loading with different joint reinforcement detail to monitor the variation in load-deflection curves at given time history. Retrofitted joint at various stress levels and with different types of FRP wrapping can be studied to observe their behavior at different loadings. Dynamic analysis of retrofitted joint at higher displacement can also be incorporated in the study.

## REFERENCES:


1. **Aci Committee 408**, Opportunities In Bond Research, American Concrete Institute Journal, Proceedings, Vol.67, No.11, Nov. 1970, Pp.857-867.

2. American Concrete Institute, ACI 352R-02, ACIASCE, Committee 352, Detroit, 2002, **Recommendations for design of beam-column-joints in monolithic reinforced concrete structures.**

3. **ATENA theory manual**, part 1 from Vladimir Cervenka, Libor Jendele and Jan Cervenka

4. **ATENA 3D** and ATENA WIN –finite element software manuals".

5. Cervenka, V., Cervenka, J., & Pukl, R**. "ATENA—A tool for engineering analysis of fracture in concrete."** Sadhana 27.4 (2002): 485-492.

6. Choudhury, A. M., A. Dutta, and S. K. Deb. (2011) "**Study on size effect of RC deficient beam-column joints with and without retrofitting under cyclic loading.**" International Journal of Civil and Structural Engineering Volume 2, No 2, 2011, ISSN 0976 – 4399

7. Choudhury, A. M., Dutta, A., & Deb, S. K. (2010) **"Study on Size effect of Retrofitted beam-column joint with Beam Weak in Flexure under Cyclic Loading".** Proceedings of 35$^{th}$ Conference on our world in concrete & structures: 25 - 27 August 2010, Singapore.

8. Ganesan, N., P. V. Indira, and Ruby Abraham. **"Steel fibre reinforced high performance concrete beam-column joints subjected to cyclic loading."** ISET J. Earthq. Technol 44.3-4 (2007): 445-456.

9. Gencoglu, M., and B. Mobasher. "**The strengthening of the deficient RC exterior beam-column joints using CFRP for seismic excitation.**" Proceedings of the 3rd international conference on structural engineering, mechanics and computation 10-12 September 2007,Cape town ,South Africa".

10. Gupta,A. and Agarwal,P. "**Performance Evaluation Of Exterior Rc Beam Column Joint strengthened With Frp Under Cyclic Load**" Fourth International Conference on Structural Stability and Dynamics (ICSSD 2012), 4–6 January, 2012.

11. Hasaballa, M., M. Mady, A. El-Ragaby, and E. F. El-Salakawy. "**Gfrp-Reinforced Concrete beam-column Joints**."(2009)".

**12.** IS 13920-1993 Edition 1.2 (2002-03), "**Indian Standard Code of Practice Ductile Detailing of Reinforced Concrete Structures Subjected to Seismic Forces**", Bureau of Indian Standards, New Delhi, 2002.

13. IS 1893-2002 **Criteria for Earthquake Resistant design of structures**.

**14.** IS 456: 2000 (Fourth Revision), "**Indian Standard: Plain and Reinforced Concrete – Code of Practice",** Bureau of Indian Standards, New Delhi, 2005.

15. ISET (1981). "**A Manual of Earthquake Resistant Non- Engineered Construction**". Indian society of earthquake technology. Roorkee.

16. Jindal. A. (2012), **"Finite Element Modelling of Reinforced Concrete Exterior Beam- Column Joint Retrofitted with Externally Bonded Fiber Reinforced Polymer (FRP) "** M.E. Thesis, Thapar University, Patiala

17. Josef,H., Alaa Sherif, and Wolfgang Roeser. "**Nonlinear finite element analysis of reinforced concrete beam-column connections.**" ACI Structural Journal 101.5 (2004).

18. Kwak, H.G., Fillipou, C.F.(1990) **"Finite Element Analysis of Reinforced Concrete Structures Under Monotonic Loading"** Structural Engineering

Mechanics and Materials**,** Report no. UCB/ SEMM-90/14.

**19.** Liu, C. (2006). **"Seismic Behaviour of Beam-Column Joint Subassemblages Reinforced with steel Fibers",** Master's Thesis, University of Canterbury, Christchurch, New Zealand.

20. Lu, Xilin, Tonny H. Urukap, Sen Li, and Fangshu Lin. "**Seismic behavior of interior RC beam-column joints with additional bars under cyclic loading.**"Earthquake and Structures 3, no. 1 (2012): 37-57.

21. Mahini, S. S., H. R. Ronagh, and A. Dalalbashi. "**Numerical modeling of CFRP-retrofitted RC exterior beam-column joints under cyclic loads.**" the 4th International Conference on FRP Composites in Civil Engineering (CICE2008). 2008.

22. Mukherjee, Abhijit, and Mangesh Joshi. "**FRPC reinforced concrete beam-column joints under cyclic excitation.**" Composite structures 70.2 (2005): 185-199.

23. Pannirselvam, N., P. N. Ragunath, and K. Suguna. "**Strength Modeling of Reinforced concrete Beam with Externally Bonded FRP Reinforcement**."American Journal of Engineering and Applied Sciences 1.3 (2008): 192.

24. Patil, S. S., and S. S. Manekari. "**Analysis of Reinforced Beam-Column Joint Subjected to Monotonic Loading**." International Journal of Engineering and Innovative Technology (IJEIT), Analysis 2.10 (2013).

25. PERUMAL, P., and B. Thanukumari. "**Use of fibre cocktails to increase the seismic performence of beam-column Joints.**" International Journal of Engineering Science and Technology 2.9 (2010): 3997-4006.

26. Rajaram, P., A. Murugesan, and G. S. Thirugnanam. "**Experimental Study on behavior of interior RC Beam Column Joints Subjected to Cyclic Loading.**"International Journal of Applied Engineering Research 1 (2010).

27. Ravi, S. Robert, and G. Prince Arulraj. "**Experimental investigation on behavior of reinforced Concrete Beam Column Joints Retrofitted with GFRP-AFRP Hybrid wrapping**." International Journal of Civil & Structural Engineering 1.2 (2012): 245-253.

28. Report on (2005) **"Earthquake Resistant Design and Construction for Beam–Column Joints in RC Buildings"** compiled by C V R Murty ,Indian Institute of Technology Kanpur.

29. Report on **"Seismic Behaviour Of Beam Column Joints In Reinforced Concrete Moment Resisting Frames"** compiled by S.R. Uma and A. Meher Prasad. Document No. :: IITK-GSDMA-EQ31-V1.0

30. Singhal, H. (2009), **"Finite Element Modeling of Retrofitted RCC Beams"** M.E. Thesis, Thapar University, Patiala.